MIT-4105-3
MITNE-116

LMFBR BLANKET PHYSICS PROJECT
PROGRESS REPORT NO. 1

June 30, 1970

Department of Nuclear Engineering
Massachusetts Institute of Technology
Cambridge, Massachusetts

Contract AT(30-1)-4105
U.S. Atomic Energy Commission

MASSACHUSETTS INSTITUTE OF TECHNOLOGY

DEPARTMENT OF NUCLEAR ENGINEERING

Cambridge, Massachusetts 02139

MIT-4105-3 MITNE-116

AEC Research and Development Contract

UC-34 Physics

LMFBR BLANKET PHYSICS PROJECT PROGRESS REPORT NO. 1

June 30, 1970

Contract AT(30-1)4105

U. S. Atomic Energy Commission

Editors:

I. A. Forbes
M. J. Driscoll
D. D. Lanning
I. Kaplan
N. C. Rasmussen

Contributors:

S. A. Ali
S. T. Brewer
D. K. Choi
F. M. Clikeman
W. R. Corcoran
M. J. Driscoll
I. A. Forbes
C. W. Forsberg
S. L. Ho
C. S. Kang
I. Kaplan
J. L. Klucar
D. D. Lanning
T. C. Leung
E. L. McFarland
P. G. Mertens
N. R. Ortiz
A. Pant
N. A. Passman
N. C. Rasmussen
M. K. Sheaffer
D. A. Shupe
G. E. Sullivan
A. T. Supple
J. W. Synan
C. P. Tzanos
W. J. Westlake

DISTRIBUTION

MIT-4105-3 MITNE-116
AEC Research and Development Contract
UC-34 Physics

1-3. U. S. Atomic Energy Commission, Headquarters,
Division of Reactor Development and Technology,
Reactor Physics Branch.

4. Argonne National Laboratory,
Liquid Metal Fast Breeder Reactor Program Office,
9700 South Cass Avenue,
Argonne, Illinois, 60439.

5. H. S. Potter, New York Patent Group,
U. S. Atomic Energy Commission,
Brookhaven Office,
Upton, New York, 11973.

6, 7. U. S. Atomic Energy Commission,
Cambridge Office.

8. Dr. Paul Greebler,
General Electric, Atomic Products Division,
175 Curtner Avenue,
San Jose, California, 95125.

9. Dr. Harry Morewitz,
Atomics International,
P. O. Box 309,
Canoga Park, California, 91305.

10. Mr. M. W. Dyos,
Advanced Reactors Division,
Westinghouse Electric Corporation,
Waltz Mill Site, P. O. Box 158,
Madison, Pennsylvania, 15663.

ABSTRACT

This is the first annual report in an experimental program for the investigation of the neutronics of benchmark mock-ups of LMFBR blankets.

During the period covered by the report, July 1, 1969 through June 30, 1970, work was devoted primarily to completion and proof-testing of the experimental facilities at the M.I.T. Reactor and to the acquisition of experimental techniques, data reduction, and analysis capabilities necessary to achieve the objectives of the program. Experiments were initiated on a steel reflected blanket constructed of uranium metal fuel clad in carbon steel tubes and surrounded by $Na_2 CrO_4$. Measurements were made that confirmed the achievement of the proper transverse spectral and spatial neutron distribution over a large central region of the test assembly.

Work is described on the development of foil and instrumental methods for neutron spectrometry, and on the application of capture-gamma techniques to blanket analysis. Improved methods for simplified LMFBR calculations are described and a discussion of the economic and technical bases for the future program effort is presented.

TABLE OF CONTENTS

LIST OF FIGURES

LIST OF TABLES

1. INTRODUCTION

1.1 Foreword

This is the first annual report of the LMFBR Blanket Physics Project. The report covers work done primarily in the period from July 1, 1969, through June 30, 1970.

The importance of the breeding ratio has long been recognized. However, the primary emphasis of fast reactor physics experiments and analysis for LMFBR development has justifiably been on the core design. The work on blanket neutronics now in progress at M. I. T. has been initiated as an important supplement to the core analysis work in progress at AEC facilities as well as other U. S. industrial organizations. The information to be derived by the Blanket Physics Project will give experimental information together with comparisons to currently available theoretical computations.

Construction of the M. I. T. Blanket Test Facility was begun in July, 1968, funded by an M. I. T. research grant. In July, 1969, support under USAEC Contract AT(30-1)4105 commenced. Construction was completed in September, 1969.

From October through December, 1969, a detailed evaluation of the performance of the facility was made using the first simulated blanket assembly. B.T.F. Blanket No. 1 was composed approximately of 50 v/o iron and 50 v/o anhydrous borax ($Na_2B_4O_7$). The construction of the facility and the evaluation program are described in detail in the topical report:

> I. A. Forbes, M. J. Driscoll, T. J. Thompson, I. Kaplan and D. D. Lanning, "Design, Construction and Evaluation of a Facility for the Simulation of Fast Reactor Blankets," MIT-4105-2, MITNE-110 (February, 1970).

Construction of the second blanket assembly was completed early in March, 1970. Blanket No. 2 is an accurate mockup of a typical LMFBR blanket. A program of foil activation measurements to establish that transverse spectral equilibrium exists in Blanket No. 2, and to measure the transverse buckling of the assembly was carried

out between March and June, 1970.

To assist the reader concerning the description of the blanket assembly, the terminology used throughout this report is as follows (refer to Fig. 4.1). The laterally horizontal x-direction and the vertical y-direction are called the transverse directions, and the z-direction is referred to as the axial direction. The axial direction is equivalent to the radial direction in the LMFBR being simulated.

After the successful completion of the transverse activation traverses, measurements of the activation of various materials in the axial direction in Blanket No. 2 were begun, and are now underway.

Work is also in progress on the measurement of neutron spectra in Blanket No. 2 using both direct spectrometer measurements (He^3 and proton recoil spectrometers) and foil activation unfolding methods (foil packet irradiation combined with the GAMANL and SAND-II codes). Prompt gamma spectroscopy on Blanket No. 2 is being carried out with a view to providing an overall blanket neutron balance. In-rod activation measurements with U^{238} foils are being made to determine the extent of heterogeneity effects.

Theoretical investigations over the past year have included work on blanket-reflector interactions, blanket economic studies, heterogeneity effects, a simplified one-group model applicable to LMFBR physics analysis, and spectrum unravelling techniques. Work has also begun on a detailed blanket optimization analysis.

1.2 Purpose and Scope of Research

The purpose of the LMFBR Blanket Physics Project is to conduct both experimental and theoretical investigations of the breeding blanket region of the LMFBR. The systematic study of a series of realistic mockups of typical blanket configurations and compositions will provide data required in the development of an economical breeder reactor.

Work on B. T. F. Blanket No. 2 (described in Chapter 3) began in March, 1970, and will continue through December, 1970. Measurements scheduled for Blanket No. 2 include:

(a) Material activation traverses: U^{238} fission and capture, Pu^{239} and U^{235} fission; Fe, Ni, Cr and Na capture to the extent proven feasible.

(b) Transverse and axial buckling measurements using Au, Mo and In foils.

(c) He^3 and proton recoil measurements of neutron spectra in selected locations.

(d) Foil packet measurements of the neutron energy spectrum as a function of axial position.

(e) Prompt gamma measurements to provide an independent method for obtaining a neutron balance.

(f) In-rod activation of annular U^{238} foils to determine the extent of heterogeneity effects.

Data analysis and methods will be as follows:

(a) Axial spectral characterization and activation rates will be calculated for comparison with all foil activation measurements. These calculations will be made with the 1DX, ANISN and XSDRN codes using various cross section sets.

(b) Two-dimensional burnup calculations will be made using the 2DB code.

(c) Neutron spectra will be derived from foil activation data using the SAND-II code.

(d) Gamma spectra will be interpreted with the aid of the GAMANL code developed at M.I.T.

(e) Neutron spectra will be derived from proton recoil data with codes developed by Bennett et al. at ANL. These will be obtained and put into operation in the near future.

In addition, work will be continued on the development of methods for the analysis of heterogeneity effects and the determination of neutron spectra from foil activation data. No major code development

work is contemplated. Other LMFBR contractors will be contacted where appropriate to solicit help in carrying out one-of-a-kind supplementary analyses. Contact will be established with various industrial groups to provide continuity between the blanket research group and design developments.

1.3 Staff

The project staff, including thesis students, during the report period was as follows:

*M. J. Driscoll, Associate Professor of Nuclear Engineering, Project Leader
*I. Kaplan, Professor of Nuclear Engineering
*D. D. Lanning, Professor of Nuclear Engineering
*N. C. Rasmussen, Professor of Nuclear Engineering
T. J. Thompson, Professor of Nuclear Engineering (on leave of absence)
F. M. Clikeman, Associate Professor of Nuclear Engineering
I. A. Forbes, Research Associate (to September 1970)
*A. T. Supple, Jr., Engineering Assistant
*G. Sullivan, Technician
S. Ahmed Ali, Research Assistant (to September 1969)
*S. T. Brewer, Research Assistant (as of September 1969), Ph. D. student
D. K. Choi, Research Assistant (to September 1969)
†*W. R. Corcoran, NDEA Trainee, Ph. D. student
J. N. Donohew, Research Assistant (to September 1969)
†*C. Forsberg, AEC Fellow, S. M. student (as of June 1970)
†S. L. Ho, I. I. E., S. M. student (to February 1970)
*C. S. Kang, Research Assistant (as of February 1970), Sc. D. student

---

*Continuing on staff as of July, 1970.

†Salary not paid from contract funds during FY 1970.

†J. L. Klucar, Special Project student (to September 1969)

*T. C. Leung, Research Assistant, Sc. D. student

E. L. McFarland, Research Assistant (from September 1969 to June 1970)

†*P. Mockapetris, S. B. student (as of February 1970)

†*N. R. Ortiz, G. E. Fellow, Sc. D. student

*A. Pant, Research Assistant (as of February 1970), S. M. student

*N. A. Passman, Research Assistant (as of February 1970), S. M. student

†*M. K. Sheaffer, U. S. Army, Ph. D. student

†D. Shupe, S. M. student, M. I. T. Physics Department

†J. W. Synan, Special Project student (to September 1969)

†*C. Tzanos, Ph. D. student (as of June 1970)

†W. J. Westlake, A. E. C. Fellow, S. M. student (to June 1970)

---

*Continuing on staff as of July 1970.

†Salary not paid from contract funds during FY 1970.

2. DESCRIPTION OF THE FACILITY

I. A. Forbes

2.1 Introduction

A detailed description of the Blanket Test Facility and of the initial evaluation tests using Blanket Assembly No. 1 is given in Reference (1). A brief description follows.

2.2 The Facility

The heart of the Blanket Test Facility is a uranium-loaded converter plate. Powered by the thermal neutron flux from the MITR thermal column, the converter generates the fast neutron flux for testing a mockup of an LMFBR blanket. The highly-thermalized flux provided by the thermal column (cadmium ratio for gold $\simeq$ 1700) helps ensure that the converter plate has the leakage spectrum and albedo characteristic of the core of a large LMFBR.

The Blanket Test Facility (B. T. F.) is located at the rear of the graphite-lined cavity, or "hohlraum," of the MITR; Figures 2.1 and 2.2 show cross-section and plan views, respectively, of the facility.

The B. T. F. irradiation region was formed by removing the rear graphite wall of the hohlraum and existing thermal exponential facility shielding, and installing a five-sided aluminum box to line the resulting cavity. The interior volume of this cavity is about 6 ft. by 6 ft. by 6 ft. The aluminum liner box is seam-welded to maintain the sealed nature of the hohlraum and prevent the leakage of A^{41} from the hohlraum into the irradiation region and the reactor building. Boral sheet is attached to the top, sides and floor of the box to reduce back-scattering of thermalized neutrons from the surrounding concrete shielding.

Shielding for the irradiation region is provided by four heavy concrete shield blocks, two stationary and two portable. The two portable blocks weigh approximately 15 tons each and can be removed

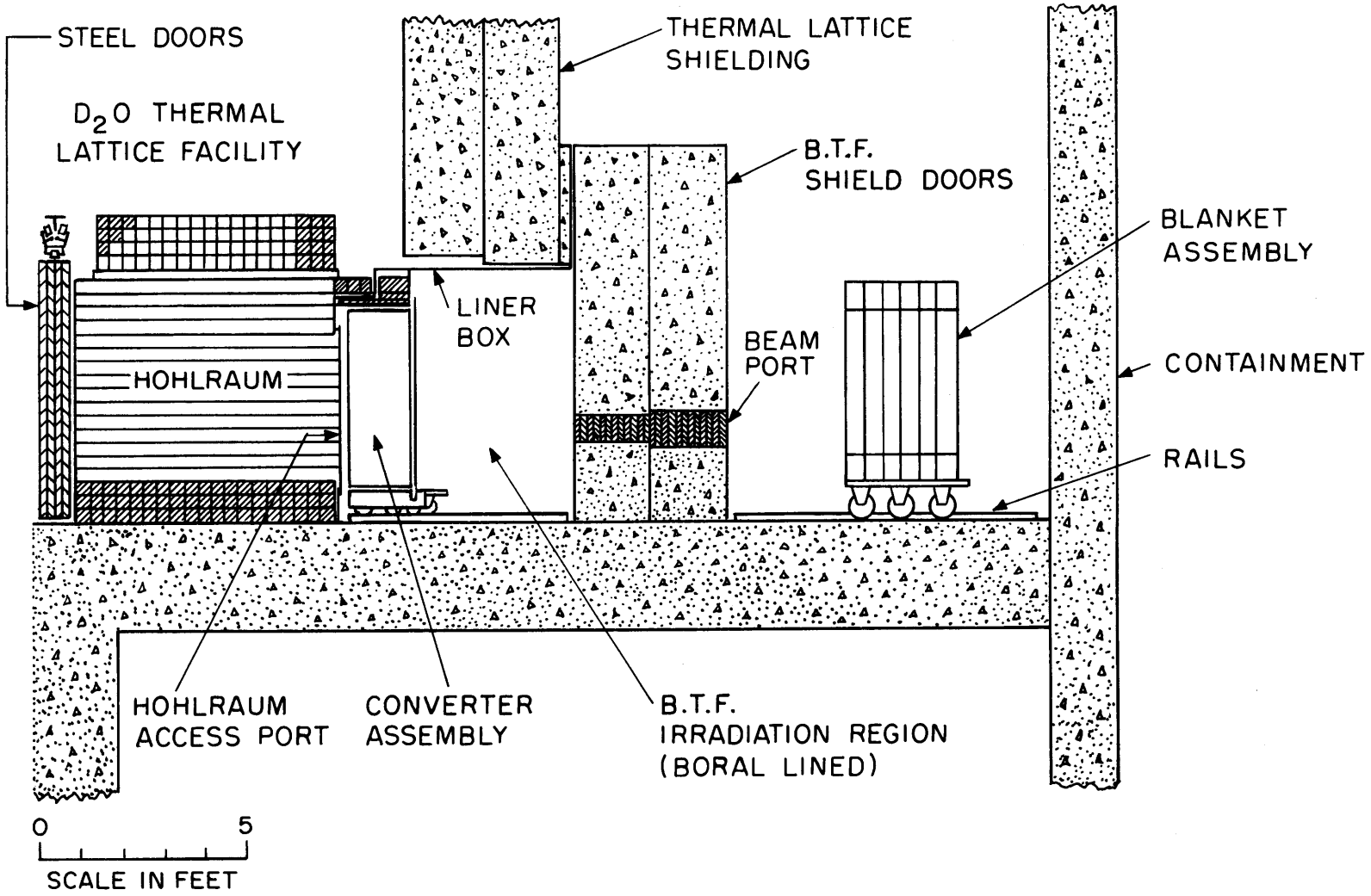

FIG. 2.1 SCHEMATIC CROSS SECTION VIEW OF HOHLRAUM AND BLANKET TEST FACILITY

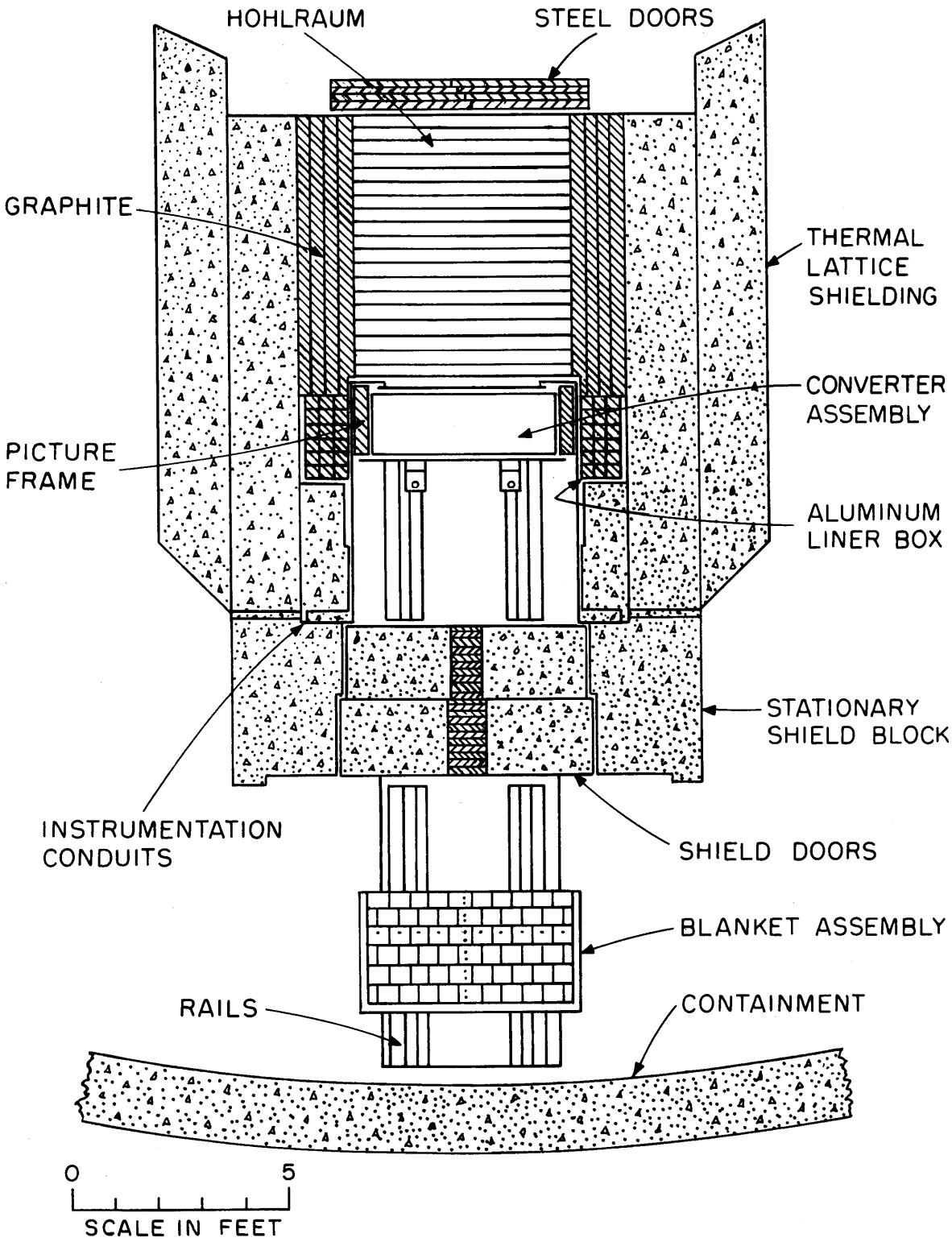

FIG. 2.2 SCHEMATIC PLAN VIEW OF THE HOHLRAUM AND BLANKET TEST FACILITY

with the reactor building's overhead crane to provide access to the irradiation region.

A set of rails, extending from the front of the irradiation region out to the reactor building containment wall, permits the insertion of the cart-mounted experimental assemblies into the irradiation region.

For operation of the Blanket Test Facility, the converter assembly is rolled to the front of the irradiation region, the simulated blanket assembly is installed directly behind it, and the concrete shield doors replaced. For operation of the thermal exponential facility and other experiments utilizing the hohlraum thermal flux, the converter assembly is replaced by a third cart, loaded with graphite and having the same dimensions as the converter assembly. The graphite cart restores the reflective properties of the hohlraum for thermal neutrons.

Changeovers from fast operation to thermal operation and vice versa are performed only when the MIT Reactor is shut down. However, personnel dose rates are low enough to permit access to the B. T. F. irradiation region when the reactor is at full power (5 Mw), for the retrieval of experimental packages (foils, etc.) from the blanket assembly.

2.3 The Converter Assembly

A schematic view of the converter assembly is shown in Fig. 2.3. The converter assembly consists of a graphite external moderator region composed of 4 in. by 4 in. reactor grade graphite stringers, and a fuel region composed of 1/2-in.-diameter, aluminum-clad UO_2 fuel rods in a close-packed, triangular-pitch array. The active fuel region is 48 in. high and 60 in. wide, and has U^{235} enrichments of 1.0999% and 1.99%. The graphite stringers and fuel rods are mounted vertically, between upper and lower grid plates, in a closed aluminum container. The container is designed to prevent any accidental rearrangement of fuel that might approach a critical assembly even if the facility were flooded with H_2O; it will also contain any A^{41} generated in the converter.

In the present loading, the graphite external moderator region is

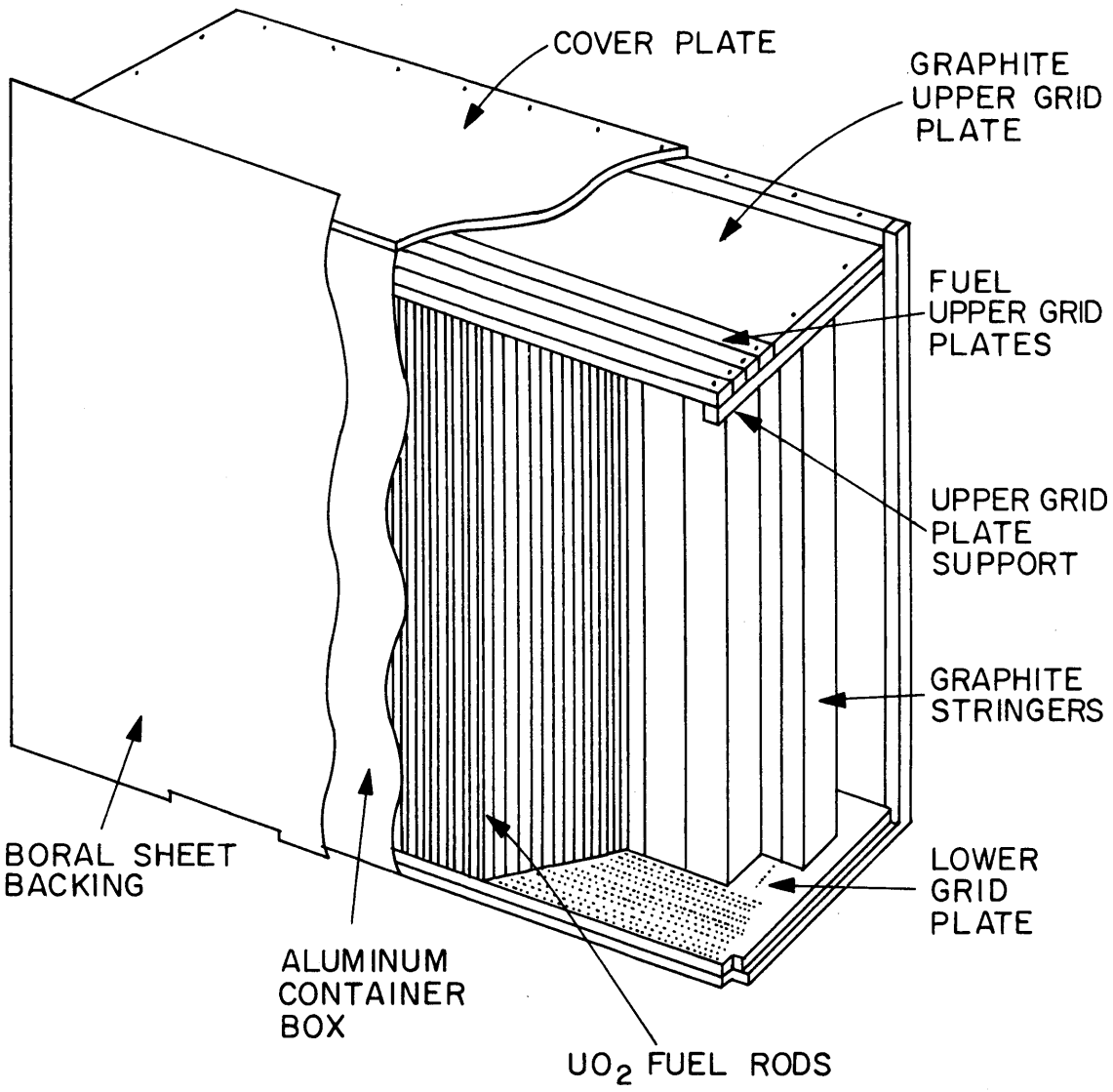

FIG. 2.3 CUTAWAY VIEW OF THE CONVERTER ASSEMBLY

8 in. thick and the UO_2 fuel region is 6.865 in. thick. However, both the graphite and fuel loadings may be readily changed (provision is made for up to 12 in. of graphite and 7.755 in. of fuel) to permit the generation of a wide range of converter leakage spectra.

2.4 Initial Evaluation Tests

When construction of the Blanket Test Facility was completed, a series of experimental runs was made to evaluate the performance of the facility with the converter assembly and the first blanket assembly.

Blanket No. 1 consisted of sixty-three subassemblies loaded on an experimental cart to form a blanket 55.4 in. high, 60.75 in. wide and 30.5 in. thick. The subassemblies were loaded with a mixture of low-carbon steel punchings and anhydrous borax powder to provide a composition of approximately 50 v/o iron and 50 v/o $Na_2B_4O_7$. This mixture contains oxygen, sodium and iron (typical blanket constituents), and simulates the neutronic properties of uranium with iron and boron so that the neutron spectra and overall spatial flux shapes generated are quite similar to those in realistic blanket assemblies.

The evaluation tests included:

(a) Dose measurements to check the biological shielding, accessibility following irradiation, and the residual activation of the converter and blanket assemblies.

(b) Measurements with bare and cadmium-covered gold foils on the sides, top and bottom of the blanket assembly to determine the extent of neutron streaming around the blanket and of back-scattering of thermalized neutrons from the surrounding concrete shielding.

(c) Mapping of the converter leakage flux shape with a matrix of gold foils.

(d) Transverse activation traverses with gold and indium foils to ensure that transverse spectral equilibrium was attained in a large central volume of the blanket, and to measure the transverse buckling.

(e) Axial activation traverses with gold and indium foils for comparison with ANISN calculations to check for correct converter spectrum generation.

The evaluation program was successfully completed by the end of December, 1969.

2.5 References

(1) Forbes, I. A., M. J. Driscoll, T. J. Thompson, I. Kaplan and D. D. Lanning, "Design, Construction and Evaluation of a Facility for the Simulation of Fast Reactor Blankets," MIT-4105-2, MITNE-110 (February, 1970).

3. BLANKET ASSEMBLY NO. 2

S. T. Brewer, I. A. Forbes, J. L. Klucar and T. Leung

3.1 Introduction

B. T. F. Blanket No. 2 is an accurate mockup of a typical LMFBR blanket composition. Subassembly boxes of low-carbon steel rectangular mechanical steel tubing are loaded with 121 uranium metal fuel rods arranged on a square lattice spacing of 0.511 in.; the 0.25-in.-diameter uranium metal fuel is clad in low-carbon steel tubing. The inter-rod volume in each subassembly is filled with anhydrous sodium chromate (Na_2CrO_4) powder. The subassembly boxes are loaded on an experimental cart to provide a blanket assembly which is 48 in. high, 59.2 in. wide and 17.72 in. thick. The blanket is backed by an 18-in.-thick low-carbon steel reflector.

The as-loaded atom densities for Blanket No. 2 are given in Table 3.2.

3.2 Description of Blanket No. 2 (J. L. Klucar and T. Leung)

3.2.1 General Description

Figure 3.1 shows a schematic view of Blanket Assembly No. 2. A 58-1/4 in. by 62-7/16 in. piece of 1-in.-thick mild steel plate welded between two 60 in. by 39 in. pieces of 1-in.-thick mild steel plate forms an "H" frame support structure which is mounted on an experimental cart. The front section of the "H" frame contains three rows of the blanket subassemblies, and the rear section is filled with seventeen 58-1/4 in. by 60 in. pieces of 1-in.-thick mild steel plate to act as a neutron reflector. Twenty-five of the subassemblies contain steel-clad uranium metal fuel rods and anhydrous sodium chromate powder. The outer subassemblies (see Fig. 3.1) are filled with the mixture of iron punchings and anhydrous borax ($Na_2B_4O_7$) powder used for Blanket Assembly No. 1 (see Section 2.4).

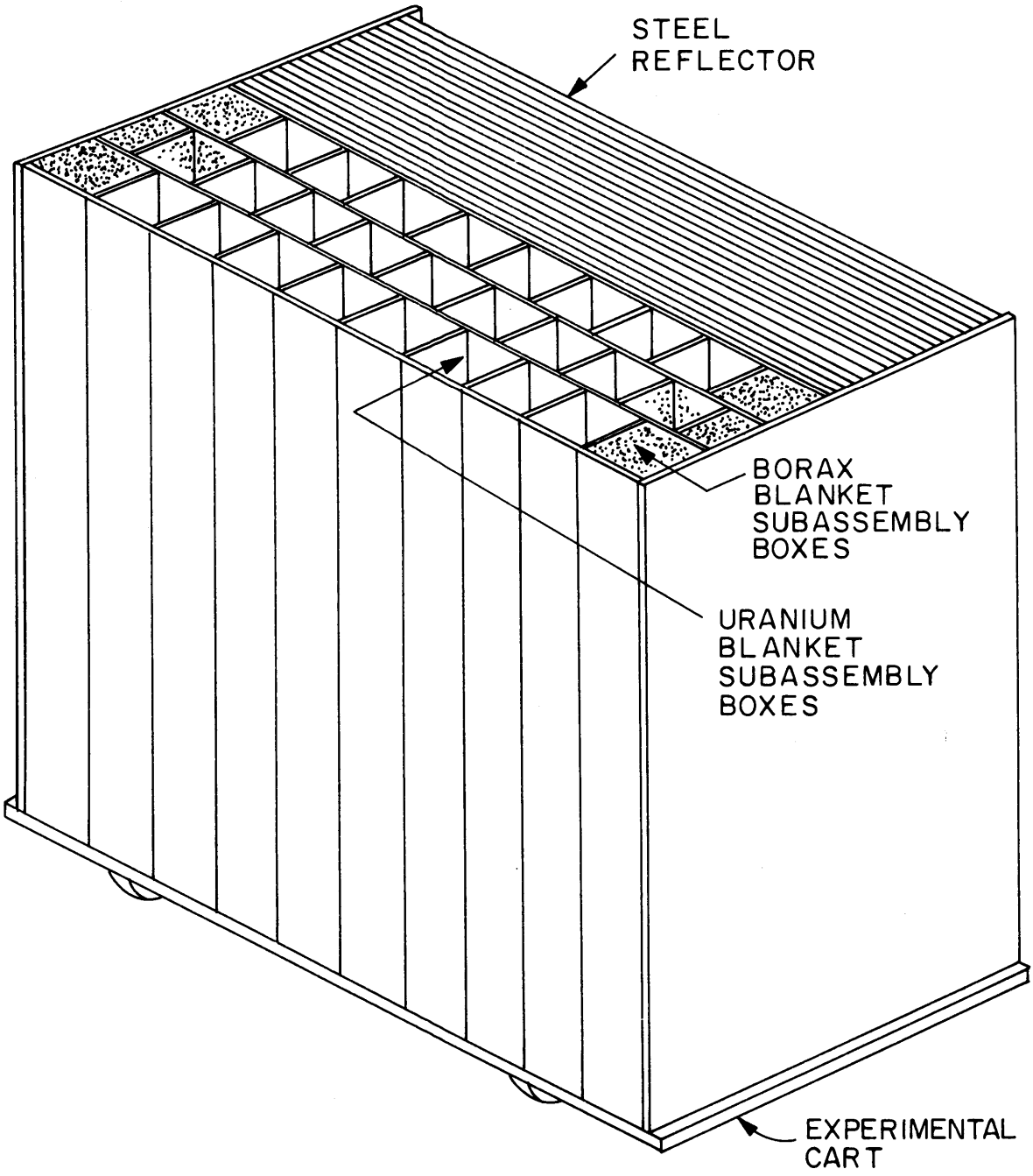

FIG. 3.1 SCHEMATIC VIEW OF BLANKET ASSEMBLY NO. 2

Twenty-six tubes are provided for foil activation traverses in the axial and transverse directions through the blanket (see Fig. 3.2). The 58-in.-long mild steel tubes have a 7/16 in. O. D. and a 0.028 in. wall thickness. A 1-in.-diameter hole, 4 in. below mid-plane, has been drilled through the reflector to provide a beam hole for fast neutron and prompt gamma spectrum measurements. In addition, a foil holder rod may be inserted in this hole for foil activation traverses through the reflector region.

3.2.2 Description of the Subassemblies

Figure 3.3 shows a schematic view of a typical subassembly. The low-carbon steel subassembly boxes are 5.92 in. square, 60 in. high and have a wall thickness of approximately 3/32 in. The bottom of each subassembly is sealed with a seam-welded steel plate. Each subassembly contains 121 fuel rods arranged in an eleven by eleven square lattice with a pitch of 0.511 in. Sixty of the rods have a U^{235} enrichment of 1.016%, and sixty-one have a U^{235} enrichment of 1.143%; the two enrichments are loaded in a checkerboard pattern within the subassembly box.

The fuel rods are held in place by upper and lower aluminum grid plates. The lower grid plate rests on the bottom closure plate, and the upper grid plate is supported on four 48-in.-long tubes which have an O. D. of 7/16 in. and a wall thickness of 0.028 in. These tubes fit over four fuel rods located near the corners of the lattice. The fuel rods are loaded through the upper grid down into the lower grid plate. The upper grid plate has cut-out sections for the traversing tubes (see Fig. 3.3) and for loading the sodium chromate powder; each tube normally contains a fuel rod unless a foil traverse is to be made.

A total of 3025 fuel rods have been fabricated at M. I. T. by recladding 48-in.-long by 0.250-in.-diameter uranium metal rods in low-carbon steel tubing. The clad tubing is 50 in. long, and has a 5/16-in. O. D. and an 0.018-in. wall thickness. Each end of the tube is closed by a press-fitted steel plug, 1/2 in. long and 9/32 in. in diameter.

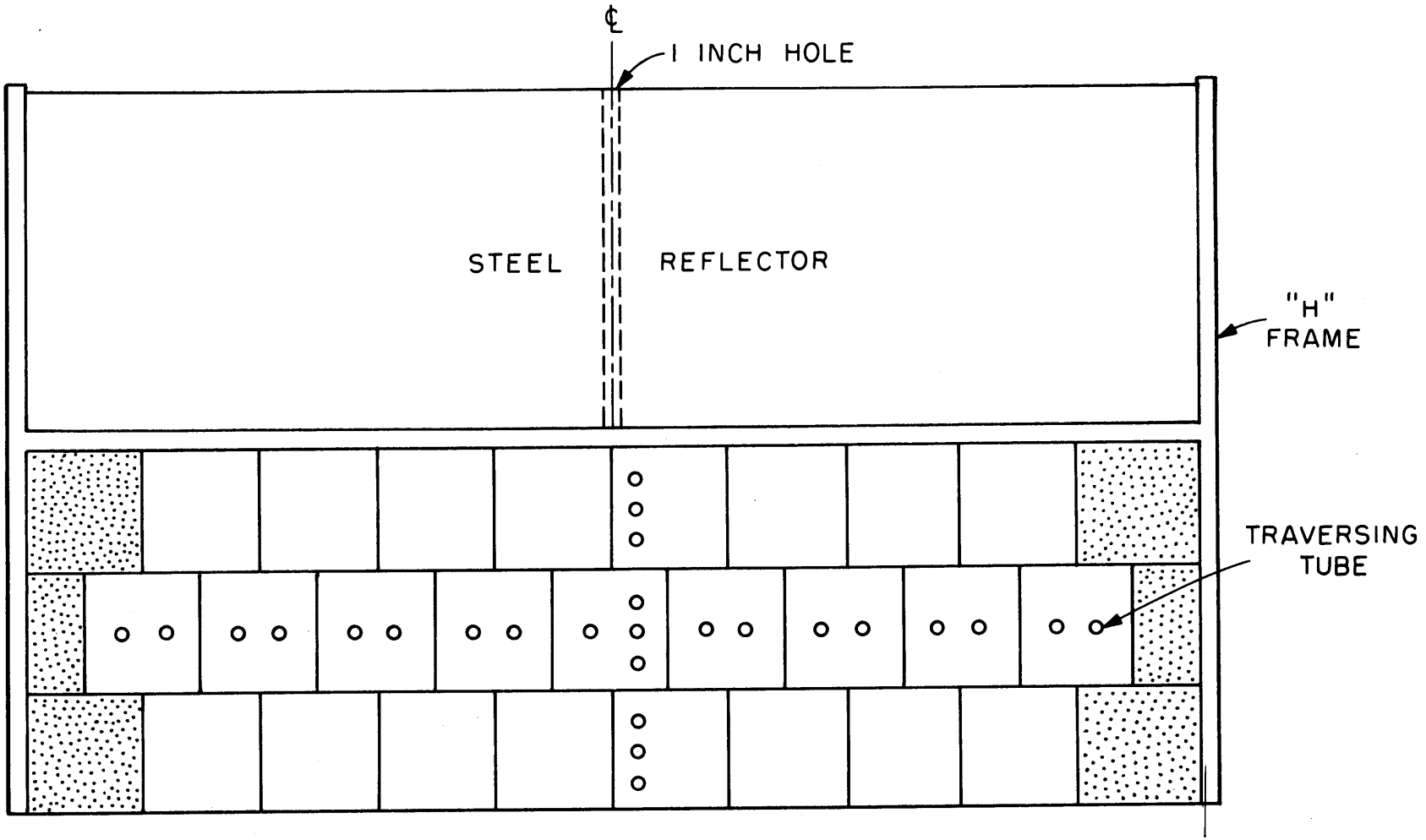

FIG. 3.2 PLAN VIEW OF BLANKET ASSEMBLY SHOWING THE TRAVERSING TUBE POSITIONS

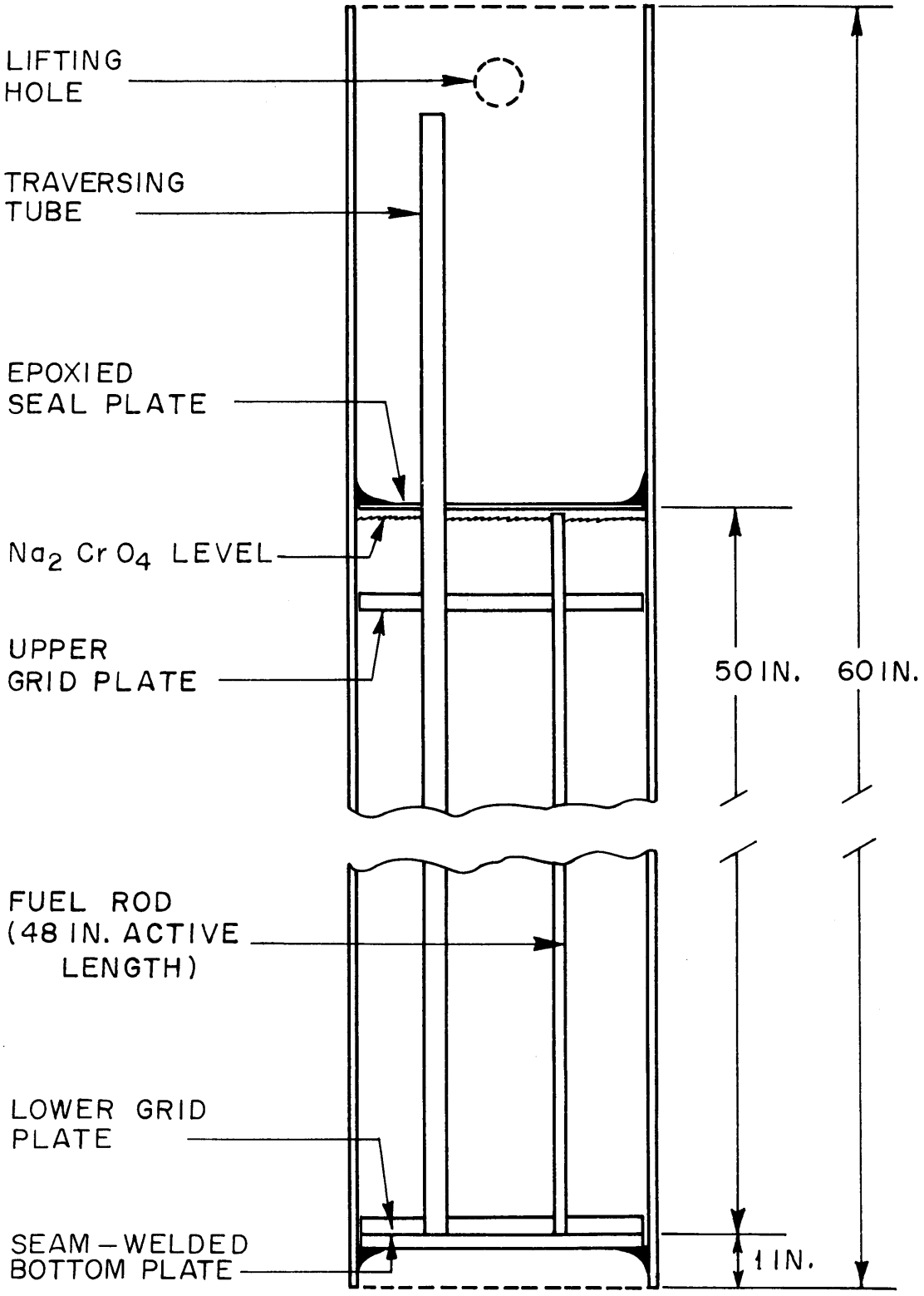

FIG. 3.3 SCHEMATIC CROSS SECTION VIEW OF BLANKET NO. 2 SUBASSEMBLY

The inter-rod volume of the subassemblies (see Fig. 3.4) is filled with anhydrous sodium chromate powder (technical grade) which has been dried and ground (see Section 3.3). The average loading of sodium chromate in a subassembly is 31.106 kg, with a standard deviation of ± 0.294 kg; the loadings vary from 30.51 kg to 31.80 kg, or ± 2% maximum deviation from the mean.

The top of each subassembly is sealed by a 0.035-in.-thick steel plate which is epoxied in place to ensure that the subassembly is air- and water-tight; the traversing tubes penetrate this plate.

A breakdown of the subassembly weight is given in Table 3.1.

TABLE 3.1
Subassembly Component Weights

Uranium metal	89.30 kg
Na_2CrO_4	31.11 kg
Cladding	13.00 kg
Subassembly box	26.55 kg
Grid plate support tubes	0.91 kg
Grid plates	0.36 kg
Total	161.23 kg

3.2.3 Atom Densities

The atom densities for Blanket No. 2 were calculated by homogenizing the material components of a subassembly at mid-height – viz. the uranium metal fuel, the anhydrous sodium chromate and the low-carbon steel cladding, support tubes and subassembly walls. The carbon content of the steel is about 0.15 w/o; other impurities, such as manganese and nickel, are negligible. The water content of the sodium chromate is 0.10 w/o.

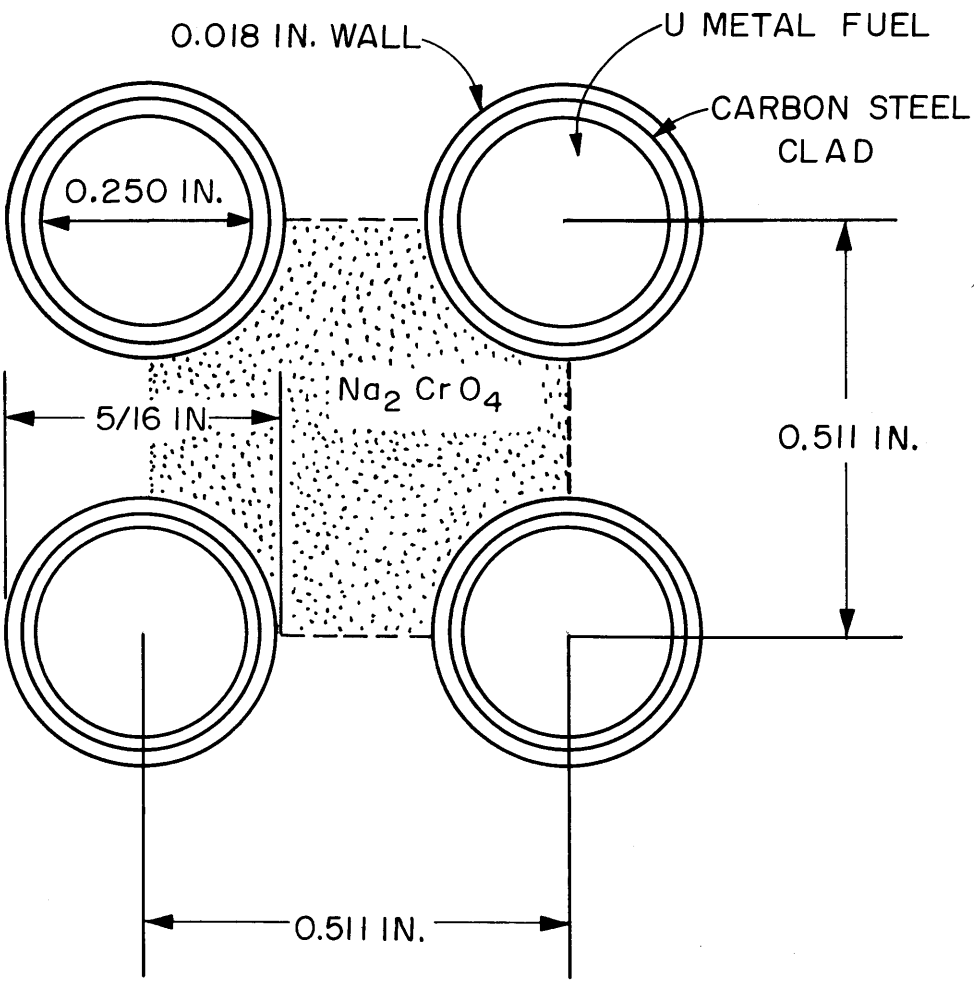

FIG. 3.4 BLANKET NO. 2 UNIT CELL

The homogenized atom densities in Blanket No. 2 are given in Table 3.2 where they are compared with the atom densities in an "equivalent realistic blanket," composed of 37.0 v/o depleted UO_2 (at 90% of theoretical density), 20.7 v/o Type 316 stainless steel (71.2 w/o Fe, 20.0 w/o Cr and 8.8 w/o Ni), 32 v/o sodium and 10.3 v/o void. It is evident that Blanket No. 2 provides a realistic blanket composition in all respects, with the exception of the small hydrogen content.

TABLE 3.2

Homogenized Atom Densities in B. T. F. Blanket No. 2

Nuclide	Blanket No. 2		Equivalent Realistic Blanket*	
U^{235}	0.000088		0.000016	
U^{238}	0.008108		0.008131	
O	0.016293		0.016293	
Na	0.008128		0.008128	
Cr	0.004064		0.003728	
Fe	0.013750	0.017814	0.012611	0.017814
Ni	0.000000		0.001475	
H	0.000073		0.000000	
C	0.000096		0.000082	

*Composed of 37.0 v/o depleted UO_2 (at 90% of theoretical density), 20.7 v/o Type 316 stainless steel, 32.0 v/o sodium and 10.3 v/o void.

3.3 Preparation of the Sodium Chromate (S. T. Brewer and J. L. Klucar)

Early in the construction of Blanket No. 2, a series of crucible drying experiments showed that the water content of the "anhydrous" sodium chromate, as delivered by the supplier, had a water content of about 0.8 w/o. Since the water content of the sodium chromate could

have a significant effect upon the spectrum in the blanket assembly (see Section 3.4), it was decided to reduce the water content to $\leq$ 0.1 w/o by drying.

3.3.1 Drying and Loading Sodium Chromate

Since sodium chromate has a low dehydration temperature (about 300° F), a simple oven drying procedure was developed. A 5-kg sample of sodium chromate heated at 400° F for 4 hours in a domestic electric oven was shown to be reduced in weight by about 0.75%. No further weight reduction was observed after 2 hours additional heating.

In each drying "run," five cans, each containing about 5 kg of sodium chromate, were baked for 8 hours. Each can of chromate was weighed before and after baking. In addition, a sample from every tenth can was "crucible-dried"; the results of the crucible drying confirmed the gross weight reduction observed in the 5-kg batches. After baking, the cans were sealed and stored in a dry atmosphere. Several cans were monitored, and no water pickup was noted during the storage period.

Since the bake-dried sodium chromate was hard and crusty, it was impossible to load it directly into the subassemblies. To reduce the dried chromate to a uniform fine powder again, a used commercial coffee grinder was purchased. The chromate was ground and stored in sealed cans. Crucible drying tests showed no significant water pickup during the grinding operation. It was found necessary to wear respirators and protective clothing when handling sodium chromate powder because of its dermatologically irritating nature.

Finally, the dried and ground sodium chromate was loaded into the subassemblies. The cans were weighed before and after the loading. The chromate was mildly vibration-compacted during the loading to ensure a uniform fill. The excellent uniformity of loading achieved by this procedure has already been noted.

3.3.2 Hydrogen Content of the Sodium Chromate

The hydrogen content of the sodium chromate was measured by two methods:

(a) prompt activation analysis;

(b) crucible drying.

Method (a) consisted of comparing the intensity of the 2.223-Mev hydrogen prompt capture gamma line of a sample of sodium chromate against that of a standard sample containing a known amount of hydrogen. Method (b) consisted of heating a sample of sodium chromate to the melting point in a crucible, cooling in a dry atmosphere, and measuring the weight loss.

The water content of the sodium chromate delivered by the supplier was determined to be 0.83 ± 0.04 w/o from the crucible drying tests and 0.77 ± 0.12 w/o (water-equivalent) from the prompt activation analysis. Samples from the dried sodium chromate loaded into the blanket subassemblies were determined to have a mean water content of 0.10 ± 0.02 w/o by the crucible drying method; prompt activation analysis confirmed that the content was ≤ 0.1 w/o.

Measurements of the pH of a solution of the sodium chromate in water confirmed that the NaOH content of the sodium chromate is negligible. Since this is the only other hydrogen-containing impurity in technical grade sodium chromate, and because prompt activation analysis identifies all hydrogen regardless of chemical form, it was concluded that the 0.10 w/o water content was a reliable figure for the final contamination level of Blanket No. 2.

3.4 The Effect of Trace Amounts of Hydrogen on the B. T. F. Spectrum (I. A. Forbes)

3.4.1 The Effect of Hydrogen in the Sodium Chromate

Excessive water content of the sodium chromate in Blanket No. 2 can have a significant effect on the spectrum in the blanket, and therefore on the foil activities measured in the axial direction in the blanket (equivalent to the radial direction in an LMFBR).

The ANISN code was used to make 16-group, 1-D, S_8 calculations of the U^{238} (n, γ) capture rate and U^{238} (n, f) fission rate through the blanket and steel reflector of Blanket No. 2. The U^{238} capture

(a typical capture reaction) and U^{238} fission (a typical threshold reaction) rates were calculated for chromate water contents of 0.0 w/o, 0.1 w/o, 0.2 w/o and 0.5 w/o. Figure 3.5 shows, for a given sodium chromate water content, the amount by which the U^{238} capture and fission rates through Blanket No. 2 differ from the zero water content case. It is seen that the error in the capture and fission rates due to the hydrogen content of the chromate is reduced to about the limit of precision in the experimental determination of the activities only when the water content of the sodium chromate is 0.1 w/o or less. It is likewise clear that commercial "anhydrous" chromate would be totally unacceptable.

The curves for 0.10 w/o water content could, in fact, be used to correct axial foil activation measurements for the hydrogen content of Blanket No. 2.

3.4.2 The Effect of Hydrogen in the Converter Assembly Graphite

Since the contamination of graphite by H_2O has been cited as a problem in fast critical assembly research[1, 2], the ANISN code was used to evaluate the effect of the estimated 300 ppm by weight of hydrogen in the converter assembly's graphite external moderator region. Calculations with and without this amount of hydrogen in the graphite showed that it had no discernible effect on the blanket spectrum.

3.5 Conclusions

An accurate and relatively inexpensive mockup of a typical LMFBR blanket has been provided by loading uranium metal fuel, clad in low-carbon steel, and anhydrous sodium chromate powder into 6-in.-square low-carbon steel subassembly boxes. This blanket assembly is closely equivalent to an LMFBR blanket containing 38.3 v/o depleted UO^2, 20.8 v/o Type 316 stainless steel, 32.0 v/o sodium and 8.9 v/o void in all important respects. The commercially-supplied sodium chromate was bake-dried to reduce its water content to 0.10 w/o before loading. ANISN calculations showed that the

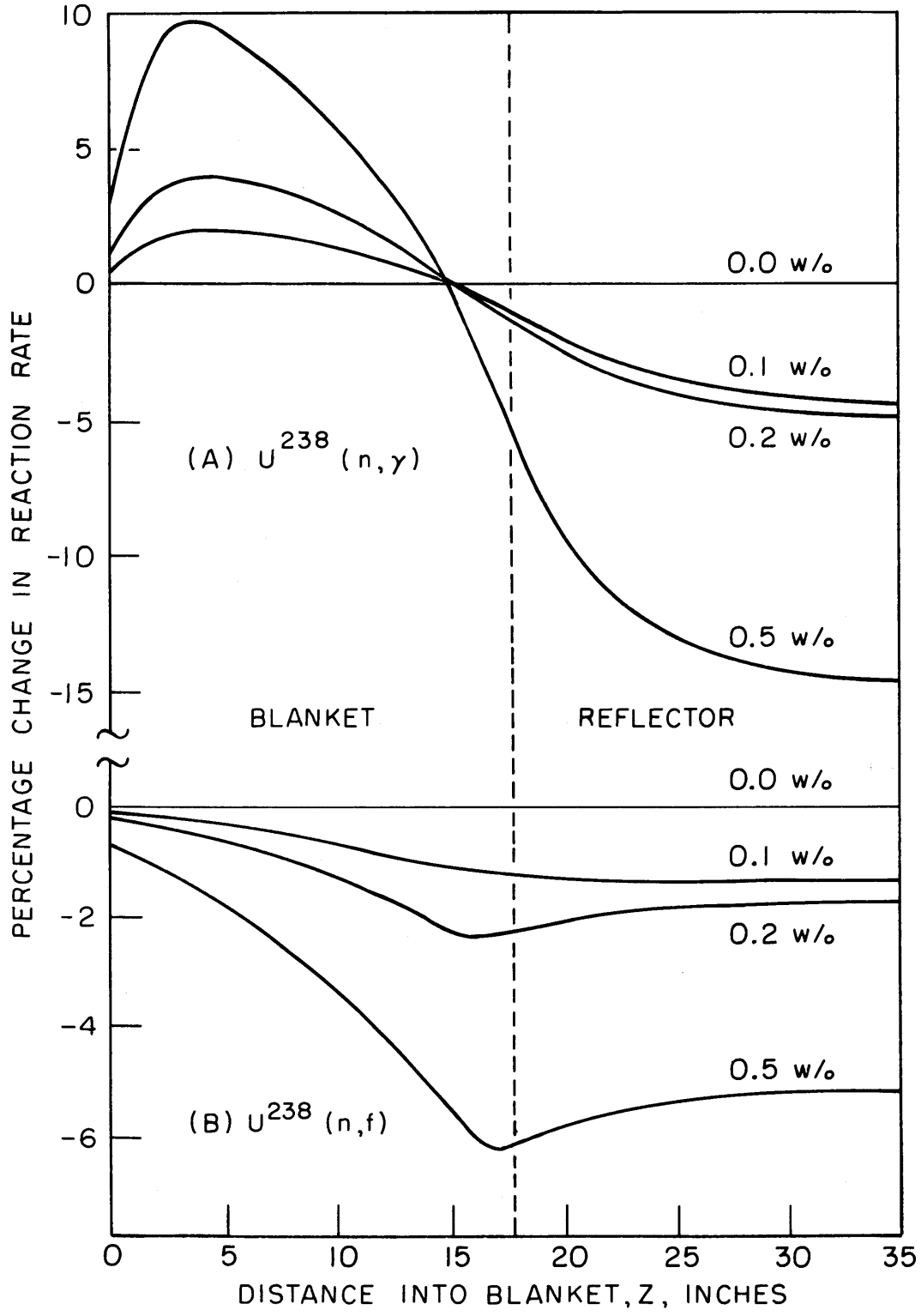

FIG. 3.5 PERCENTAGE ERROR IN REACTION RATES IN BLANKET NO.2 AS A FUNCTION OF THE SODIUM CROMATE WATER CONTENT

errors in measured foil activities in Blanket No. 2 due to the hydrogen content are reduced to acceptable levels only when the water content of the sodium chromate is reduced to 0.10 w/o.

3.6 References

(1) Levine, M.M., "Report from Atomic Energy Establishment, Winfrith," issued by B.N.L. (February, 1970).

(2) Palmedo, P.F., H. Ludewig and A.L. Aronson, "Effect of Hydrogen Content of Graphite in Fast Critical Experiments," A.N.S. Trans., Vol. 13, No. 1, p. 253 (June, 1970).

4. FOIL ACTIVATION MEASUREMENTS

T. Leung

4.1 Introduction

Foil activation measurements are being made in Blanket No. 2 for the purpose of providing detailed reaction rate data through the blanket and steel reflector.

Transverse foil activation traverses to establish that transverse spectral equilibrium exists in Blanket No. 2, and to measure the transverse buckling, have been completed. Activation traverses in the axial direction through the blanket and reflector are currently being made to determine the axial activation rates for Au, In, Mo, U^{238} capture and fission, and Pu^{239} and U^{235} fission; Fe, Ni, Cr and Na capture rates will also be measured to the extent possible.

Measurements to date have been made with gold, indium and molybdenum foils. 16-group cross sections for the $Au^{197}(n, \gamma) Au^{198}$ and $In^{115}(n, n') In^{115m}$ reactions are given in Table 4.1; they were obtained by collapsing the 620-group activation cross sections of the SAND-II[1] library over a typical LMFBR core spectrum. The $Au^{197}(n, \gamma) Au^{198}$ reaction has a sufficiently high cross section over the entire energy range to act as a neutron detector over the whole energy spectrum; it is also particularly sensitive to thermal or epithermal contamination of the blanket spectrum. The $In^{115}(n, n') In^{115m}$ reaction has a 400-keV threshold and is a suitable detector of high energy neutron behavior. The $Mo^{98}(n, \gamma) Mo^{99}$ reaction has a very small cross section above about 1 keV, but has a relatively large cross section below this energy; it is a suitable indicator of the behavior of neutrons in the upper eV range.

TABLE 4.1

16-Group Activation Cross Sections for Gold and Indium

Group	E_L	Activation Cross Sections, barns	
		$Au^{197}(n, \gamma)Au^{198}$	$In^{115}(n, n')In^{115m}$
1	3.5 MeV	0.0215	0.341
2	1.4 "	0.0586	0.275
3	0.9 "	0.0974	0.0960
4	0.4 "	0.141	0.0161
5	100 keV	0.287	0.00032
6	17 "	0.630	0.0
7	3 "	1.59	0.0
8	0.55 "	6.02	0.0
9	100 eV	11.8	0.0
10	30 "	23.2	0.0
11	10 "	7.02	0.0
12	3 "	700	0.0
13	1 "	35.4	0.0
14	0.4 "	23.8	0.0
15	0.1 "	43.2	0.0
16	Thermal	92.3	0.0

4.2 Transverse Foil Activation Measurements

4.2.1 Experimental Procedure

The size and weight of the gold, indium and molybdenum foils are listed in Table 4.2. The foils were taped into recessed spots milled in 5/16-in.-diameter low-carbon steel foil holder rods. The foil

TABLE 4.2

Description of Foil Materials

Foil Material	Reaction	Diameter	Thickness	Weight	Half Life of Radioactive Isotope
Gold	$Au^{197}(n, \gamma)Au^{198}$	1/8 inch	10 mil	0.038 gm	64.8 hours
Indium	$In^{115}(n, n')In^{115m}$	1/4 inch	10 mil	0.060 gm	4.5 hours
Molybdenum	$Mo^{98}(n, \gamma)Mo^{99}$	1/8 inch	25 mil	0.057 gm	66 hours

holders were inserted into the 3/8-in. I. D. traversing tubes in the blanket subassemblies (see Fig. 3.2) prior to irradiation. Figure 4.1 shows a schematic view of the foil irradiation positions in the blanket assembly. Typical irradiation time for the foils was between four and ten hours.

Following irradiation, the foils were removed from the blanket and counted.

The activity of the gold foils was recorded by an automatic counting and sample-changing system, using standard techniques. A thalium-activated sodium iodide crystal was used for counting the 412-keV principal photopeak (and also the higher energy photopeaks) of Au^{198}. The baseline discriminator was set at the lowest point in the spectrum below the photopeak at about 300 keV.

The molybdenum foils were counted individually. A well-type, thalium-activated sodium iodide crystal was used for counting the 780-keV photopeak of Mo^{99}. A single-channel analyzer was used to straddle the peak; the channel width was approximately 130 keV.

Detection of the $In^{115}(n, n')In^{115m}$ reaction is complicated by the competing $In^{115}(n, \gamma)In^{116}$ capture reaction. The In^{116} activity consists of gamma rays with energies greater than the 335-keV gamma rays from the In^{115m} activity, so that there can be Compton-effect counts from In^{116} activity underneath the 335-keV photopeak. The resonance integral for the capture reaction is about 2640 barns; as a result, the 54-min half-life In^{116} activity may not be negligible even a few hours after the end of the irradiation. To minimize this effect, the counting of the 4.5-hour half-life In^{115m} activity was begun at least 8 hours after the end of irradiation.

The indium foils were counted in the same counting system as the molybdenum foils. A single-channel analyzer was used to straddle the 335-keV photopeak of In^{115m}; the channel width was approximately 120 keV.

After counting, the raw data were corrected for decay, background and deadtime, and reduced to relative activity per milligram of foil at the end of irradiation.

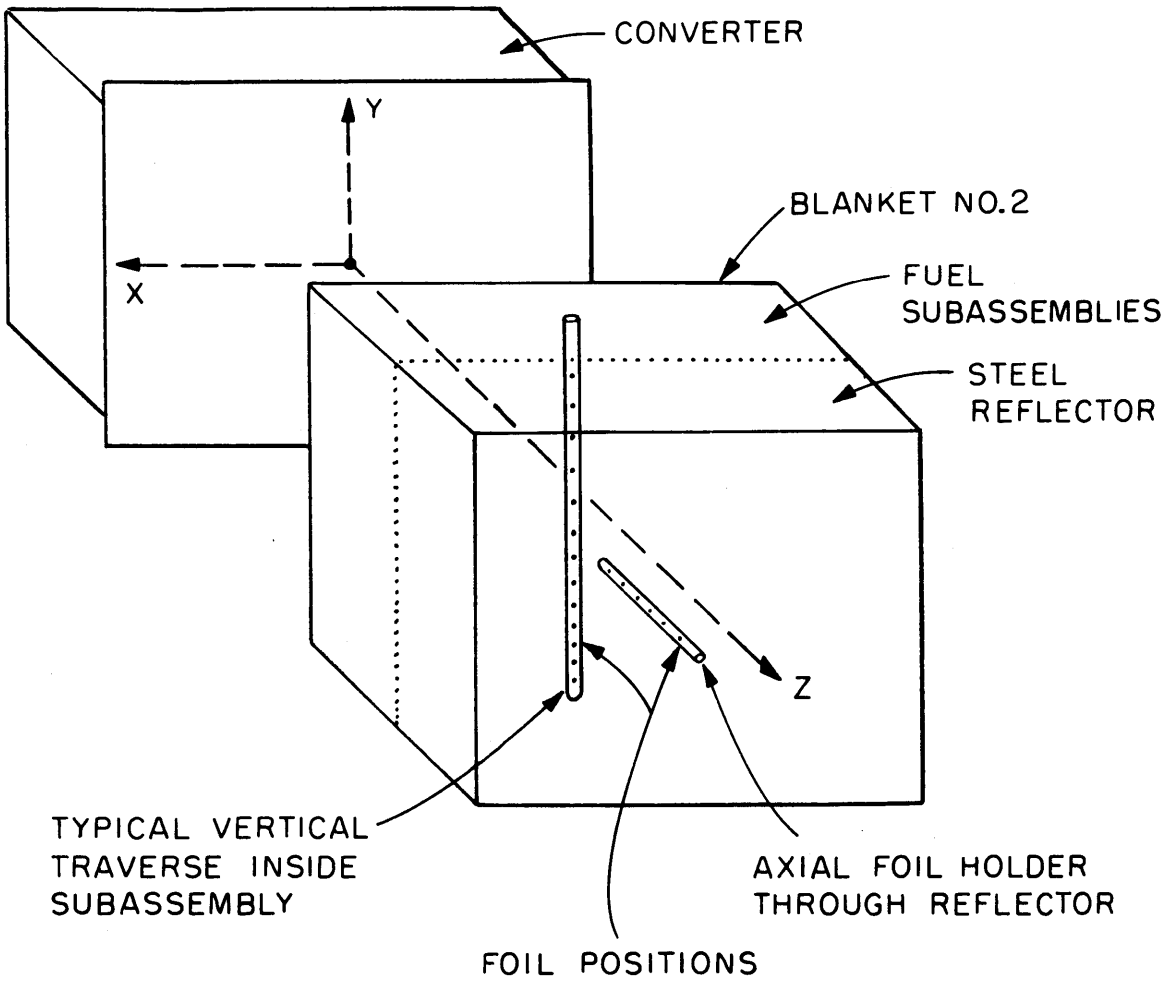

FIG. 4.1 SCHEMATIC VIEW OF THE CONVERTER AND BLANKET ASSEMBLY SHOWING THE FOIL IRRADIATION POSITIONS

4.2.2 Vertical Traverses

Vertical (Y-direction) activation traverses were made with gold, indium and molybdenum foils at various depths into the blanket. The vertical traverses were made 1.5 in. off the horizontal centerline (X = -1.5 in.) (see Fig. 4.1 for the coordinate system used).

Figure 4.2 shows the vertical activation traverses for gold, and Figure 4.3 shows the vertical activation traverses for indium and molybdenum. The standard deviation in the foil activities is smaller than the diameter of the experimental points in the figures. The fitted cosine curves were obtained by the least-squares method over all the experimental points. It is seen that all the gold, indium and molybdenum vertical activation traverses are well approximated by the relation,

$$A(Y) = A(0) \cos\left(\frac{\pi Y}{60}\right),$$

where A is the foil activity and Y is in inches.

Figure 4.4 shows the vertical gold-to-indium, indium-to-molybdenum and gold-to-molybdenum activation ratios at various depths into the blanket. It is seen that the activation ratios are constant from X = -15 in. to X = + 15 in., indicating that vertical spectral equilibrium is reached over a central region of the blanket about 2-1/2 ft. in height. As expected, these activation ratios are a function of the depth (Z-direction) into the blanket. The increase in the gold-to-indium activation ratio and the decrease in the indium-to-molybdenum and gold-to-molybdenum activation ratios with increasing depth into the blanket indicate the softening of the neutron spectrum.

4.2.3 Horizontal Traverses

Horizontal (X-direction) activation traverses were made with gold, indium and molybdenum foils at two distances into the blanket, Z = 0 (converter-blanket interface) and Z = 8.88 in. The horizontal traverses were made 3.0 in. above and below the vertical centerline (Y = +3.0 in. and Y = - 3.0 in.).

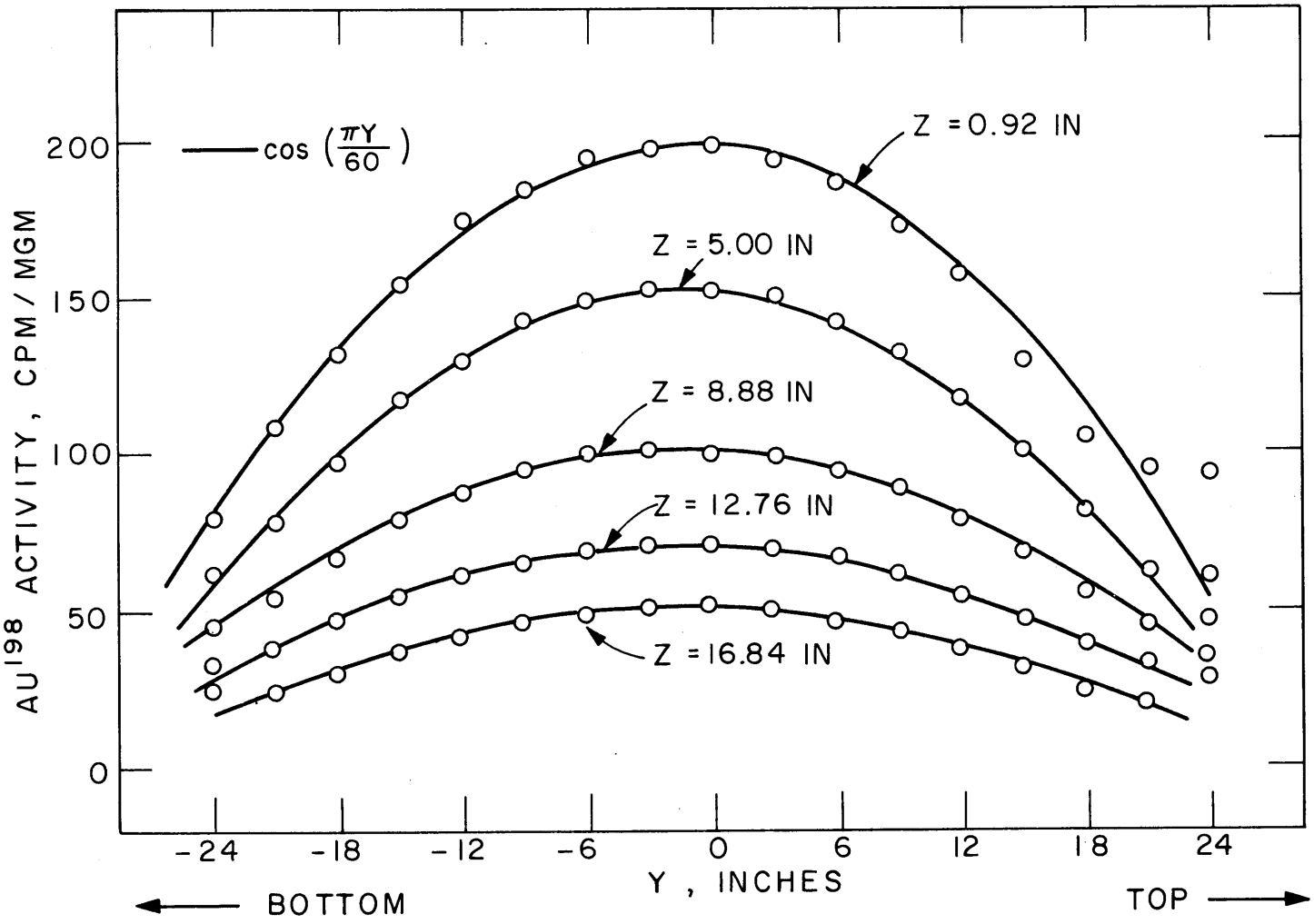

FIG. 4.2 GOLD VERTICAL ACTIVATION TRAVERSES IN BLANKET NO. 2

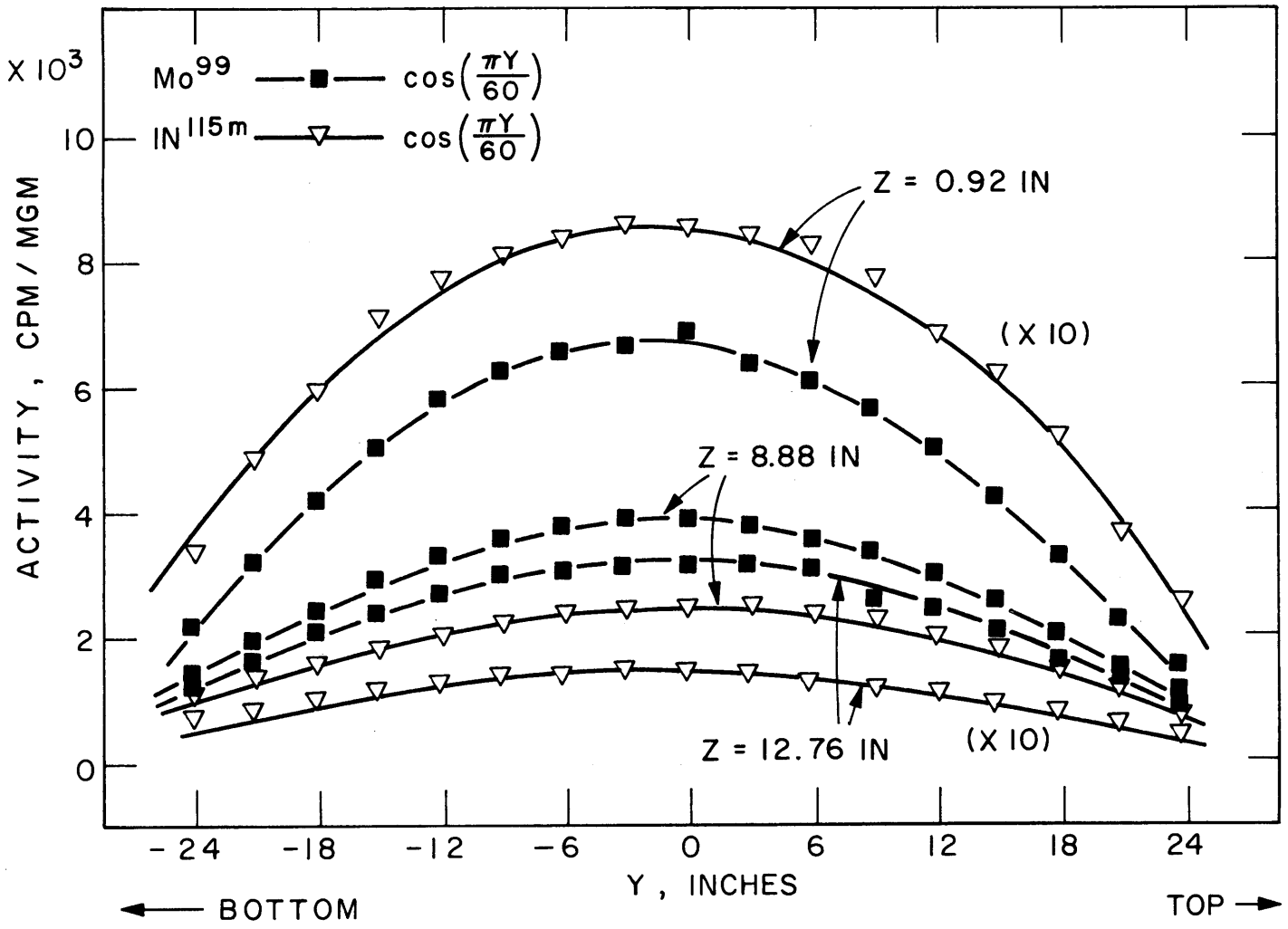

FIG. 4.3 VERTICAL ACTIVATION TRAVERSES IN BLANKET NO.2

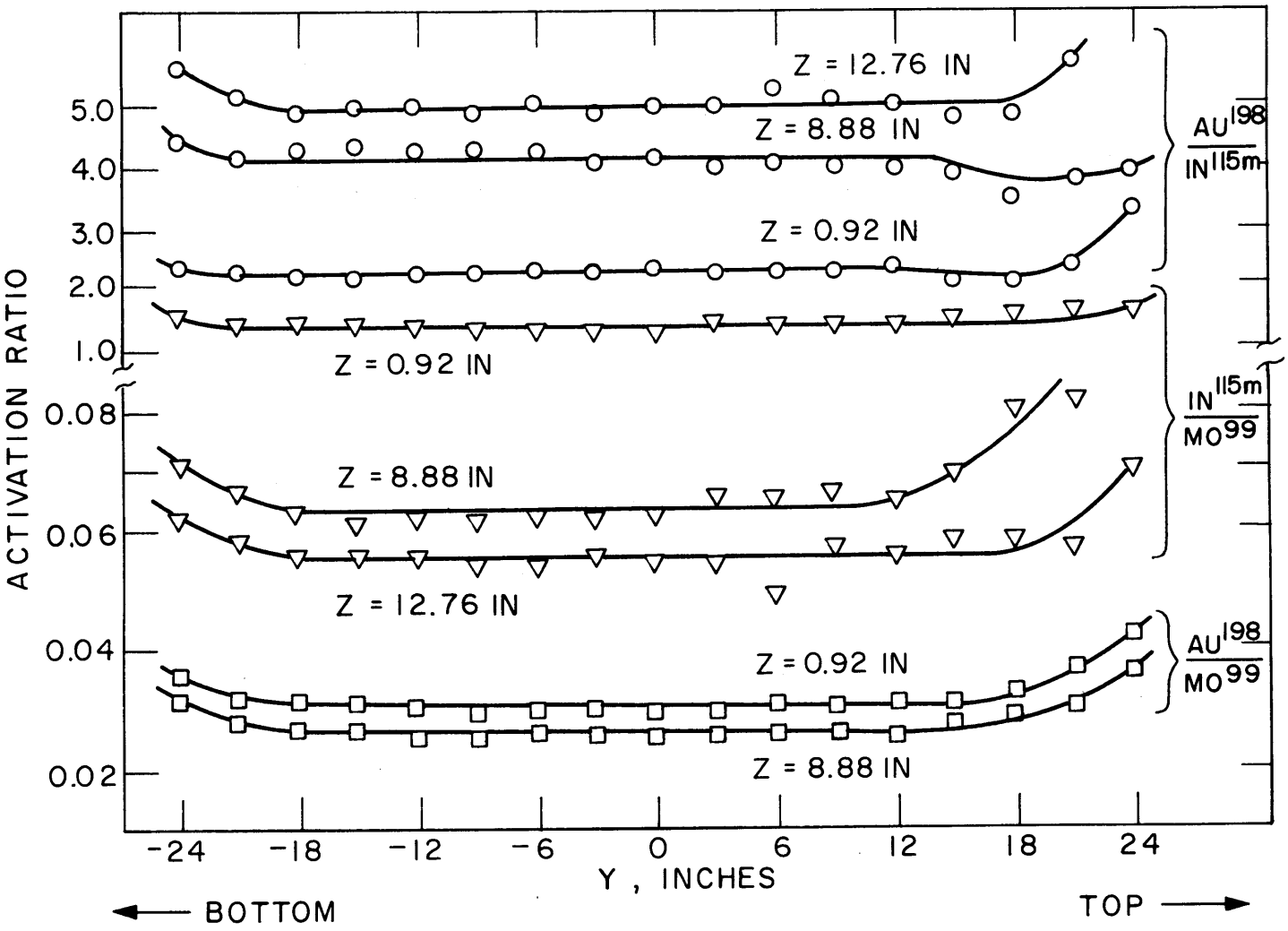

FIG. 4.4 VERTICAL ACTIVATION RATIOS IN BLANKET NO. 2

Figure 4.5 shows the horizontal activation traverses for gold, and Figure 4.6 shows the horizontal activation traverses for indium and molybdenum. Again, the standard deviation in the foil activities is smaller than the diameter of the experimental points, and the fitted cosine curves were obtained by least-squares fit over all the experimental data. It is seen that all the gold, indium and molybdenum horizontal activation traverses are well approximated by the relation,

$$A(X) = A(0) \cos\left(\frac{\pi X}{74}\right),$$

where A is the foil activity and X is in inches.

Figure 4.7 shows the horizontal gold-to-indium, indium-to-molybdenum and gold-to-molybdenum activation ratios at Z = 0 and Z = 8.8 inches. It is seen that the activation ratios are constant from Y = -15 inches to Y = +15 inches, indicating that horizontal spectral equilibrium is reached over a central region of the blanket about 2-1/2 feet wide.

4.3 Axial Activation Traverses

Axial (Z-direction) activation traverses are currently being made in Blanket No. 2. The axial traverses in the blanket are made in the same traversing tubes as were used for the horizontal and vertical traverses. The axial traverses through the low-carbon steel reflector are made by taping the foils into recessed spots milled in a 31/32 inch-diameter, low-carbon steel bar; the bar is inserted into the 1 inch-diameter hole drilled through the steel reflector (see Fig. 3.2) for irradiation.

Figure 4.8 shows axial activation traverses for gold and indium; the standard deviation in the foil activities is smaller than the diameter of the experimental points. The solid lines are the results of 16-group, 1-D, S_8 calculations with the ANISN code; the activation cross sections given in Table 4.1 were used. These are preliminary results only, and further measurements and improved multigroup calculations (using better cross section data, especially for iron) will be made.

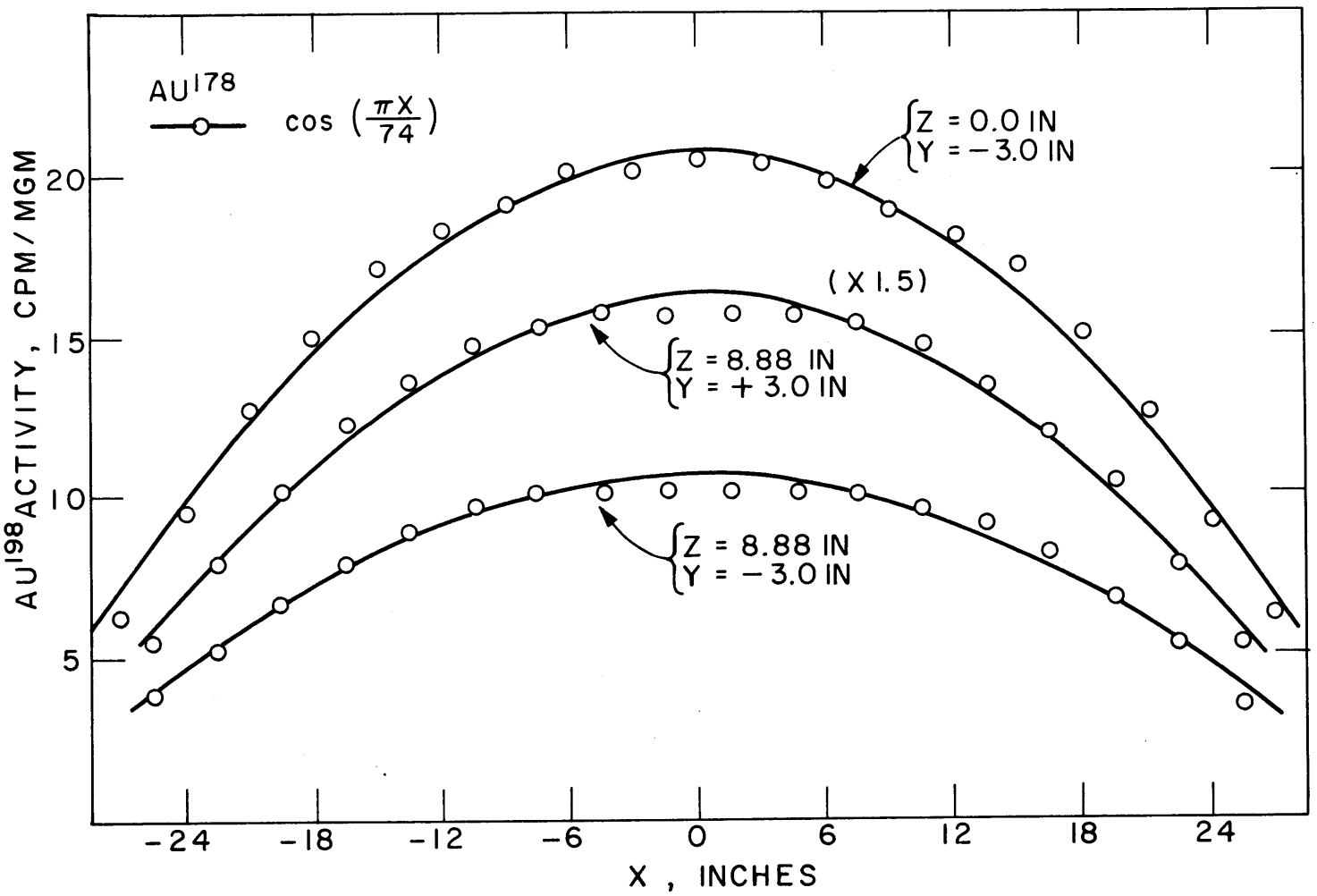

FIG. 4.5 GOLD HORIZONTAL ACTIVATION TRAVERSES IN BLANKET NO. 2

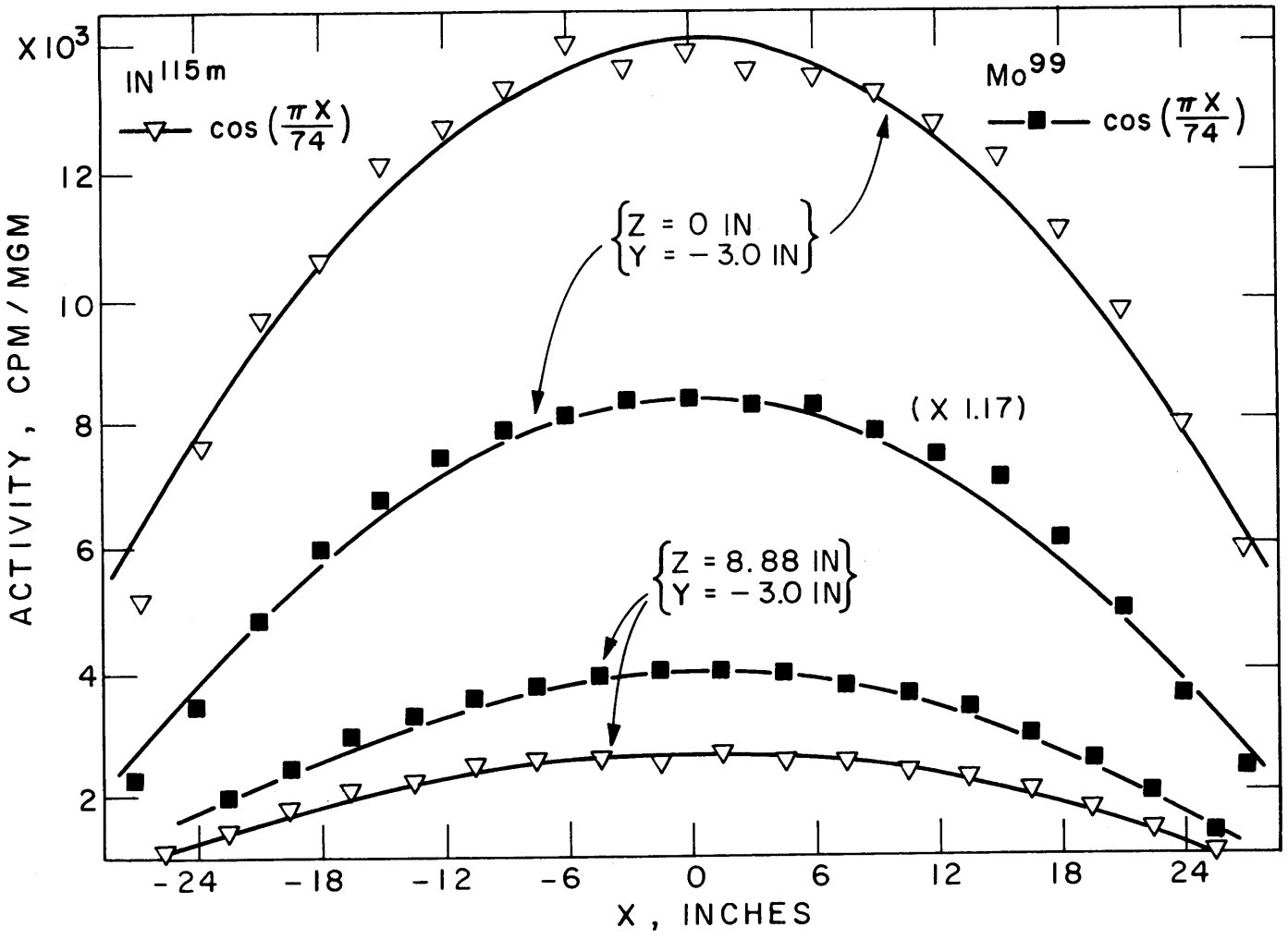

FIG. 4.6 HORIZONTAL ACTIVATION TRAVERSES IN BLANKET NO. 2

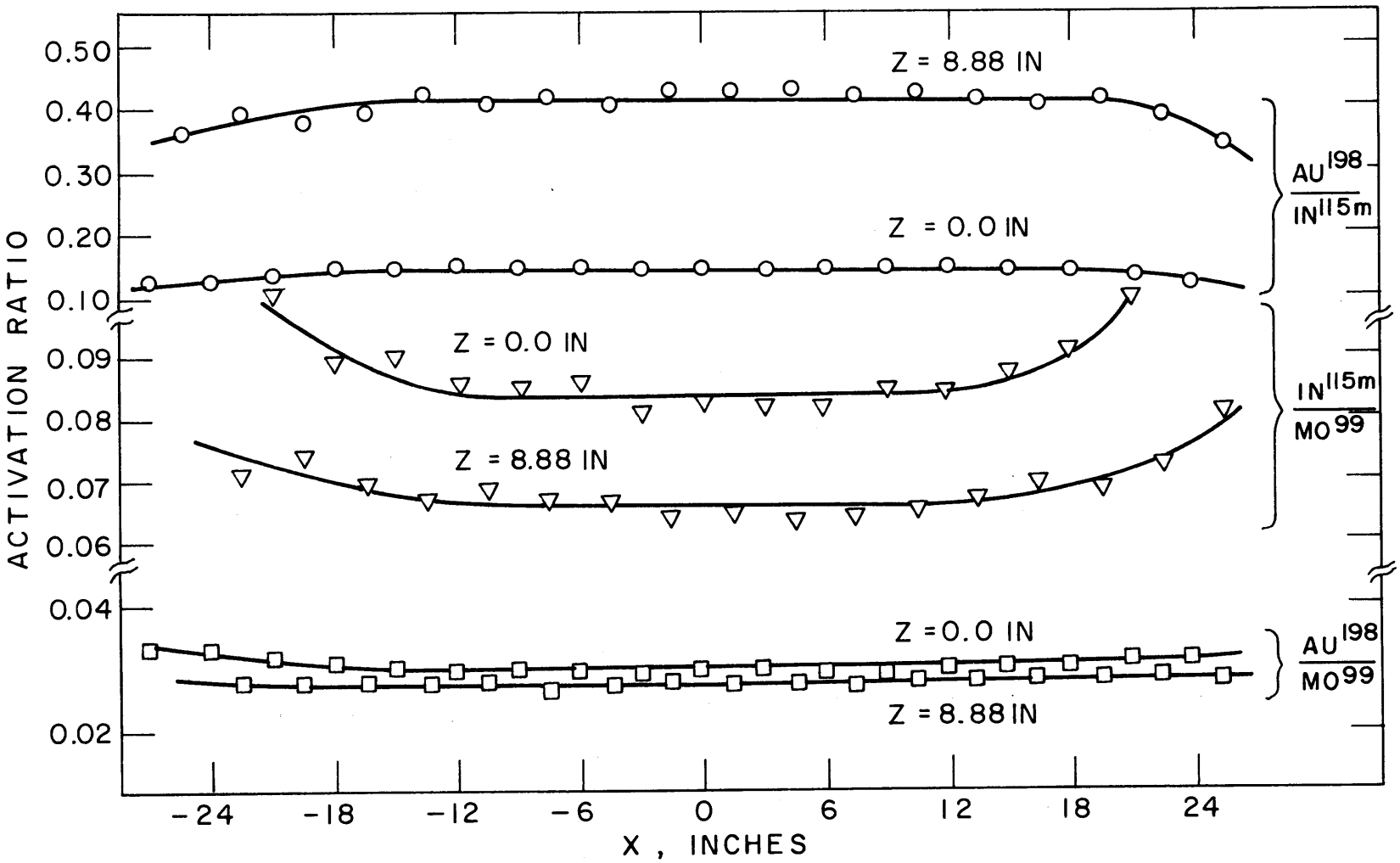

FIG. 4.7 HORIZONTAL ACTIVATION RATIOS IN BLANKET NO. 2

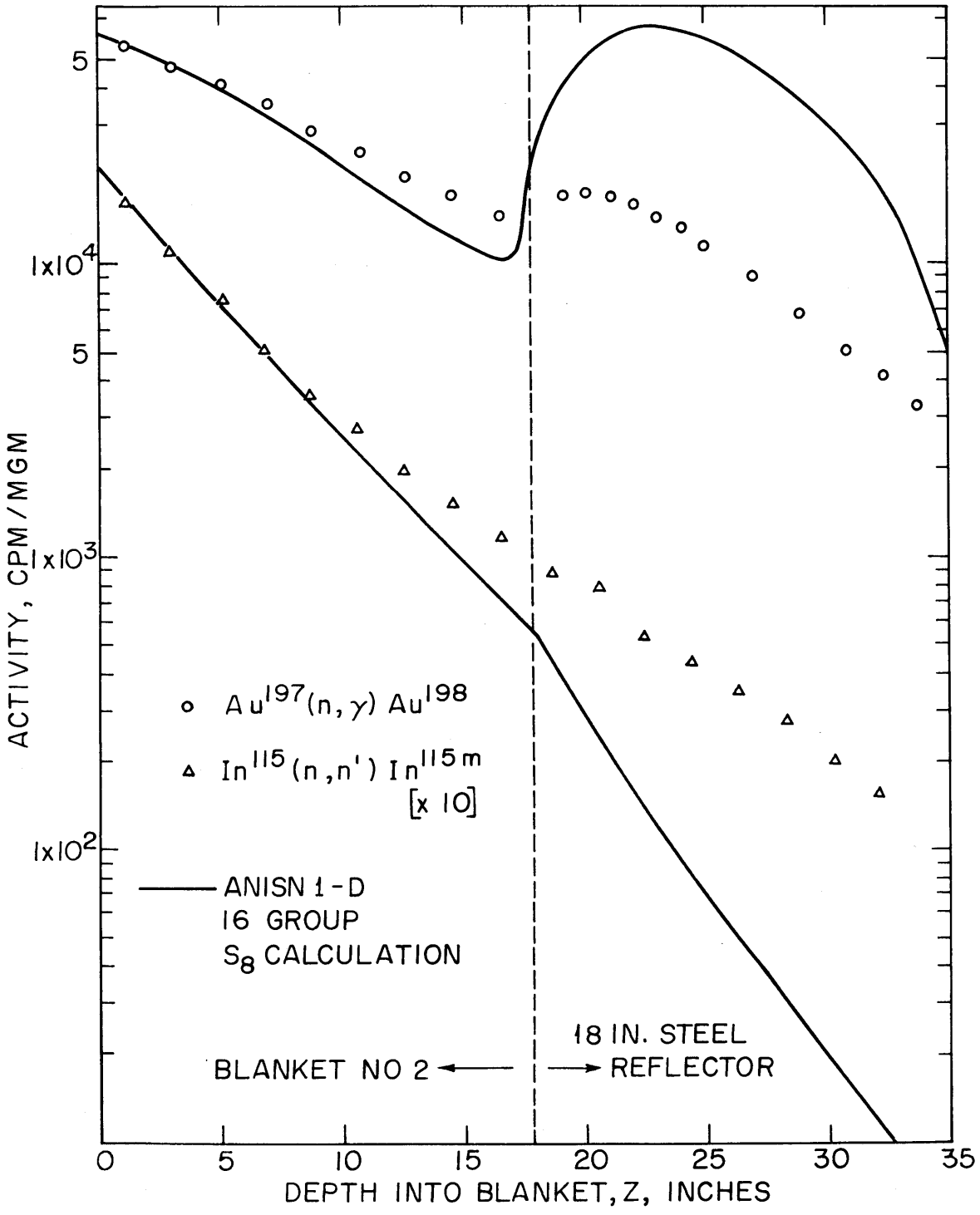

FIG. 4.8 AXIAL ACTIVATION TRAVERSES IN BLANKET NO.2

Measurements of the axial activation rates for U^{238} capture and fission, and Pu^{239} and U^{235} fission will be made; also Fe, Ni, Cr and Na capture rates to the extent possible.

4.4 Conclusions

The horizontal and vertical activation traverses with gold, indium and molybdenum foils in Blanket No. 2 show that the horizontal and vertical spatial distributions of the neutron flux in the blanket assembly have the desired cosine dependence; furthermore, these cosine distributions have constant width and height through the thickness of the blanket. Hence the neutron flux in Blanket No. 2 can be described by the relation,

$$\phi(X, Y, Z, E) = \cos\left(\frac{\pi X}{74}\right) \cos\left(\frac{\pi Y}{60}\right) \phi(Z, E) ,$$

and the transverse leakage from the assembly can be accounted for by means of a simple buckling term in numerical calculations. The transverse buckling is given by the relation,

$$B^2 = \left(\frac{\pi}{H}\right)^2 + \left(\frac{\pi}{A}\right)^2 ,$$

where H and A are the effective height and width, respectively, of the neutron flux distribution in the blanket. Numerically,

$$H = 60 \pm 1.5 \text{ in.} = 152.4 \pm 3.8 \text{ cm} ,$$

$$A = 74 \pm 1.5 \text{ in.} = 188.0 \pm 3.8 \text{ cm} ,$$

and $$B^2 = 0.000704 \pm 0.000024 \text{ cm}^{-2} .$$

Since transverse leakage from the blanket assembly accounts for only about 16% of the total blanket neutron balance (about 9.6% vertically and 6.4% horizontally), the ± 3.4% uncertainty in the transverse buckling will contribute an uncertainty of only ± 0.54% to the blanket neutron balance.

The experimental foil activation ratios show clearly that transverse spectral equilibrium is attained in a large (approximately 2-1/2 feet square) central region of Blanket No. 2. The activation ratios also indicate the softening of the neutron spectrum with increasing

axial (Z-direction) depth into the blanket.

The gold and indium axial activation traverses also confirm the expected axial spectral softening. Future work involving foil activation measurements in Blanket No. 2 will concentrate on the axial activation traverses.

4.5 References

(1) McElroy, W.N. et al., "A Computer-Automated Iterative Method for Neutron Flux Spectra Determination by Foil Activation," AFWL-TR-67-41 (August, 1967).

5. INSTRUMENTAL NEUTRON SPECTRUM MEASUREMENTS

N. R. Ortiz

5.1 Introduction

Over the past twenty years, considerable effort has been made to develop spectrometers capable of measuring neutron energies from a few kilovolts through a few MeV. Spectrometry in this region is desired to provide physics data essential for the design and analysis of fast reactors.

As part of the LMFBR Blanket Physics Project program at M.I.T., the fast neutron spectrum in the blanket assemblies will be measured at selected locations in the blanket. The instrumental methods to be used for this are:

(a) LiI crystal -- for the MeV region;

(b) He^3 spectrometer -- capable of neutron spectrum measurements down to about 100 keV;

(c) proton recoil spectrometer -- capable of neutron spectrum measurements down to the low keV region.

The work to date has been concentrated on measurements with the He^3 detector, but measurements are planned using the proton recoil spectrometer and the LiI crystal.

5.2 Measurements with the He^3 Spectrometer

5.2.1 Description of the He^3 System

The He^3 system consists of two silicon semiconductor detectors in a sandwich configuration; the space between the two detectors is filled with He^3 gas. A small tank of He^3 gas is provided to fill the detector to the desired operating pressure. The absorption of a neutron by a He^3 nucleus will result in the emission of a triton and a proton according to the reaction,

$$_2He^3 + _0n^1 \rightarrow {}_1H^3 + {}_1H^1 + 764 \text{ keV}.$$

If the triton and the proton are each absorbed in a semiconductor detector (as determined by a coincidence unit), and the signals from the two detectors are added, the total energy of the reaction is obtained. A block diagram of the system is shown in Fig. 5.1.

The advantages of the He^3 spectrometer[1] are:

(a) the $He^3(n, p)$ reaction cross section starts with a large value for thermal neutrons and varies smoothly with energy, having no known resonances;

(b) there are no excited daughter products, so that the reaction products, the triton and the proton, contain the entire energy of the reaction.

The disadvantages of the He^3 spectrometer are:

(a) the competing effect of elastic scattering of neutrons by He^3;

(b) the high Q value makes the measurement of neutron energies below about 100 keV difficult.

5.2.2 Energy Calibration and Response Function

The energy calibration of the multichannel analyzer was made using the thermal neutron source from port 2CH1 at the M.I.T. reactor. In a thermal flux, a 573-keV proton and a 191-keV triton are produced. By counting the signal from one detector only, a peak is obtained in the channel corresponding to the proton energy of 573 keV; by summing the signals due to both the proton and the triton in coincidence, a peak is obtained in the channel corresponding to an energy of 764 keV. A linear relationship between channel number and energy is then assumed to provide the energy calibration of each channel.

A Californium-252 neutron source was used to obtain the energy response function of the He^3 system. The neutron energy spectrum of this source was assumed to be given by the expression,[2]

$$N(E) = CE^{1/2} \exp(-E/T),$$

where E is the neutron energy, and T = 1390 keV.

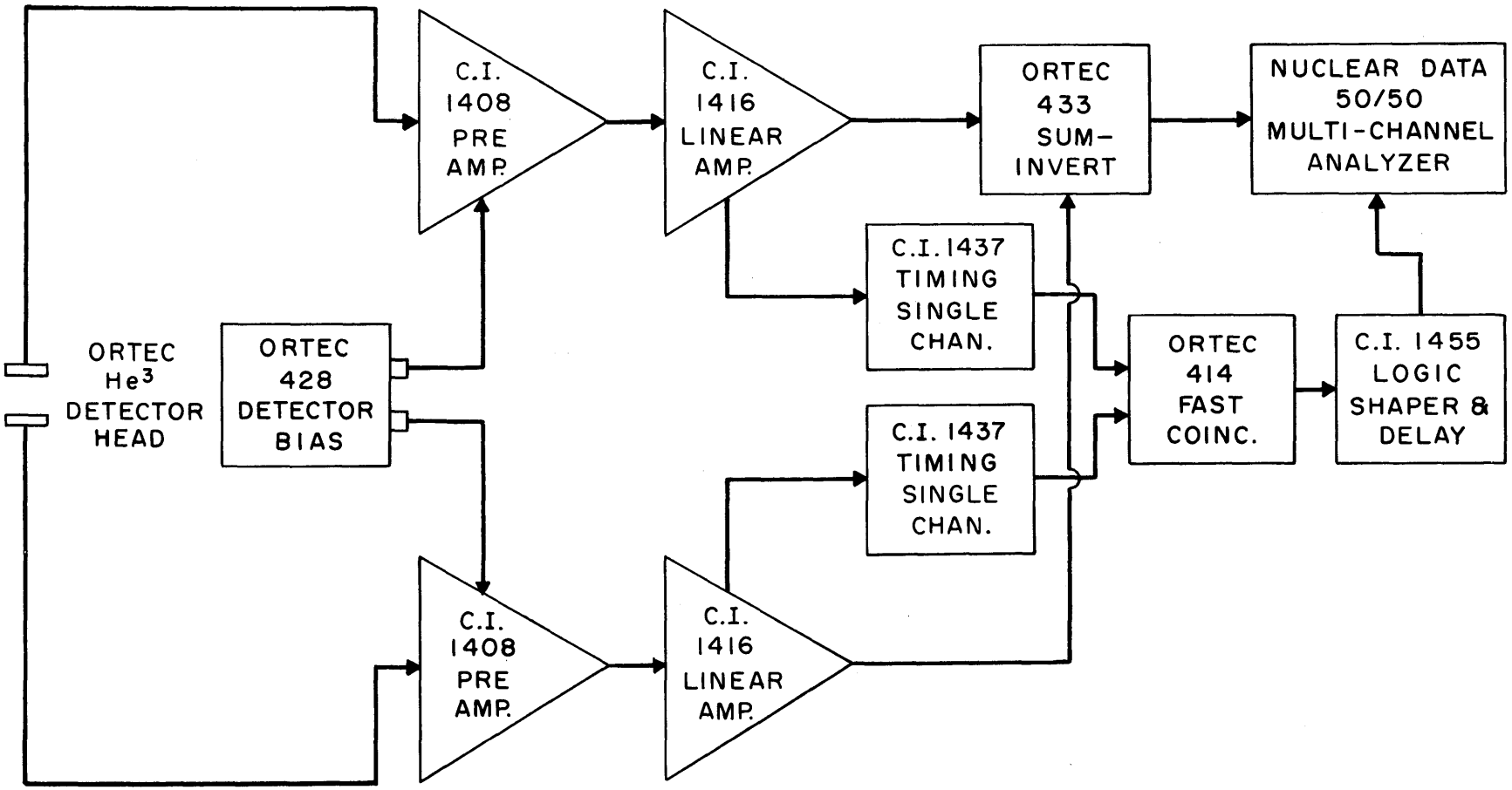

FIG. 5.1 He-3 NEUTRON SPECTROMETER ELECTRONIC SYSTEM

The Cf^{252} spectrum was measured with the He^3 detector by hanging both the Cf^{252} source and the detector from the ceiling of a large shielded room to minimize the effects of neutron back-scattering from the walls. The effect of elastic scattering of neutrons by He^3 nuclei is decreased by the coincidence requirement between the two detectors. The background count rate from the silicon detectors was measured by evacuating the detector of He^3 and replacing it in the neutron flux.

Figure 5.2 shows the Cf^{252} fission spectrum and the corresponding charged particle energy spectrum detected. The difference between the two spectra results from the energy dependence of the He^3 absorption cross section and the efficiency of the detector. The ratio of the theoretical spectrum to the measured spectrum gives the energy response function of the system. Knowing the response function, any unknown spectrum can be measured and corrected to obtain the true neutron spectrum.

5.2.3 He^3 Spectrum Measurements in the Blanket Test Facility

Preliminary runs have been made with the He^3 detector in an effort to measure the energy spectrum of the neutron beam from the 1-in.-diameter hole drilled through the iron reflector of Blanket Assembly No. 2 (see Fig. 3.2). The He^3 detector was placed two feet from the rear surface of the reflector; flux intensity limitations of the detector prevented its being placed closer to the reflector. The measured neutron spectrum and background are shown in Fig. 5.3 (no correction has been made for the response function of the detector). According to the energy calibration, most of the neutrons are in the energy region below 100 keV. This is a much softer spectrum than should be characteristic of the rear of the blanket assembly. Since no collimation was provided for the neutron beam between the back of the reflector and the detector for these preliminary runs, it is likely that low energy neutrons leaking out of the rear face of the iron reflector and/or backscattering from the concrete shielding surrounding the detector contaminated the beam spectrum.

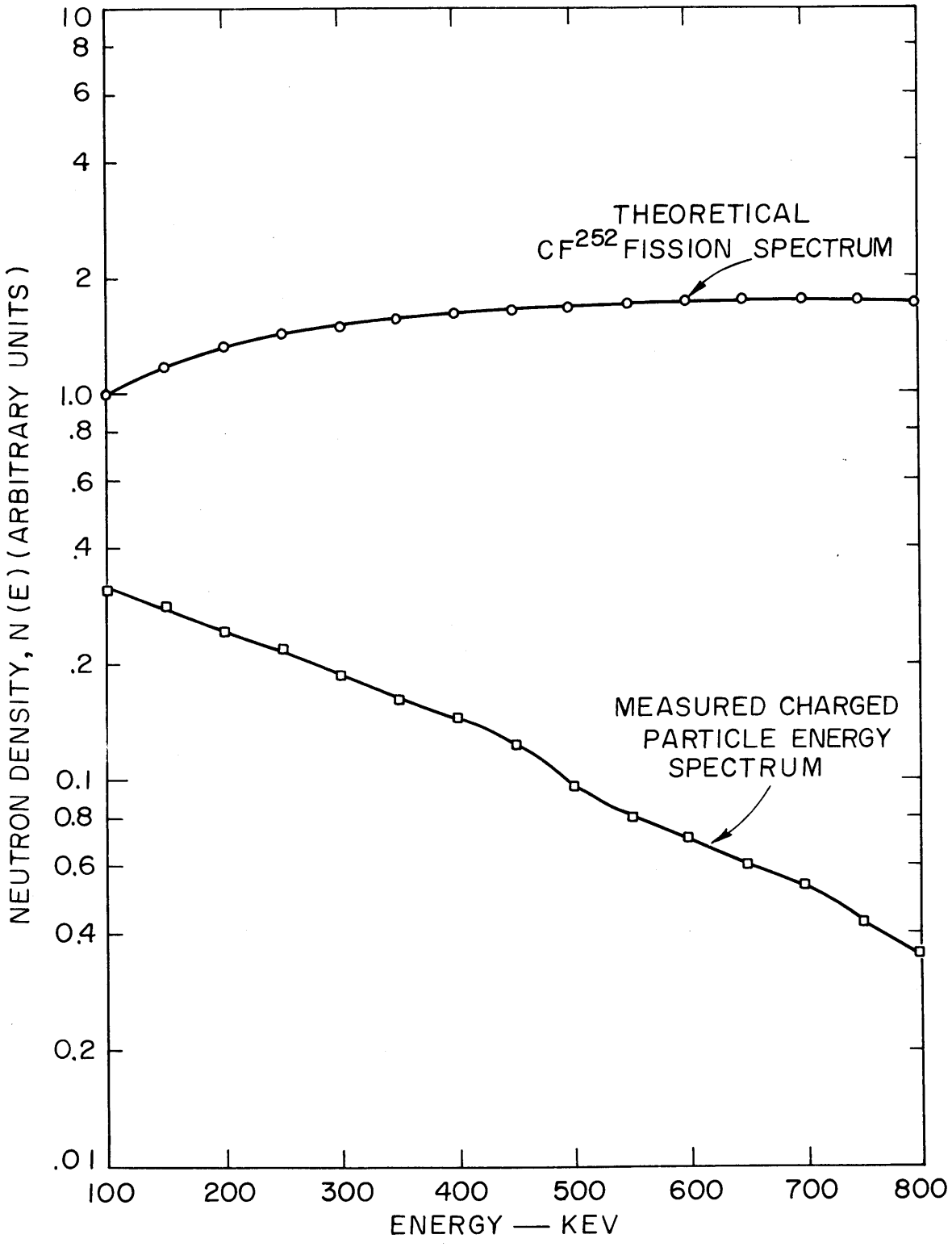

FIG. 5.2 CALIFORNUM-252 CALIBRATION OF He-3 SYSTEM

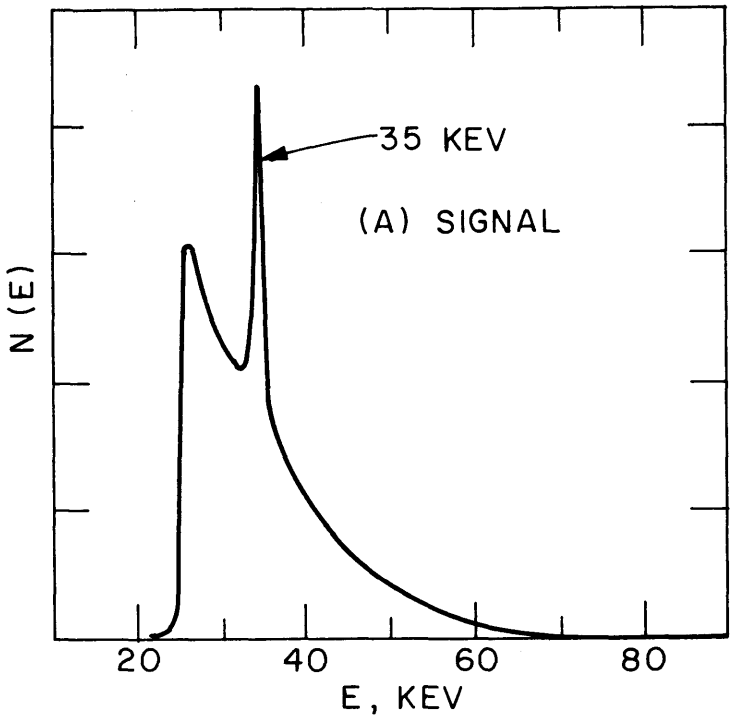

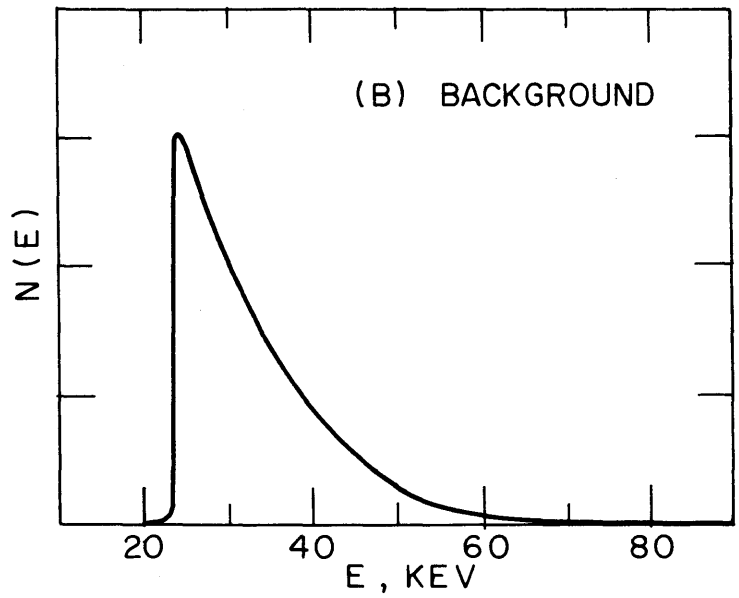

FIG. 5.3 HE^3 SPECTRUM OF THE NEUTRON BEAM FROM THE 1 IN. DIAMETER PORT THROUGH THE REFLECTOR OF B.T.F. BLANKET NO. 2

Future measurements with the He^3 detector will incorporate two changes in the system to improve the results:

(a) a collimator between the rear face of the iron reflector and the detector (shown in Fig. 5.4) to minimize beam contamination;

(b) replacement of the sum amplifier (adder) with a difference amplifier to improve the low-energy resolution of the system.[3]

Table 5.1 shows that the difference between the proton and triton energies changes much more rapidly at neutron energies in the low keV region than does the sum of the proton and triton energies. Replacement of the sum amplifier by a difference amplifier should improve the system resolution by up to a factor of twenty.

5.3 Conclusions and Future Work

Instrumental neutron spectrum measurements will be made in Blanket Assembly No. 2, using three different methods, to provide a mapping of the differential neutron spectrum through the blanket.

Measurements with the He^3 spectrometer are underway. Changes are presently being made to improve beam collimation and low-energy resolution.

Measurements with the proton recoil spectrometer have been severely delayed by the manufacturer's prolonged postponements of the delivery dates for the detectors. However, two detectors have now been obtained on loan from E. F. Bennett of A.N.L., and are presently being calibrated. The proton recoil measurements will be made using essentially the same methods as those developed by E. F. Bennett at A.N.L.[4, 5]

Although initial spectrum measurements are being made on the neutron beam from the 1-in.-I.D. hole through the steel reflector of Blanket No. 2, future measurements will also be made with the detectors placed inside a specially-designed blanket subassembly.

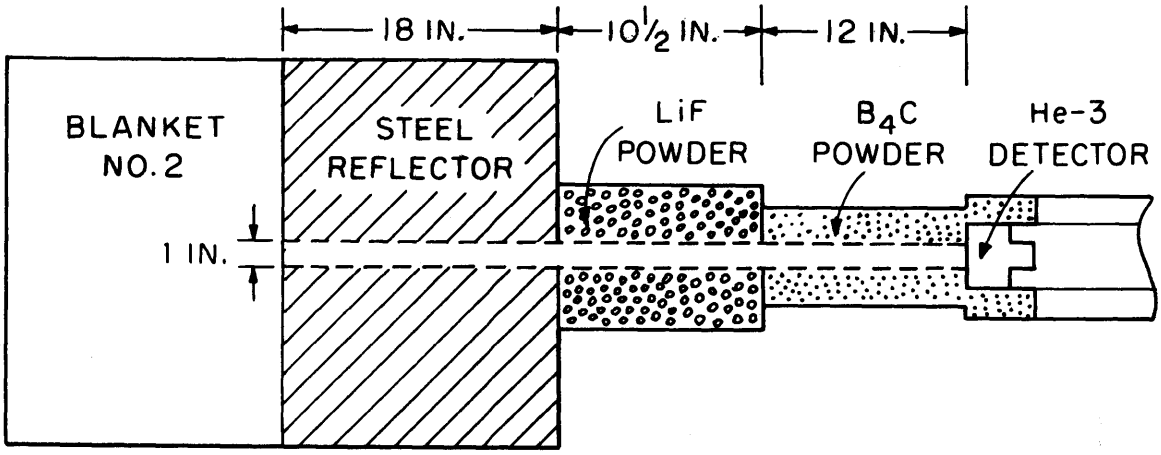

FIG. 5.4 NEUTRON BEAM COLLIMATOR
(NOT TO SCALE)

TABLE 5.1 Neutron Spectroscopy – He^3 System

E_1 (keV)	V	W (keV)	$V^2 + W$	E_3 (keV)	E_4 (keV)	Δ $E_3 - E_4$ (keV)	Σ $E_3 + E_4$ (keV)
0	0	573	23.94	573	191	382	764
0.5	0.18	573.25	23.94	582	182.5	400	764.5
1.0	0.25	573.50	23.95	586	179	407	765.0
1.5	0.31	573.75	23.96	589	176.5	412.5	765.5
2.0	0.35	574	23.96	591	175	416	766.0
3.0	0.43	574.50	23.97	595	172	423	767.0
100	2.50	623	25.08	760.9	103.1	657.8	864.0

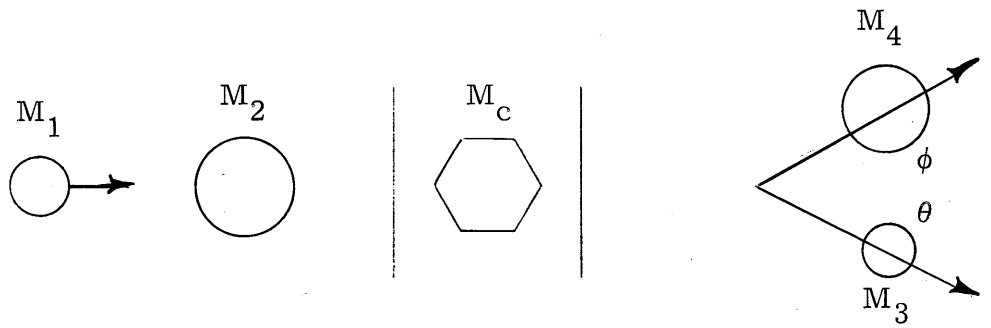

1) $\sqrt{E_3} = V \pm \sqrt{V^2 + W}$ 2) $V = \frac{\sqrt{M_1 M_3 E_1}}{M_3 + M_4} \cos\theta$ 3) $W = \frac{M_4 Q + E_1(M_4 - M_1)}{M_3 + M_4}$

5.4 References

(1) Fowler, J., and L. Marion, "Fast Neutron Physics, Part I," Interscience Pub., Inc., New York (1960).

(2) Green, L., "Transmission Measurement of the Cf^{252} Fission Neutron Spectrum," NSE, 37, 232-242 (1969).

(3) Jeter, T. R., "Recent Improvements in Helium-3 Solid State Neutron Spectrometry," IEEE Trans. Nuc. Sci., 422 (1967).

(4) Bennett, E. F., "Fast Neutron Spectroscopy by Proton-Recoil Proportional Counting," NSE, 27, 16-27 (1967).

(5) Bennett, E. F., "Neutron Spectrum Measurement in a Fast Critical Assembly," NSE, 27, 28-33 (1967).

6. NEUTRON SPECTRA FROM FOIL ACTIVATION

S. L. Ho and N. A. Passman

6.1 Introduction

The purpose of the work reported in this chapter is to evaluate determination of neutron spectra by using foil activation. Although this technique is one of long standing in the field of experimental reactor physics, a number of possible improvements were investigated. One major objective of the present work was to develop a one-step, simultaneous multifoil-counting procedure based on Ge(Li) spectrometry. This technique includes the use of the GAMANL code (1) developed at M.I.T. to extract individual nuclide activities, which can in turn be fed into existing codes, such as SAND II (2) to unfold the energy spectrum of the neutrons in which the foil materials were irradiated. This approach is preferable to methods which employ individual foil counting, since it is much more amenable to automation.

6.2 Experimental Procedures

One of the more important steps in all foil activation methods is the selection of the foil materials to be used. Criteria for selection generally include: capture cross-section shape (resonance or threshold) which emphasizes a particular part of the neutron spectrum, intermediate half life (hours to days) to facilitate activation and counting, and a distinctive decay gamma spectrum. In the present case, this latter criterion is particularly important because of the need for simultaneous resolution of all photopeaks in a common spectrum. It rules out the use of fission foils, or nuclides identified primarily through the ubiquitous 0.511-MeV photopeak. Table 6.1 lists the target materials found most useful for the present applications, in which most of the neutron flux lies in the range 100 eV to 5 MeV.

TABLE 6.1

Materials Used for Neutron Spectrum Determination

Target	Product Nuclide	Half Life (Hours)	Predominant γ Analyzed (MeV)
Au	Au-198	65	0.412
W	W-187	24	0.479
Mn	Mn-56	2.58	0.847
Mo	Mo-99	67	0.141
Na	Na-24	15	1.368
In	In-115m	4.5	0.335
Ni	Co-58	1728	0.810
Ti	Sc-48	44	0.983

The above materials are used in the form of powder smaller than 35 mesh (16.5-mil diameter). Metal powder was used, except for sodium which was used as carbonate. The materials are homogeneously mixed before loading in the foil capsule in order to subject all materials to the same average neutron environment and to provide the same mean counting geometry. A polyethylene vial was employed for the foil capsule in the early runs. However, because the hydrogen in the polyethylene can seriously perturb a fast spectrum, more recent work has employed a tube of one of the "foil" materials, typically nickel, as the capsule itself.

The counting equipment and procedures involved use of Ge(Li) detectors, their attendant electronic systems, and the code GAMANL to interpret the multichannel analyzer spectra. The essential features of these counting systems has already been described in articles and recent topical reports dealing with M.I.T. practice in this field.

6.3 Preliminary Results

Powder-containing capsules have been irradiated in the 6CH1 Transistor Irradiation Facility at the MITR. This facility was designed to produce a fission spectrum of neutrons for radiation damage studies on semiconductors. Figure 6.1 shows the unfolded $\phi(E)$ above 1 MeV compared with the theoretical fission spectrum. Also shown are the effects of changing the specified error tolerance (in terms of percent standard deviation, S.D.) fed into SAND-II. The introduction of an apparently spurious flux dip at 6.5 MeV due to overly restrictive error limits is clearly shown in Figure 6.1, and is a typical consequence of the SAND-II algorithm (4). If intelligently applied, however, SAND-II will indeed give reasonable results.

The spectrum above 1 MeV is determined primarily from the threshold foil activities, while that below 10 keV is characterized mainly through resonance absorption. In the limited experimental work to date, it has proven more difficult to unfold nonanomalous spectra in the lower energy region. This result would also appear to be in essential agreement with the experiences reported by Newman (4), who applied SAND-II to ordinary individual-foil experiments in an LMFBR spectrum; and we also expect to be able to achieve equally suitable results eventually through diligent error analysis and sensitivity studies.

6.4 Discussion

The objective of the work discussed in this chapter is, of course, the determination of the energy spectrum of the ambient neutrons in the blanket mock-up. At the least, these measurements will provide a valuable supplement to, and check upon, the instrumentally determined spectra above 1 keV. Below 1 keV the foil method may well be the only proven, convenient approach.

During the coming year a number of aspects of the foil method will be improved upon:

(1) An evaluation will be made of the relative merits of the powder (this work) vs. foil (see, for example, reference (4) for a recent

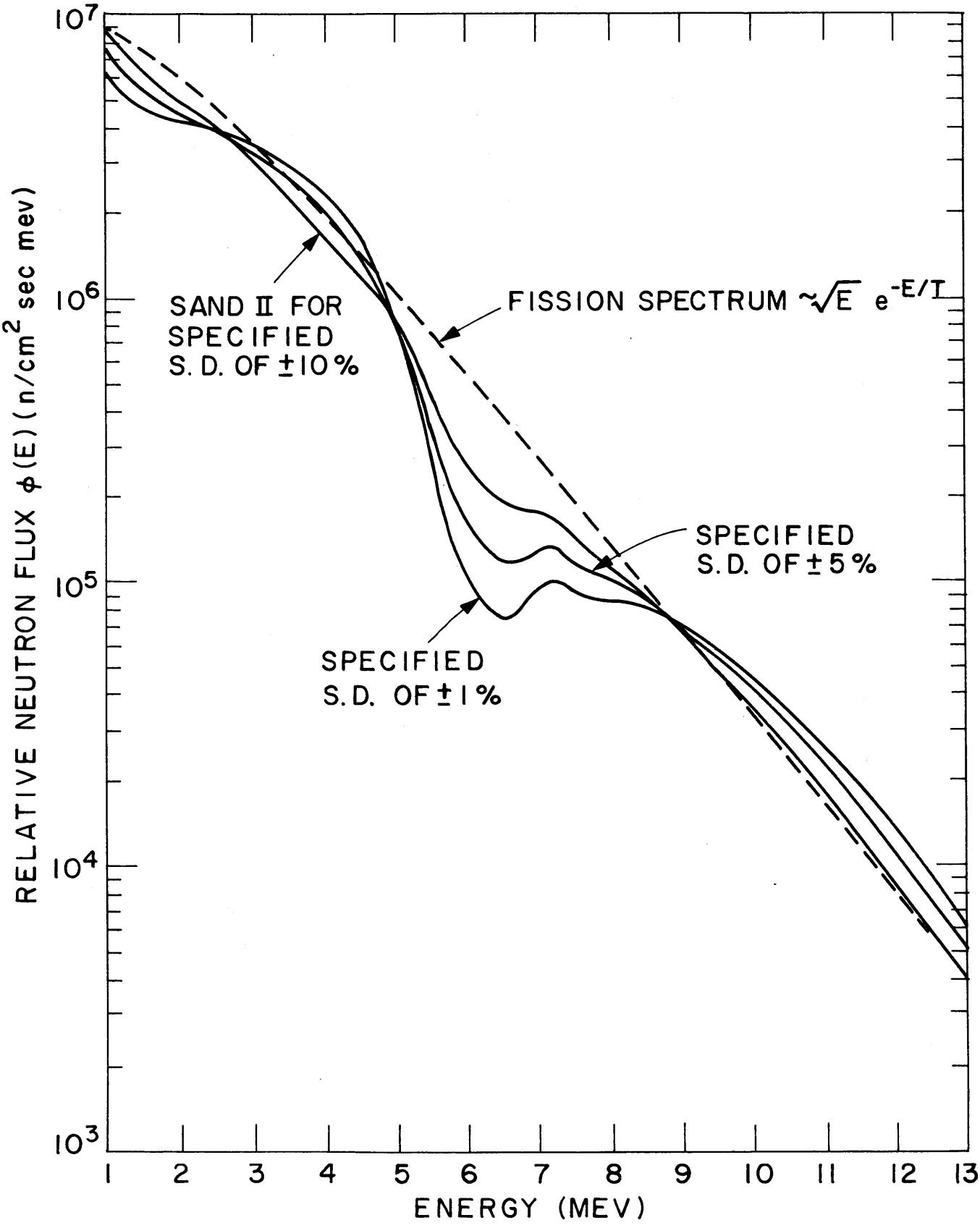

FIG. 6.1 COMPARISON OF FLUX UNFOLDED BY SAND II WITH FISSION SPECTRUM

application very similar to that of present concern) versions of the material activation technique. While the powder capsule method is more suited to automation, it must still be shown that good results can be achieved with the smaller selection of suitable foil materials, and that the use of fine, widely dispersed particles can eliminate the need for resonance self-shielding corrections.

(2) Alternative unfolding techniques to SAND-II will be evaluated. It seems prudent to require that each set of data be unfolded by at least two independent schemes to help insure against erroneous interpretation of the data.

(3) Alternative gamma analysis methods to GAMANL will be evaluated. It is possible, for example, to achieve close to an on-line data analysis capability using the project's PDP/8L computer and available data processing program packages (5).

(4) An irradiation in a 1/E spectrum will be carried out to check the accuracy of the method below 1 keV and to establish a detection system response function suitable for correcting out idiosyncracies introduced into unknown spectra by the overall data processing complex.

This work has presently advanced to the stage where there does not appear to be any serious obstacle to implementation of the material activation technique for determination of blanket mock-up spectra.

6.5 References

(1) Harper, T., T. Inouye, N.C. Rasmussen, "GAMANL, A Computer Program Applying Fourier Transforms to the Analysis of Gamma Spectral Data," MIT-3944-2, August 1968.

(2) Berg, S. and W.M. McElroy, "A Computer-Automated Iterative Method for Neutron Flux Spectra Determination by Foil Activation," AFWL-TR-67-VI, Vol. II (1967).

(3) Ho, S.L., "Measurement of Fast and Epithermal Neutron Spectra Using Foil Activation Techniques," S.M. Thesis, M.I.T. Nuclear Engineering Department, January 1970.

(4) Newman, D.F., "Determination of the Absolute Neutron Flux Spectrum in the PCTR Neutron Cavity from Multiple Foil Activity Measurements," S.M. Thesis, University of Washington, 1970.

(5) Series 50/50 Physics Analyzer Basic Software Instruction Manual, Nuclear Data, Inc., January 1970.

7. NEUTRON SPECTRUM MEASUREMENTS BY PROMPT GAMMA SPECTROMETRY

C. Forsberg and D. Shupe

7.1 Introduction

Work is presently being carried out as part of the LMFBR Blanket Physics Project to develop a neutron spectrometer based on the analysis of the prompt gamma spectrum due to neutron capture by a selected target material.

7.2 Principle of Operation

When a neutron is captured by a target nucleus, the resulting excited nucleus emits one or more prompt gamma rays. The relative intensities of these prompt gamma rays are functions of the incident neutron energy. Hence, it may be possible, in principle at least, to determine the spectrum of the incident neutrons by analyzing the spectrum of the prompt gammas emitted by the target material.

7.3 Spectrometer Development

At present, tantalum-181 is being investigated as the preferred target material. It is anticipated that a tantalum spectrometer would have its greatest sensitivity in the measurement of neutron energies between 10 eV and 1 keV – a region where other methods are not entirely adequate.

Ta^{181} target material is being irradiated at the M.I.T. reactor in both thermal and fission neutron fluxes; irradiations will also be made shortly in a 1/E neutron flux. The purpose of these measurements is to determine whether the prompt gamma spectrum of Ta^{181} shows sufficient variation as a function of neutron energy to make this approach worthwhile. This work is continuing, and will also involve analytical evaluations which take into account recent experimental and

theoretical information published on the variation of the prompt gamma yield of Ta^{181} with incident neutron energy.[1, 2]

A tantalum spectrometer system is currently being designed and assembled. Following evaluation tests, it will be used for neutron spectrum measurements in the Blanket Test Facility if it shows sufficient promise of successful performance.

7.4 References

(1) Wasson, O. A., R. E. Chrien, M. A. Lone, M. R. Bhat and M. Beer, "Resonance Neutron Capture in $^{181}Ta(n, \gamma)^{182}Ta$," Nuclear Physics, A132, 161-176 (1969).

(2) Yost, K. J., "A Method for the Calculation of Neutron-Capture Gamma-Ray Spectra," NSE, 32, 62-75 (1968).

8. APPLICATIONS OF PROMPT GAMMA SPECTROSCOPY TO LMFBR RESEARCH

C. S. Kang

8.1 Introduction

The techniques of prompt gamma-ray spectroscopy, using high resolution lithium-drifted germanium detectors, have been highly developed at M.I.T. and at other institutions. It is the purpose of the present work to investigate the application of prompt gamma spectroscopy methods in several areas of interest to the research program of the LMFBR Blanket Physics Project.

One such area has already been noted; prompt gamma spectroscopy was used to determine the hydrogen content of the sodium chromate powder used in Blanket Assembly No. 2 (see section 3.3.2). The two primary areas now being investigated are:

(a) the determination of the relative reaction rates of the constituent materials of Blanket No. 2 for comparison with similar results to be obtained by conventional foil-counting methods;

(b) the feasibility of fast neutron spectroscopy by analysis of energy shift or broadening of the 2.223-MeV capture gamma line resulting from neutron capture by hydrogen or other materials.

These two areas are discussed below.

8.2 Determination of Reaction Rates

Work is presently under way in an effort to measure the relative reaction rates of constituent materials of Blanket Assembly No. 2 (viz. U^{238}, Na, Cr and Fe). This is to be accomplished by measuring the relative intensities of the characteristic prompt gamma rays resulting from neutron capture by these materials. Measurements of the reaction

rates will aid in determining the overall blanket neutron balance for Blanket No. 2.

Preliminary prompt gamma spectrum measurements have been made using the gamma beam from the 1 inch-I.D. beam hole through the steel reflector of Blanket No. 2 (see Fig. 3.2). Further measurements will be made through the coming year.

8.3 Fast Neutron Spectroscopy

An investigation is also being made of the feasibility of measuring fast neutron spectra by analysis of the energy shift in the 2.223-MeV prompt gamma line resulting from neutron capture by hydrogen.

Preliminary evaluation measurements are being made with a Cf^{252} fission neutron source. Work to establish the feasibility of this method will continue, and, if successful, measurements will be made in Blanket No. 2.

8.4 Conclusions

Work is currently being performed to measure material reaction rates in Blanket No. 2 using prompt gamma spectroscopy, and to develop a method for fast neutron spectroscopy based on the analysis of the hydrogen prompt gamma line. Work in both these areas will continue in the coming year.

9. HETEROGENEITY EFFECTS IN LMFBR BLANKET FUEL ELEMENTS

W. J. Westlake, Jr.

9.1 Introduction

If the detailed reaction rates within a unit cell have appreciable spatial variation, the neutron economy will differ from that predicted by a reactor model employing homogenized material regions. An investigation of the reaction rate distributions within a fuel rod is one method of determining the influence of heterogeneity effects on the neutron balance. The effects attributed to heterogeneities in LMFBR's are expected to be most significant in the blanket where severe spectral degradation can occur.

It has been shown that the predominant heterogeneity effects are due to the spatial dependence of the U^{238} fission and capture reaction rates within a fuel rod in LMFBR cores and fast critical assemblies (1). Intra-rod distributions of fission and capture reaction rates can be measured directly using uranium foil activation techniques. The purpose of the present work was to perform such foil activations within the 0.25 inch-diameter, uranium metal fuel rods in Blanket Assembly No. 2.

9.2 Experimental Technique

The experimental work consisted of irradiating both 1/16 inch-diameter, depleted uranium foils and 1/4 inch-diameter, two-piece depleted uranium foils, placed within a 1/4 inch-diameter blanket fuel rod of metallic uranium, 1.016% enriched in U^{235} (see Fig. 9.1). Blanket fuel rods containing the depleted uranium foils were loaded in Blanket Assembly No. 2 in various locations (see Fig. 9.2). During irradiation, the rods were rotated at 1 rpm in order to cancel out the effects of the blanket flux gradient.

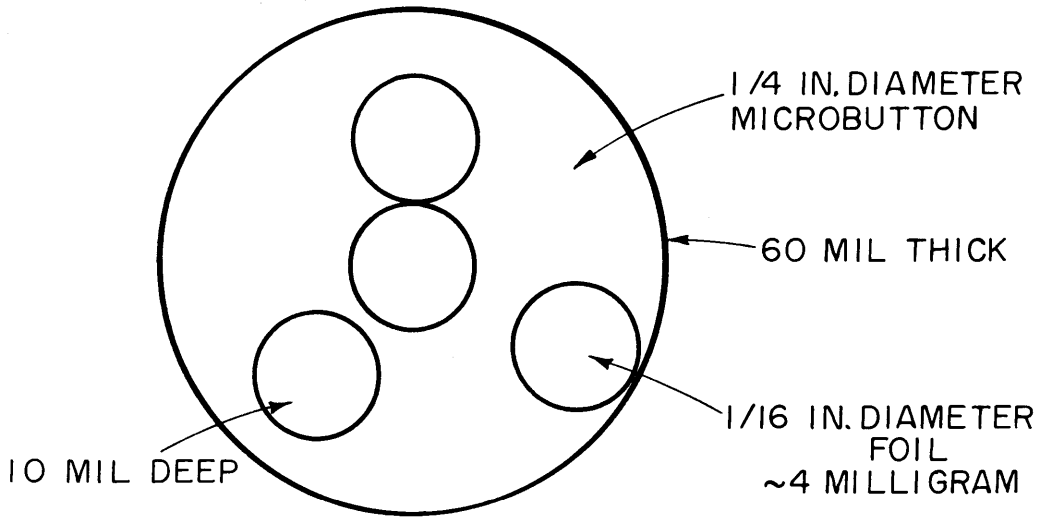

MICROBUTTON AND 1/16 IN.
FOIL POSITIONS

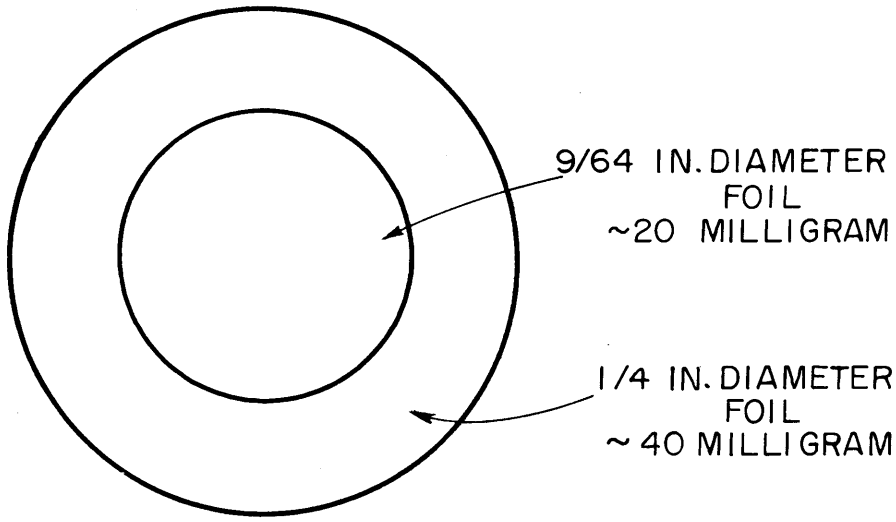

TWO-PIECE CONCENTRIC
FOIL SET

FIG. 9.1 SCHEMATIC DRAWINGS OF FOIL GEOMETRIES

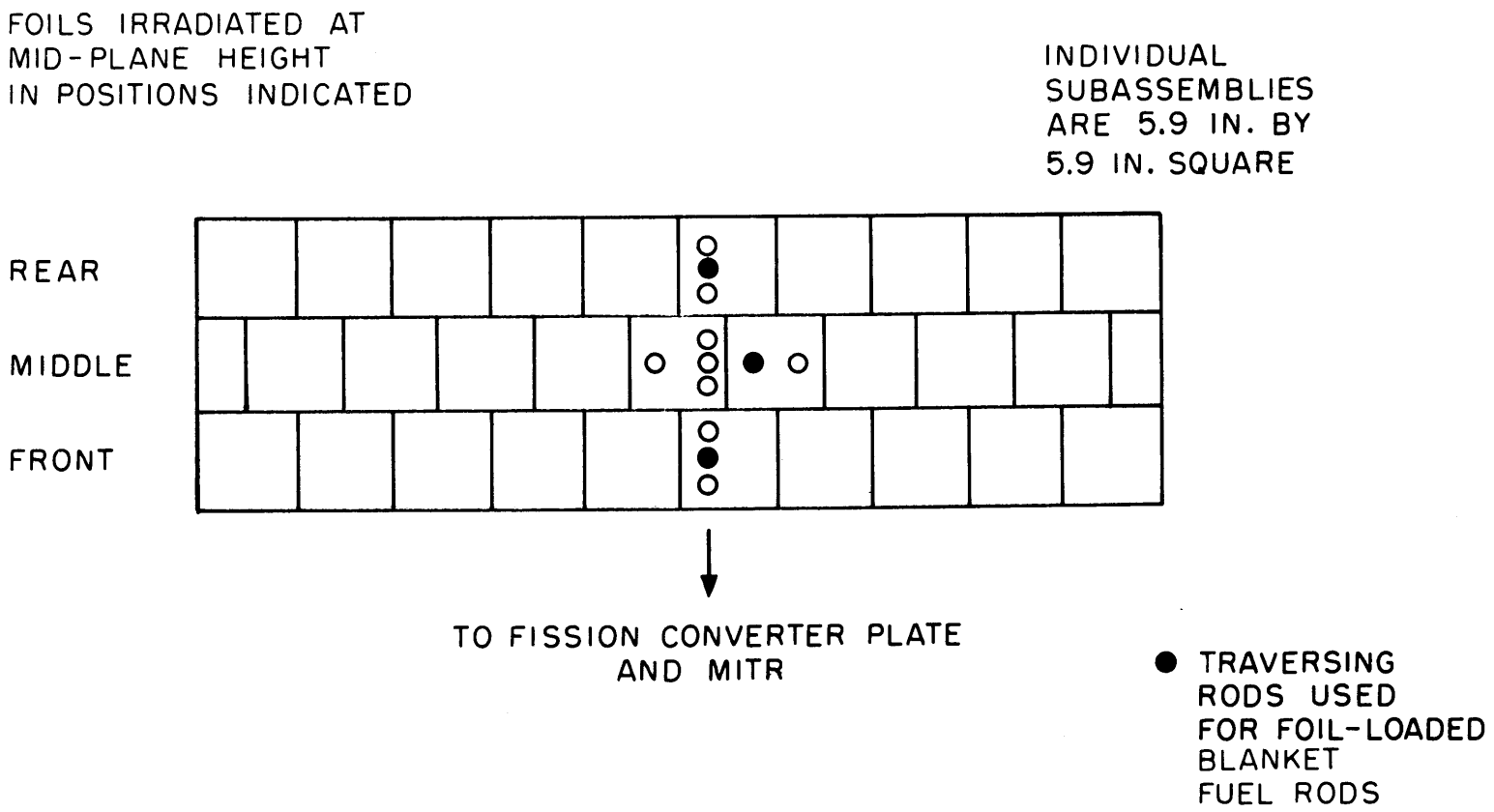

FIG. 9.2 SCHEMATIC PLAN VIEW OF BLANKET TEST ROD POSITIONS

The foils were removed from the blanket following irradiation and gamma-counted with a NaI(Tl) scintillation crystal detector and single-channel analyzer counting system. The fission product and Np^{239} activities (due to the (n, f) and (n, γ) reactions on U^{238}, respectively) were counted.

9.3 Experimental Results

The measured intra-rod U^{238} capture and fission reaction rate distributions obtained in the foil irradiation runs are shown in Figures 9.3, 9.4 and 9.5 (the three measurement positions in Blanket No. 2 are shown in Fig. 9.2).

The U^{238} capture rate distributions shown in Figs. 9.3 and 9.4 clearly indicate a significant difference between the rod centerline and rod surface reaction rates. This difference approaches 20% for the microbutton foil irradiation results obtained with the test fuel rod placed in the rear row of the blanket assembly (see Fig. 9.3). A 7% to 14% variation in the regional U^{238} capture rates was obtained with the two-piece foil sets (see Fig. 9.4). There is good agreement between the microbutton and two-piece foil measurements, but greater confidence must be given to the two-piece foil results. Because of their greater weight (65 milligrams as opposed to 4 milligrams for the microbutton foils), count rates were higher and the importance of foil material loss due to flaking during handling was reduced. The microbutton foil data shown in Fig. 9.3 would seem to indicate that the intra-rod U^{238} capture rate depression is greater in the front row of the blanket assembly than in the middle row – which is in disagreement with the expected results. It is possible that the errors in the centerline foil activities were large enough to produce sufficient error in the normalized activities to explain this result. In any event, the more reliable two-piece foil data (see Fig. 9.4) does not appear to corroborate this result.

The two-region foil set results shown in Fig. 9.5 indicate (with the exception of one of the four foil sets included) that the regional variation in the U^{238} fission rate is the same for all runs within $\pm$ 1.5%,

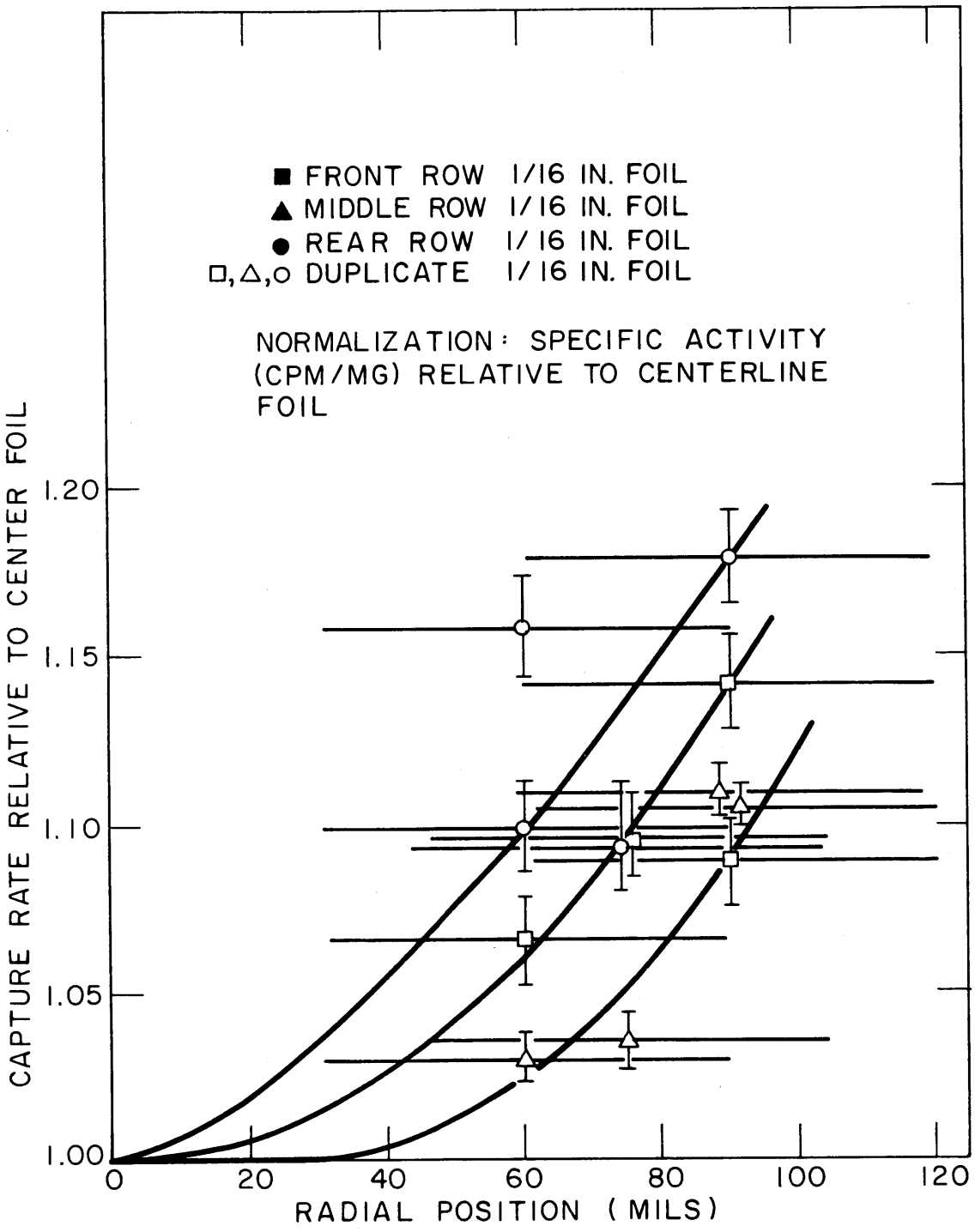

FIG. 9.3 RELATIVE RADIAL U-238 CAPTURE RATE DISTRIBUTION IN BLANKET FUEL RODS

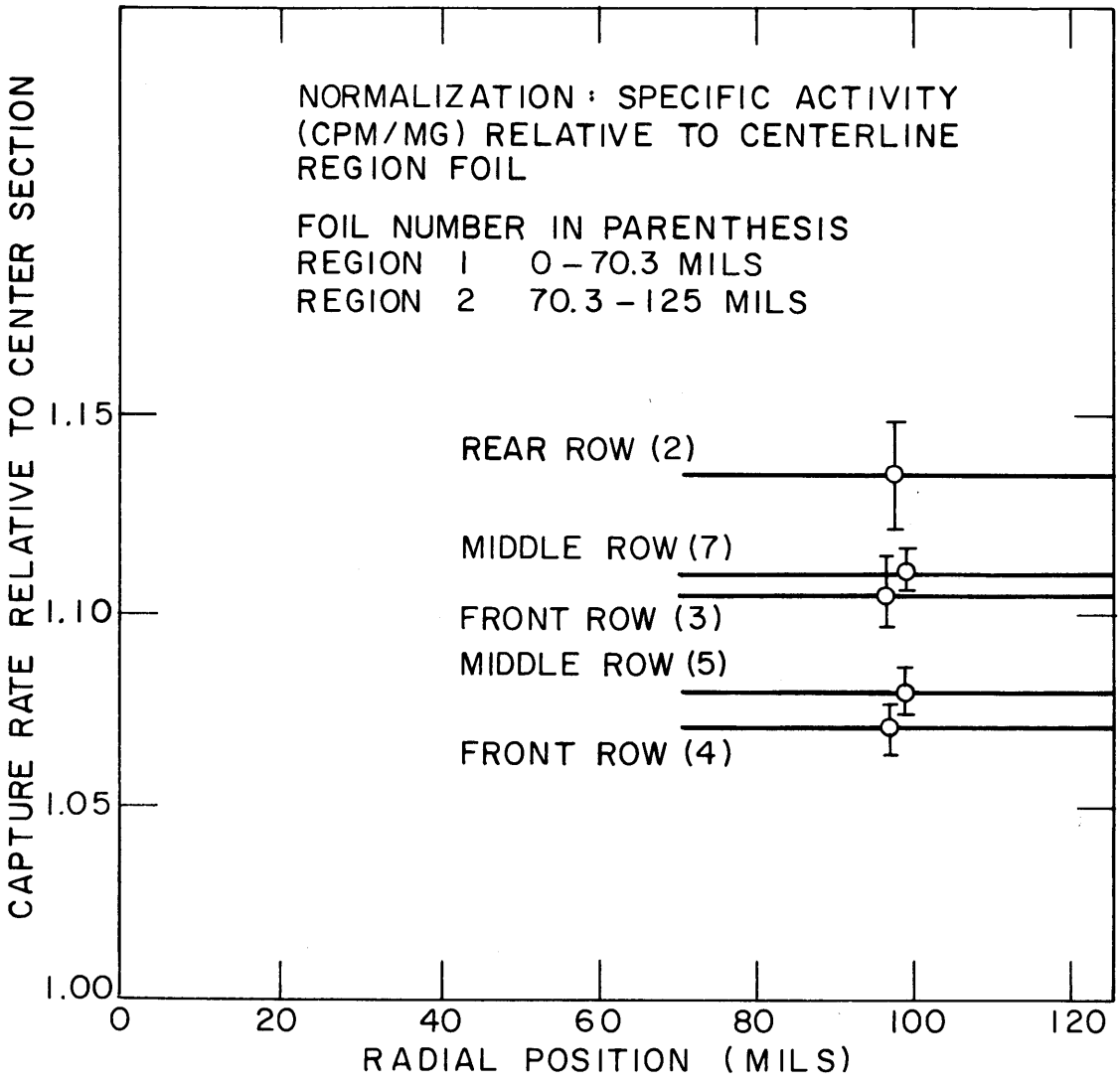

FIG. 9.4 RELATIVE TWO-REGION RADIAL U-238 CAPTURE RATE DISTRIBUTION IN BLANKET FUEL RODS

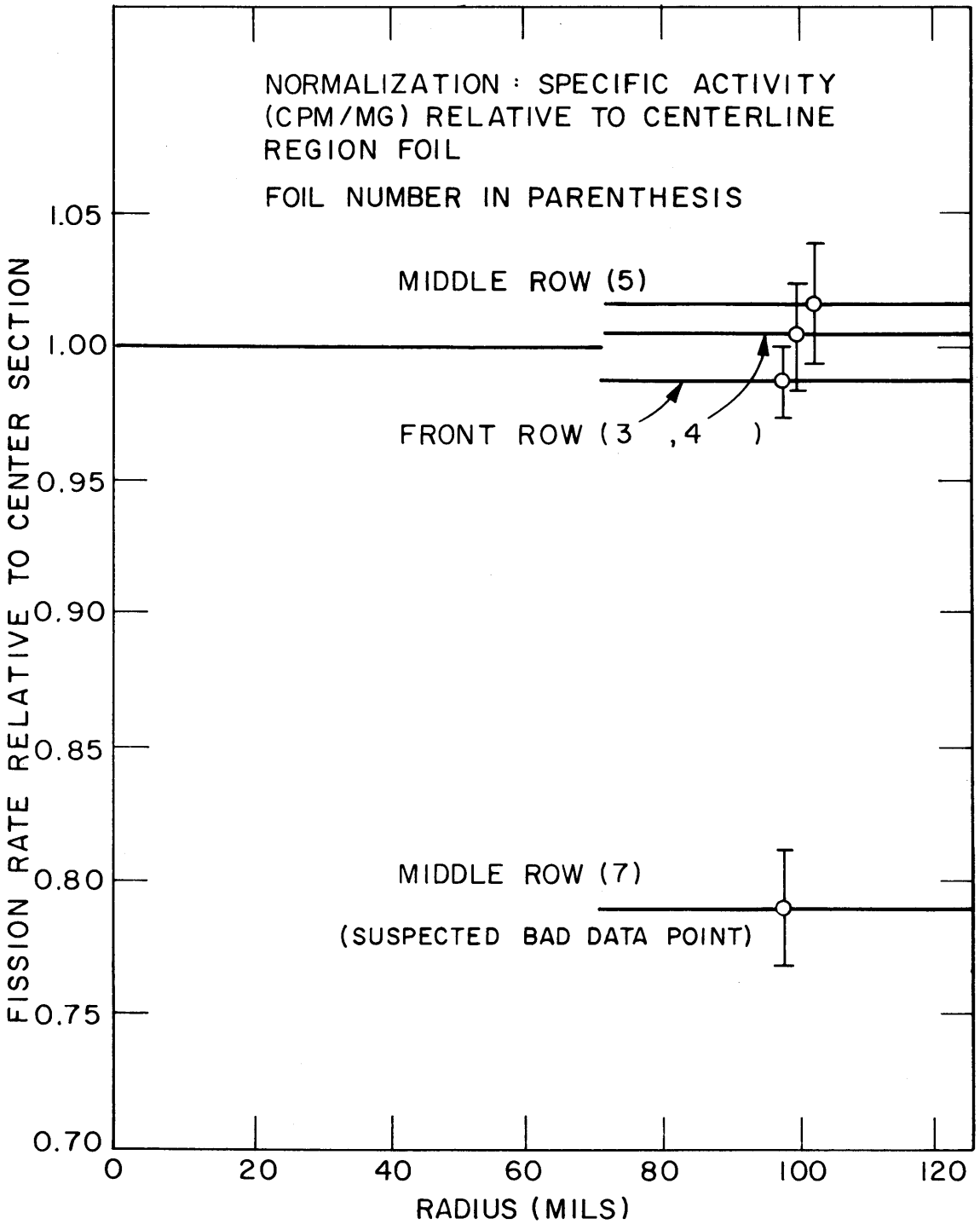

FIG. 9.5 RELATIVE TWO-REGION RADIAL U-238 FISSION RATE DISTRIBUTION IN BLANKET FUEL RODS

is much less than the regional variation found in the U^{238} capture rate, and is therefore negligible in terms of its effect upon the blanket neutron balance.

The ANISN code was used for 16-group, 1-D, S_8 transport theory calculations on several models of a Blanket No. 2 unit cell. No corrections were made for resonance self-shielding effects in the multigroup cross sections. The calculated fuel rod surface to fuel rod centerline reaction rate variations were -0.4% and +3.2% for U^{238} fission and capture, respectively. The calculated intra-rod capture rate variation (3.2%) is considerably smaller than the measured variation (10% to 20%). The large disagreement should be due in large part to the effects of resonance self-shielding.

To check the effect of U^{238} resonance self-shielding, several gold two-piece annular foil sets were irradiated in the test fuel rod in Blanket No. 2. The two-region gold foil measurements showed that the Au^{197} capture rate did indeed have much less spatial dependence than the U^{238} capture rate; the specific activity of the two gold foils differed by less than 1% in all cases. Thus it is clearly resonance self-shielding and not overall flux depression which is the cause of the depression in the U^{238} capture rate.

9.4 Conclusions

The predominant heterogeneity effect in fast reactor blankets is that due to the spatial dependence of the U^{238} capture rate within a fuel rod. The intra-rod U^{238} capture and fission rate distributions have been measured in the 0.25 inch-diameter, uranium metal fuel of B.T.F. Blanket No. 2. The measured rod surface to rod centerline reaction rate variation was found to be between 10% and 20% for U^{238} capture and between -1.5% and +1.5% for U^{238} fission.

When two-piece annular gold foils were irradiated in the test fuel rod, the specific activities of the two foils were found to differ by less than 1% (as opposed to 7% to 14% for U^{238}). This demonstrates that the observed U^{238} capture rate is largely due to U^{238} resonance self-shielding.

It should be noted that the fuel rods in Blanket No. 2 are metallic and therefore have approximately twice the uranium density of the UO_2 which would be used in a real LMFBR blanket. This is offset to some extent by the fact that blanket fuel rods will probably have larger diameters (about 0.5 inch). On the other hand, the oxygen contained in the UO_2 will provide appreciable internal moderation, which should wash out some of the resonance flux depression encountered in the metallic fuel.

Heterogeneity measurements will be continued on Blankets No. 2 and No. 3. A UO_2-fueled blanket subassembly, containing metallic sodium in the inter-rod volume, is being constructed in order to provide further data on blanket heterogeneities. The Blanket No. 2 unit cell calculations will be refined and improved.

9.5 References

(1) Edison, G., "The Effect of Heterogeneity on Reactivity in a Large Carbide LMFBR," Trans. Am. Nucl. Soc. 12, 276 (1969).

(2) Westlake, W.J., Jr., "Heterogeneous Effects in LMFBR Blanket Fuel Elements," S.M. Thesis, M.I.T. Nuclear Engineering Department, June 1970.

10. BLANKET-REFLECTOR INTERACTIONS

S. Ahmed Ali

10.1 Introduction

In preparation for the experimental research program involving Blanket Assemblies No. 2 and No. 3, an investigation was made of the effect of the reflector thickness and composition upon the detailed neutron reaction rates in the blanket. The ANISN code was used to perform 16-group (modified Hansen-Roach cross-section set), 1-D, S_8 transport theory calculations on a model of the Blanket Test Facility consisting of the converter, Blanket No. 2 and a reflector. A variety of reflector thicknesses and compositions were examined.

10.2 Effect of Reflector Thickness

To examine the effect of reflector thickness on blanket reaction rates, ANISN calculations were made for reflector thicknesses varying from zero to 30 inches; the blanket thickness remained constant at 18 inches. The calculations were made for two reflector compositions – an iron reflector and a "reflector" having the same composition as the blanket.

Figure 10.1 shows (a) the total absorption rate plus the lateral leakage rate in the blanket (i.e., $\Sigma_a \phi + DB^2 \phi$), and (b) the leakage rate from the blanket into the reflector, as functions of the reflector thickness for both the iron reflector and for the extended blanket. The normalization is to one thermal source neutron per second in the converter assembly. It is seen that an 18-inch reflector of either iron or blanket material is effectively infinite, since the absorption and leakage rates are not changed by making the reflector thickness greater than 18 inches. The total fission rate in the blanket was found to be similarly affected. These calculations showed that the 18 inch-thick reflector used on Blanket No. 2 would be effectively infinite in extent in terms of its effect on the blanket neutron balance, as intended.

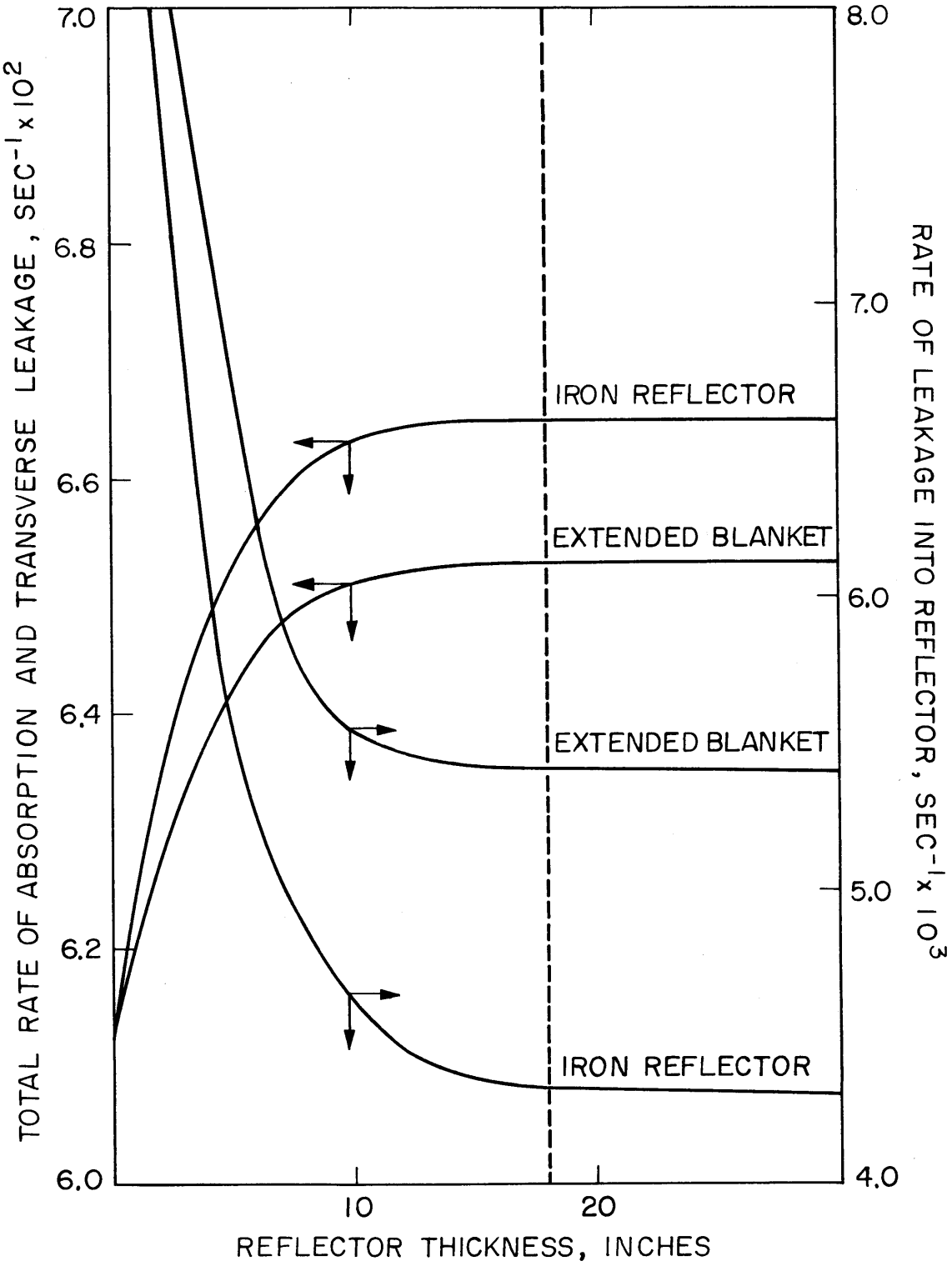

FIG. 10.1 TOTAL ABSORPTION AND LEAKAGE RATES IN BLANKET NO. 2 AS A FUNCTION OF REFLECTOR THICKNESS

10.3 Effect of Reflector Composition

In order to examine the effect of the reflector composition on the blanket reaction rates, the ANISN code was used to calculate the axial variation of the U^{238} capture rate in Blanket No. 2 for a variety of reflector compositions. The reflector thickness remained constant at 18 inches.

Figure 10.2 shows the U^{238} axial (Z-direction) capture rate in Blanket No. 2 for reflectors composed of Na, Fe, Fe_3O_4, ZrO_2 and BeO; these are compared to a base case composed of blanket material, i.e., an extended blanket. It is seen that the U^{238} capture rate in the blanket is increased only slightly by using an iron or sodium reflector instead of extending the blanket. The increase in the U^{238} capture rate at the outer edge of the blanket is greatest for the lightest reflector materials. A BeO reflector would increase the total capture rate in Blanket No. 2 by about 10%. This would give rise to an essentially equivalent increase in blanket plutonium production. Alternatively, Pu^{239} production could be maintained constant using a thinner blanket. Both aspects would have potential economic advantages. As can also be seen in Fig. 10.2, the reflector-induced flux perturbation does not propagate more than about 8 inches back into the blanket, and hence the choice of reflector material has no appreciable effect upon the core.

10.4 Conclusions

ANISN calculations have shown that an 18-inch reflector for Blanket Assembly No. 2 is effectively infinite. It was further found that the total absorption rate in the 18 inch-thick blanket is only 2% higher with an 18-inch iron reflector than if the blanket is extended 18 inches further (see Fig. 10.1), and also very little different from the Na reflected case. These facts led to the choice of an 18-inch iron reflector for Blanket No. 2.

Calculations to determine the effect of the reflector composition on blanket reaction rates have shown that light reflectors providing external moderation can produce a significant increase in blanket capture rates (about 10% for a BeO reflector). Consideration is

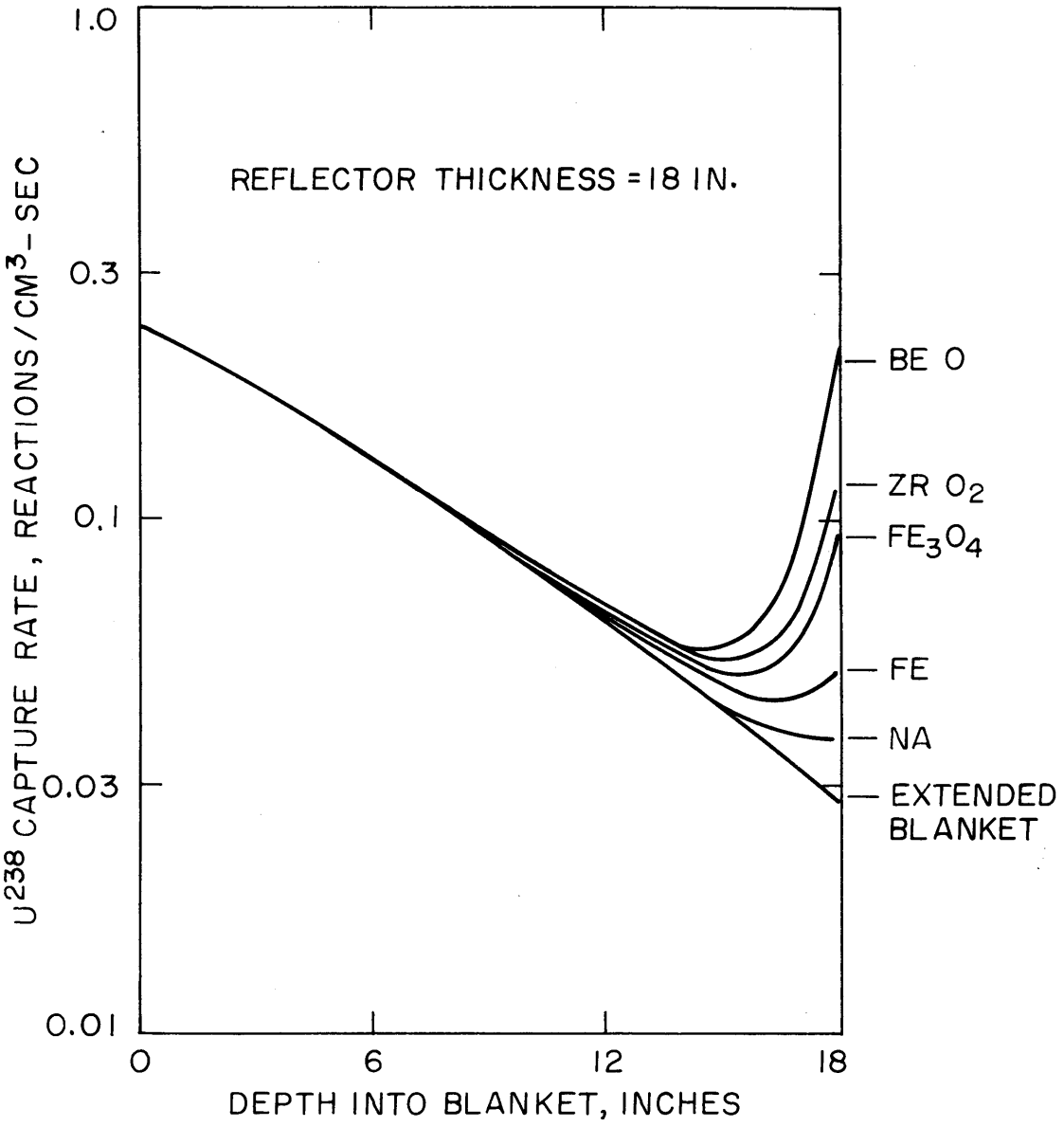

FIG. 10.2 U^{238} CAPTURE RATE IN B.T.F. BLANKET NO. 2 FOR DIFFERENT REFLECTOR COMPOSITIONS

therefore being given to replacing the iron reflector of Blanket No. 2 by a graphite or BeO reflector for the Blanket No. 3 experiments. ANISN calculations will be made shortly to determine the effects of a graphite reflector.

11. A ONE-GROUP MODEL FOR FAST REACTOR CALCULATIONS

M. K. Sheaffer

11.1 Introduction

A key assumption underlying the present research with the Blanket Test Facility is that these studies can be conducted efficiently without the use of a critical assembly. This makes it highly desirable that core spectral properties be characterized in a concise manner. As will be described below, investigation of this area resulted not only in the development of two simple core characterization parameters, but also in a flexible and surprisingly accurate one-group method for core neutronic calculations. A detailed description of this method will be presented in the topical report:

> M. K. Shaeffer, M. J. Driscoll and I. Kaplan, "A One-Group Method for Fast Reactor Calculations," MIT-4105-1, MITNE-108 (September 1970).

11.2 Spectral Characterization Parameter, S

The primary theoretical basis for this model is continuous slowing-down theory, which has demonstrated previous successes in correlating the energy spectra of fast reactors.[1, 2, 3] Application of slowing-down theory yields the following familiar expression for the capture escape probability for a weakly absorbing infinite medium:

$$P(E_o \rightarrow E) = e^{-\int_E^{E_o} \frac{\Sigma_a(E)}{\xi\Sigma_s(E)} \cdot \frac{dE}{E}}, \qquad (11.1)$$

where $P(E_o \rightarrow E)$ is the probability that a neutron of energy E_o will reach a lower energy E without capture, and where

$$\frac{\Sigma_a(E)}{\xi\Sigma_s(E)} = \frac{1}{M(E)}$$

is the reciprocal of the moderating ratio, M(E), of the medium.

Avaev has shown[4] that the inverse moderating ratio term in the integral of Eq. (11.1) is best replaced by the modified form:

$$\frac{1}{M(E)} = \frac{\Sigma_a(E)}{\Sigma_a(E) + \xi\Sigma_s(E)}, \tag{11.2}$$

for strongly absorbing media. This suggests that the starting point in the search for a spectral characterization parameter might well be a function of the form:

$$S' = \frac{\Sigma_a}{\Sigma_a + \xi\Sigma_s}, \tag{11.3}$$

where the cross sections in Eq. (11.3) have been averaged over the flux spectrum. Although there is no particular reason to expect that flux averaging will do anything but define a mean spectral index, it is desirable to average over $\phi(E)$ in order to preserve reaction rates when the one-group cross sections are used in criticality calculations.

Application of one-group theory now permits two important simplifications:

(a) Leakage can be accounted for by adding the familiar DB^2 term to Σ_a;

(b) criticality can be determined by applying the neutron balance,

$$\Sigma_a + DB^2 = \nu\Sigma_f .$$

Equation (11.3) is thereby modified to the form:

$$S'' = \frac{\nu\Sigma_f}{\nu\Sigma_f + \xi\Sigma_s} . \tag{11.4}$$

Several practical considerations can now be taken into account to simplify calculation of the terms appearing in Eq. (11.4). First, while the slowing-down power, $\xi\Sigma_s$, should theoretically include both elastic and inelastic scattering, only the former will be included: comparison of Figs. 11.1 and 11.2 shows that in the energy range where important cross sections, such as the fission cross section of Pu^{239}, are strong functions of energy, elastic scattering predominates. Second, in the interests of simplicity, the scattering cross

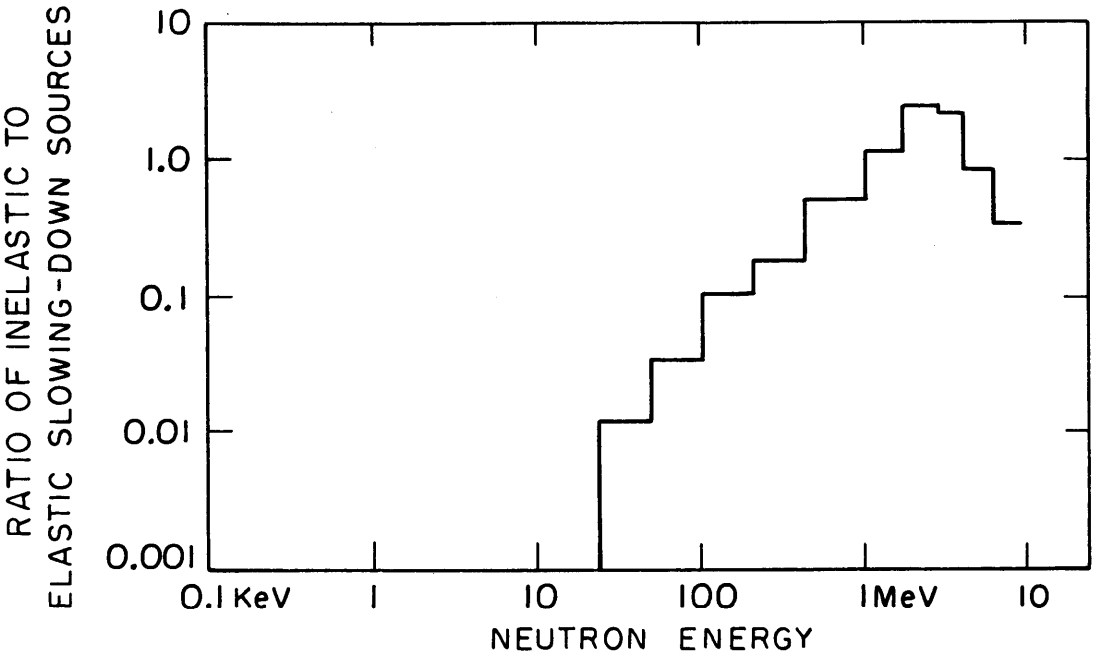

FIG. II.1 COMPARISON OF INELASTIC AND ELASTIC SLOWING-DOWN SOURCES IN TYPICAL LMFBR CORE

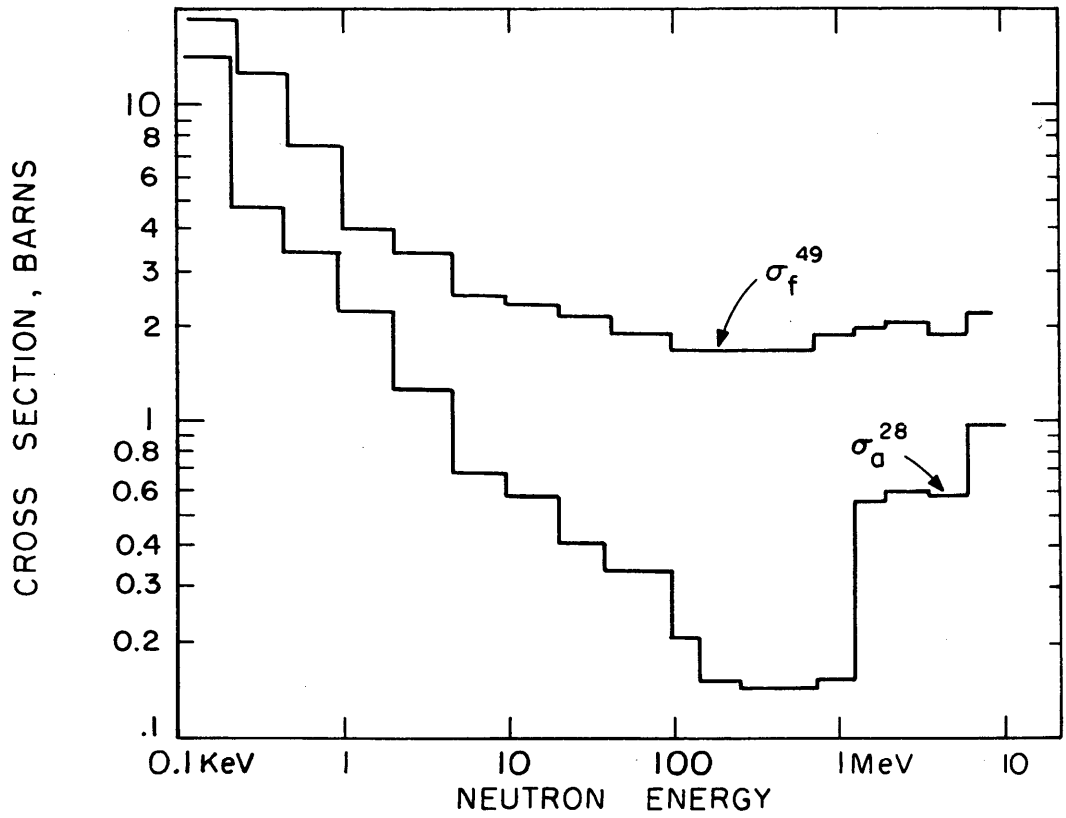

FIG. II.2 TYPICAL VARIATION OF CROSS SECTION WITH ENERGY

section, Σ_s, will be replaced by the transport cross section, Σ_{tr}, since it can be shown that $\xi\Sigma_s$ and $\xi\Sigma_{tr}$ do in fact have the same general magnitude and functional dependence.

The candidate characterization parameter then becomes:

$$S = \frac{\nu\Sigma_f}{\nu\Sigma_f + \xi_{el}\Sigma_{tr}} . \tag{11.5}$$

11.3 Theoretical Considerations for a Characterization Parameter for Threshold Fission

Investigation of the spectral parameter, S, as discussed in the next section, revealed its usefulness in correlating all cross sections except those for fission of the fertile isotopes. Such a result was not unexpected because of the nature of the threshold process and the neglecting of inelastic slowing-down, which predominates in this energy region.

If the cross section for threshold fission is idealized as having step-function dependence with a constant value, σ_{fT}, above a threshold energy, E_T, then the one-group averaged cross section is given by the relation,

$$\bar{\sigma}_f = \frac{\int_0^\infty \sigma_f(E)\ \phi(E)\ dE}{\int_0^\infty \phi(E)\ dE} = \sigma_{fT} \cdot \frac{\int_{E_T}^\infty \phi(E)\ dE}{\phi_{TOTAL}} . \tag{11.6}$$

It is next assumed that the flux above E_T is proportional to the uncollided neutron flux, or,

$$\bar{\sigma}_f = c\ \sigma_{fT}\ \frac{\phi_{UNCOL}}{\phi_{TOTAL}} . \tag{11.7}$$

A neutron balance gives

$$\nu\Sigma_f\ \phi_{TOTAL} = \Sigma_R\ \phi_{UNCOL} , \tag{11.8}$$

where Σ_R is the effective removal cross section for first flight neutrons. Combining Eq. (11.7) and Eq. (11.8) yields:

$$\bar{\sigma}_f = c\,\sigma_{fT}\,\frac{\nu\Sigma_f}{\Sigma_R} \quad . \tag{11.9}$$

Equation (11.9) suggests that the ratio,

$$R = \frac{\nu\Sigma_f}{\Sigma_R} , \tag{11.10}$$

is an approximate spectral characterization parameter for threshold cross sections. Two important features of this parameter should be emphasized. First, regardless of core composition, the shape of the neutron flux above 1 MeV is essentially equivalent to the fission spectrum, $\chi(E)$. Hence, σ_R may be computed from the relation,

$$\sigma_R = \frac{\int_{E_T}^{\infty} \chi(E)\left[\sigma_a(E) + \sigma_{el}(E\rightarrow E') + \sigma_{in}(E\rightarrow E')\right] dE}{\int_{E_T}^{\infty} \chi(E)\, dE} , \tag{11.11}$$

where $E' < E_T$. Equation (11.11) reveals the important fact that σ_R depends only on the cross sections of each element and is independent of the core spectrum. Hence, microscopic removal cross sections can be computed easily from multigroup sets and are constant, regardless of the core composition. This cross section can also be determined experimentally using the classical sphere transmission technique.

Second, examination of Eq. (11.5) reveals that S is a function of $\nu\Sigma_f$; hence, it is also a function of R if the core contains any fertile isotopes. The iteration procedure required to perform criticality calculations using S and R (described in the next section) is considerably simplified if Eq. (11.5) and Eq. (11.10) are combined to yield,

$$R = \frac{S}{1 - S} \cdot \frac{\xi\Sigma_{tr}}{\Sigma_R} . \tag{11.12}$$

11.4 Development and Numerical Tests of σ Correlation

The procedure used to develop and evaluate a correlation between one-group averaged cross sections and S and R was as follows.

First, a reference multigroup cross section set, in this case the 26-group ABBN set,[5] was selected and fundamental mode spectra were calculated for forty-five representative fast reactor cores (see Table 11.1). The cases investigated included oxide-, carbide- and metal-fueled cores having compositions in the range typical of large, liquid metal cooled, fast breeder reactors.

Next, the 26-group spectra were used to collapse fission, absorption and transport cross sections into one-group averaged values. The parameters S and R were then calculated for each case. Ten of the cases having S values uniformly over the full range encountered were selected to develop the cross-section correlations, and the other cases were reserved to test the completed one-group model.

The existence of a correlation between one-group σ values and S and R was then investigated. It was found that there was a linear relationship between the cross-section values and S or R on a log-log plot. Hence, it was decided to adopt the convention,

$$\sigma = \sigma_1 S^g \quad \text{and} \quad \sigma = \sigma_1 R^g \,. \tag{11.13}$$

Figures 11.3 and 11.4 show some sample cross-section plots supporting these choices of functional dependence.

A least-squares fit was then performed to determine the two parameters σ_1 and g using the ten sets of data selected; all forty-three materials of the ABBN set were correlated.

11.5 Iterative Procedure for Applying the One-Group Model

The iterative procedure required to obtain the values of S and R for any core is as follows. An initial value of S is estimated; the cross sections, σ_{tr_i}, are then calculated, and R is determined from Eq. (11.11). $\nu\Sigma_f$ is then computed, and a new value of S is calculated from Eq. (11.5). This procedure is repeated until S has converged to within the required precision (typically about 1%). The iteration was

TABLE 11.1

Composition (Volume Percent) of Fast Reactor Cores Investigated

	OXIDE CORES					CARBIDE CORES					METAL CORES			
No.	PuO_2	UO_2	Na	Fe	No.	PuC	UC	Na	Fe	No.	Pu	U	Na	Fe
1	5	20	50	25	1	5	20	50	25	1	5	30	50	15
2	5	30	50	15	2	5	25	50	20	2*	5	20	50	25
3	5	30	40	25	3	5	30	40	25	3	5	30	40	25
4	5	35	35	25	4	5	35	35	25	4	5	35	35	25
5*	5	25	50	20	5*	7	18	50	25	5	5	25	50	20
6	5	25	45	25	6	5	25	45	25	6	5	25	45	25
7	5	25	40	25	7	5	25	40	25	7	5	25	40	25
8*	5	25	25	25	8	5	25	25	25	8*	5	25	25	25
9	5	25	10	25	9	5	25	10	25	9*	5	25	10	25
10	5	25	0	25	10	5	25	0	25	10	5	25	0	25
11*	8	22	45	25	11	5	30	50	15	11	8	22	45	25
12	7	28	40	25	12	8	22	45	25	12	3	27	45	25
13	9	26	40	25	13	4	26	45	25	13	7	28	40	25
14*	4	27	45	24	14	7	28	40	25	14	9	26	40	25
15	5	26	45	24	15*	9	26	40	25	15*	3.5	26.5	45	25

*Denotes cores used for correlation.

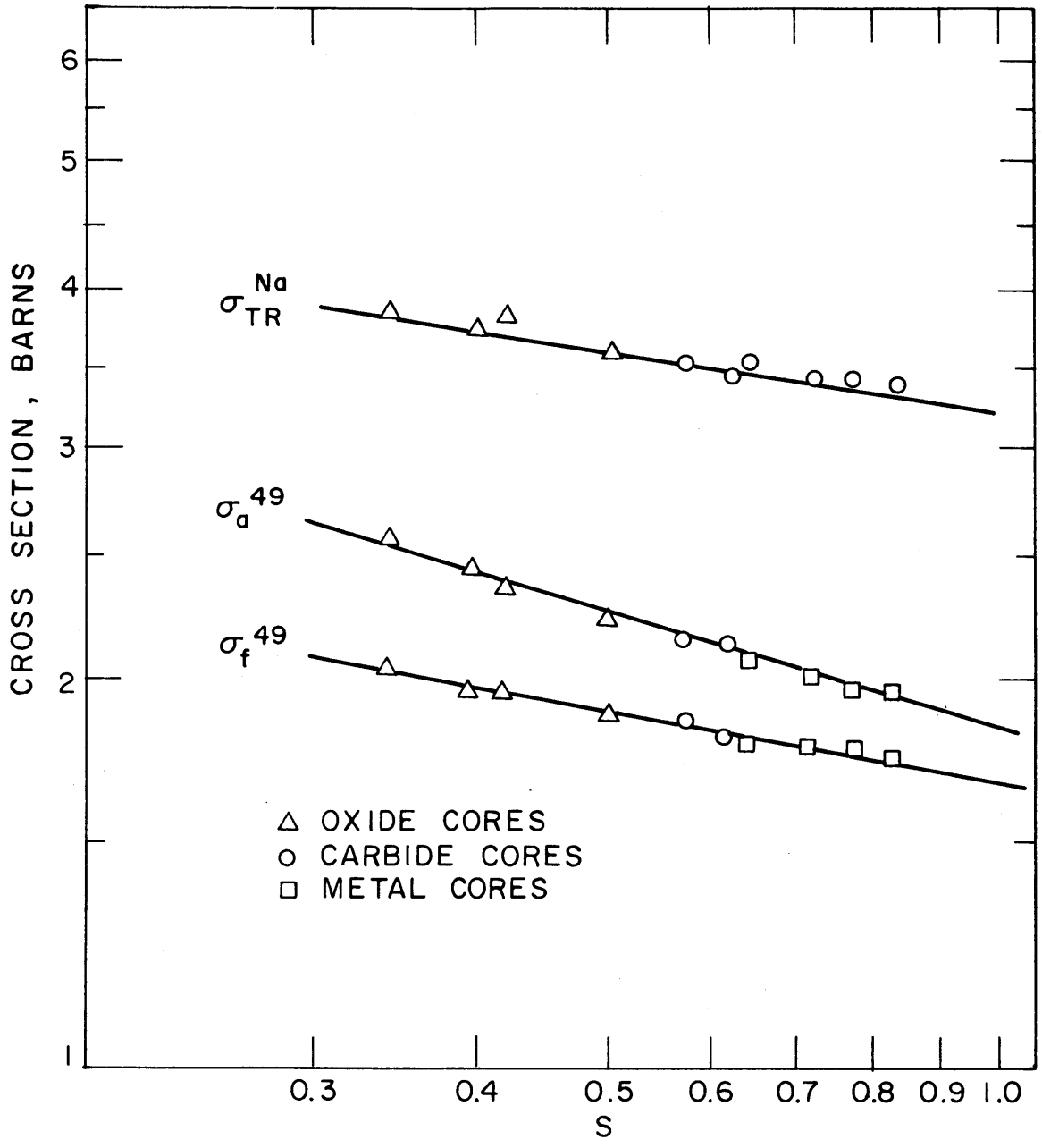

FIG. II.3 TESTS OF CROSS SECTION CORRELATION

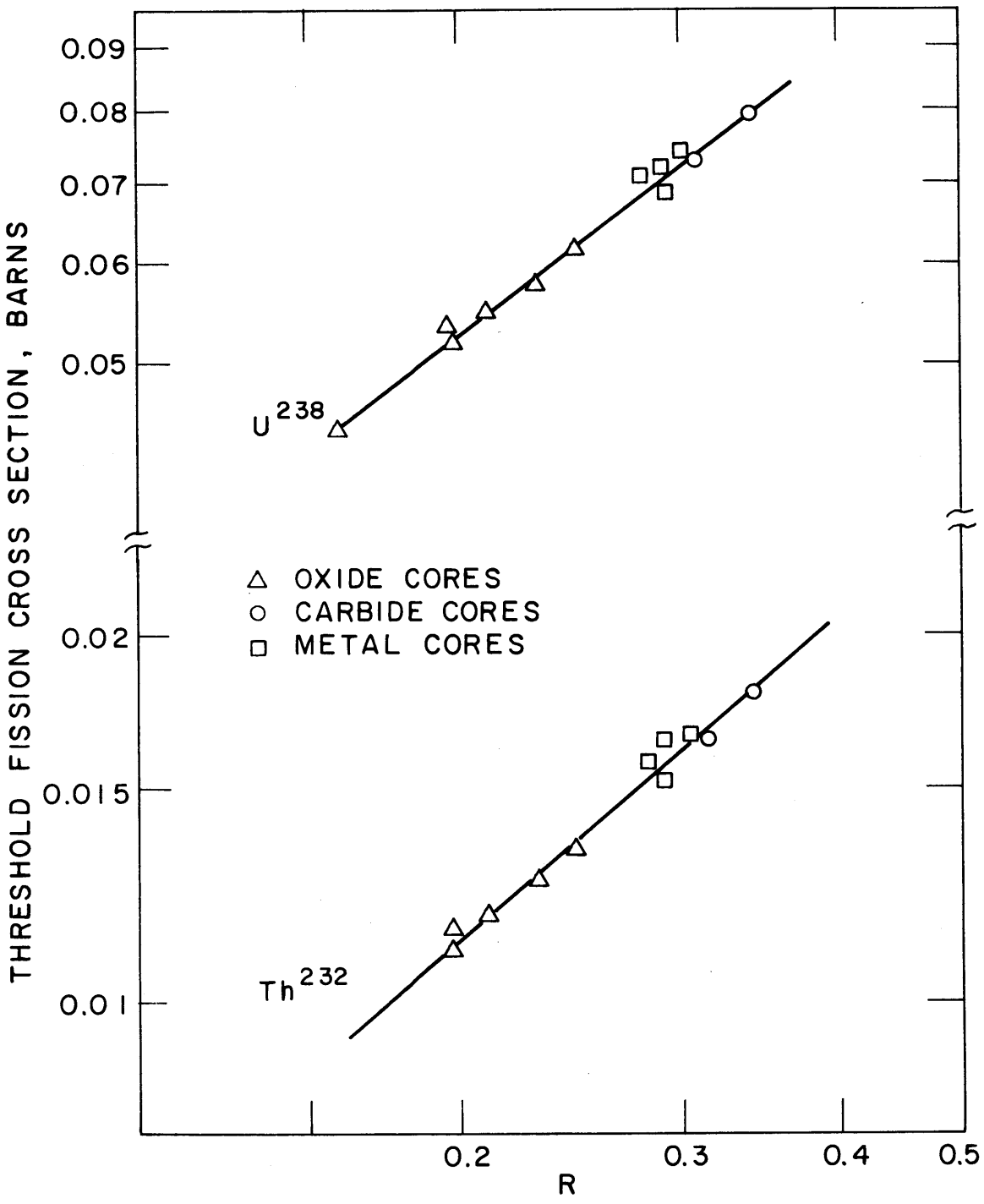

FIG. II.4 TESTS OF CROSS SECTION CORRELATION FOR THRESHOLD FISSION

found to converge rapidly; in the forty-five test cases considered, no more than two iterations were required to obtain S and R. Once S and R are known, all other cross sections (e.g., Σ_a) necessary for the one-group calculation can be evaluated.

11.6 Comparison of 1-Group and 26-Group Results

Tables 11.2, 11.3 and 11.4 show the errors in material buckling (B^2), critical enrichment (ϵ), infinite multiplication factor (k_∞), reactivity ($\Delta k/k$), core conversion ratio (b_i) and the ratio of fertile to fissile fissions (δ_{28}) for the aforementioned cases. The errors in B^2, k_∞ and δ_{28} were calculated directly, since all calculations were based on the fundamental mode approximation. The errors in the other parameters were estimated using suitable one-group equations.[6] As can be seen from the tabulated results, the average errors are 1.77% in B^2, 0.218% in ϵ, 0.59% in k_∞, 0.69% in $\Delta k/k$, 2.19% in b_i and 2.17% in δ_{28}. This is remarkably good agreement.

11.7 Further Extensions of the One-Group Model

Although the forty-five initial test cases all involved liquid metal cores fueled with Pu^{239} and U^{238}, a series of parametric studies has demonstrated its usefulness for all practical fuel, cladding, coolant, structural and control materials. Further utilization of the model[7] has indicated also its ability to account for spectral effects in sodium voiding, and recent research has applied the model successfully in predicting prompt neutron lifetimes. Present investigation is aimed toward extending the model to treat Doppler temperature effects and blanket region calculations.

TABLE 11.2 Comparison of 1-Group and 26-Group Calculations for Oxide Cores

Core	$B^2 \times 10^{3**}$	$\Delta B^2/B^2$ (%)	$\Delta \epsilon$ (%)	$\Delta k_\infty/k_\infty$ (%)	$\Delta k/k$ (%)	Δb_i (%)	$\Delta \delta_{28}$ (%)
1	1.542	1.77	.221	1.15	-.622	1.82	4.51
2	1.283	-1.18	-.090	-.334	.338	-.365	1.11
3	1.293	-1.27	-.686	-.189	.330	-.918	2.58
4	1.130	-4.10	-.211	-.886	.900	-1.76	1.77
5*	1.412	.564	.054	.433	-.179	.655	2.81
6	1.436	.638	.059	.508	-.195	.358	3.49
7	1.423	.435	.041	.379	-.135	.122	3.39
8*	1.378	-.229	-.023	-.074	.075	-.685	3.04
9	1.336	-.968	-.102	-.637	.337	-1.74	2.77
10	1.287	-1.61	-.175	-.132	.581	-3.01	2.58
11*	3.146	2.07	.478	.340	-.954	2.92	4.23
12	2.606	.952	.136	.215	-.378	.951	3.07
13	3.752	1.99	.421	.076	-.922	2.68	3.83
14*	.694	-2.45	-.104	-.266	.440	-1.18	3.02
15	1.407	.322	.028	.360	-.096	.144	3.17
	Average:	1.37	0.142	0.399	0.432	1.29	3.02

*Denotes core used to develop correlation.

**As determined by one-group model.

TABLE 11.3 Comparison of 1-Group and 26-Group Calculations for Carbide Cores

Core	$B^2 \times 10^{3**}$	$\Delta B^2/B^2$ (%)	$\Delta \epsilon$ (%)	$\Delta k_\infty/k_\infty$ (%)	$\Delta k/k$ (%)	Δb_i (%)	$\Delta \delta_{28}$ (%)
1	2.224	2.18	.311	.342	-.868	.792	2.55
2	2.100	1.12	.125	-.229	-.410	-.228	1.07
3	2.046	-.493	-.042	-.842	.157	-.198	.781
4	1.895	-2.65	-.175	-1.50	.745	-3.13	.127
5*	3.516	2.79	.668	.196	-1.35	3.49	2.97
6	2.176	1.31	.141	-.110	-.462	-.394	1.67
7	2.123	.798	.088	-.289	-.291	-.871	1.50
8	2.027	.390	.045	-.520	-.148	-1.39	1.11
9	1.924	-.057	-.007	-.801	.023	-2.03	.661
10	1.850	-.399	-.050	-1.13	.162	-2.76	.345
11	1.973	-.264	-.024	-.841	.090	-1.14	-.297
12	4.262	2.15	.503	-.044	-1.06	3.55	2.37
13	1.287	-1.15	-.073	-.960	.200	-2.43	1.58
14	3.655	1.69	.266	-.095	-.732	.862	1.20
15*	5.119	2.59	.591	-.0009	-1.27	3.85	1.92
	Average:	1.34	0.207	0.527	0.538	1.81	1.34

* Denotes core used to develop correlation.

** As determined by one-group model.

TABLE 11.4 Comparison of 1-Group and 26-Group Calculations for Metal Cores

Core	$B^2 \times 10^{3**}$	$\Delta B^2/B^2$ (%)	$\Delta \epsilon$ (%)	$\Delta k_\infty/k_\infty$ (%)	$\Delta k/k$ (%)	Δb_i (%)	$\Delta \delta_{28}$ (%)
1	4.168	-2.75	-.345	-.750	1.27	-1.87	-2.55
2*	4.265	-.392	-.071	-.598	.194	-.660	-.541
3	4.415	-3.11	-.375	-1.05	1.40	-3.49	-2.11
4	4.427	-4.47	-.454	-1.31	1.91	4.50	-2.63
5	4.219	-1.57	-.233	-.652	.749	-1.32	-1.59
6	4.360	-1.77	-.258	-.827	.836	-2.28	-1.52
7	4.284	-1.84	-.270	-.752	.874	-2.16	-1.56
8*	4.044	-2.14	-.321	-.580	1.04	-1.86	-2.04
9*	3.797	-2.44	-.377	-.340	1.22	-1.40	-2.59
10	3.629	-2.65	-.416	-.144	1.34	-.995	-2.99
11	7.759	.923	.246	.172	-.508	7.37	.177
12	1.729	-8.19	-.471	-2.83	2.48	-7.46	-.866
13	6.943	-.691	-.133	-.009	.359	2.12	-1.49
14	9.283	.720	.188	.457	-.399	8.49	-.225
15*	2.447	-5.14	-.414	-2.08	1.88	-6.13	9.52
	Average:	2.59	0.305	0.837	1.10	3.47	2.16

* Denotes core used to develop correlation.

** As determined by one-group model.

11.8 References

(1) Driscoll, M.J., "Characterization of Neutron Spectra in Fast Reactors," Sc.D. Thesis, M.I.T., Department of Nuclear Engineering (December, 1965).

(2) Driscoll, M.J., and I. Kaplan, "A Simple Shape Function for Correlating Fast Reactor Spectra," Trans. A.N.S., Vol. 9, No. 1 (June, 1966).

(3) Dunn, F.E., and M. Becker, "Analytic Representation of Fast Reactor Flux and Importance Spectra," Trans. A.N.S., Vol. 11, No. 1 (June, 1968).

(4) Avaev, V.N., "The Shape of the Spectrum of Moderated Neutrons in Absorbing Media," Atomnaya Energiya, 18, 6, 584-588 (June, 1965).

(5) Bondarenko, I.I., et al., "Group Constants for Nuclear Reactor Calculations," Consultants Bureau, New York (1964).

(6) Driscoll, M.J., M.I.T. Course 22.94 Notes (1968), and Supplement No. 1 (1969).

(7) Pate, Z.T., "Severe Reactivity Excursions in Fast Reactors," Sc.D. Thesis, Department of Nuclear Engineering, M.I.T. (March, 1970).

12. LMFBR BLANKET FUEL DEPLETION AND ECONOMIC STUDIES

S. T. Brewer

12.1 Introduction

A study of LMFBR blanket fuel management economics is being made as part of the LMFBR Blanket Physics Project. This work, scoping and parametric in nature, has the objective of determining the effect on plant power cost (mills/kWh) of various blanket design parameters, such as composition (fissile, fertile, structure and coolant), size, irradiation time, fuel management scheme, core/blanket/reflector configuration, etc. By pointing out trends in the optimum design of LMFBR blankets, and the relative economic importance of the aforementioned design parameters, LMFBR Blanket Physics Project planners will be aided in designing future assemblies and experiments so as to yield the most useful results.

A base parameter in this work is the core size or rated capacity of the plant. Since very large plants have recently been forecast,[1] a wide range of plant sizes (100 MWe to 5000 MWe) will be examined. One obvious effect is that blanket economic benefit diminishes with increasing core size; indeed, for some sufficiently large core volume, the sale of plutonium bred in the blanket will not compensate for the fabrication and reprocessing costs of the blanket. This result has been confirmed by simple hand calculations.

Fuel economics calculations require:

(a) a cost analysis model;

(b) a physics/depletion model to supply the load and discharge inventories needed in the cost analysis calculations.

These are described below.

12.2 Cost Analysis Model

A survey of methods used in estimating levelized power costs reveals vast disparities in definitions, assumptions and interpretations. Unfortunately, it is not clear that these differences in accounting methods and interpretations will not distort technical or engineering choices.

A cost analysis model, similar to that of Vondy,[2] has been derived for the present work. With LMFBR blankets, the problem of the tax treatment of appreciating fuel is introduced. Unlike Vondy, the present model assumes that the revenue from the sale of plutonium is taxable. The model has been so derived that all cost components are separable and additive.

12.3 Physics/Depletion Model

12.3.1 Requirements of the Model

Cost studies require the load and discharge inventories of important fuel isotopes in individual batches. This necessitates depletion, or "burnup," calculations which yield isotope concentrations as functions of irradiation time.

Blanket physics/depletion calculations are more involved (than those for the core) for three main reasons:

(a) the spectrum softens rapidly with increasing distance from the core-blanket interface;
(b) the spectrum hardens with time due to the large relative buildup of plutonium;
(c) heterogeneous self-shielding effects are stronger in the softer blanket spectrum.

Conventionally, the first two of these difficulties may be overcome by increasing the number of energy groups. The second may also be offset by recollapsing multigroup cross-section sets occasionally during burnup. Both tactics require increased computer expense.

The effects of energy, spatial and time detail on LMFBR physics/depletion calculations have been the subject of several recent studies.[3, 4, 5] In particular, Little et al.[3] have found that

satisfactory core inventory results can be obtained with very few energy groups, and that the few group cross sections need not be recalculated periodically during burnup. An early objective of the present work has been to determine whether similar conclusions could be reached for blankets, in order to provide a simplified physics/depletion model suitable for the parametric studies.

12.3.2 Effect of the Number of Energy Groups

In order to examine the effect of the number of energy groups on blanket physics/depletion calculations, a reference LMFBR configuration (shown in Fig. 12.1) was selected and parallel depletion calculations were performed using 26 energy groups (Run A) and one group (Run B). The two-dimensional, multigroup diffusion theory code, 2DB,[6] was used for both runs.

The parent cross-section data were taken from ENDF/B and were processed by the cross-section generating code, 1DX,[7] at BNWL[8] to produce two, heterogeneity-corrected, 26-group cross section sets (one each for the core and blanket). These final 26-group sets served throughout depletion Run A. The one-group data for Run B were obtained by collapsing the 26-group sets (by zone), at time zero, using the Run A initial solution. This one-group set remained in effect throughout the Run B calculation.

Runs A (26 groups) and B (1 group) covered 600 full power days, with physics calculations (flux shape, local spectrum and neutron balance) at 150-day intervals. The core and axial blanket were replaced at 300 days, corresponding to an average core burnup of about 100,000 MWD/MT. The radial blanket was assumed to be left in place for the full 600 days. The energy release over the 600 days was equivalent to a reactor power of 2576 Mwt, or approximately 1000 Mwe.

Table 12.1 shows representative Pu^{239} concentrations obtained in Runs A and B; only five of the fifteen radial blanket zones are included. Similar results were obtained for U^{238} and the higher plutonium isotopes.

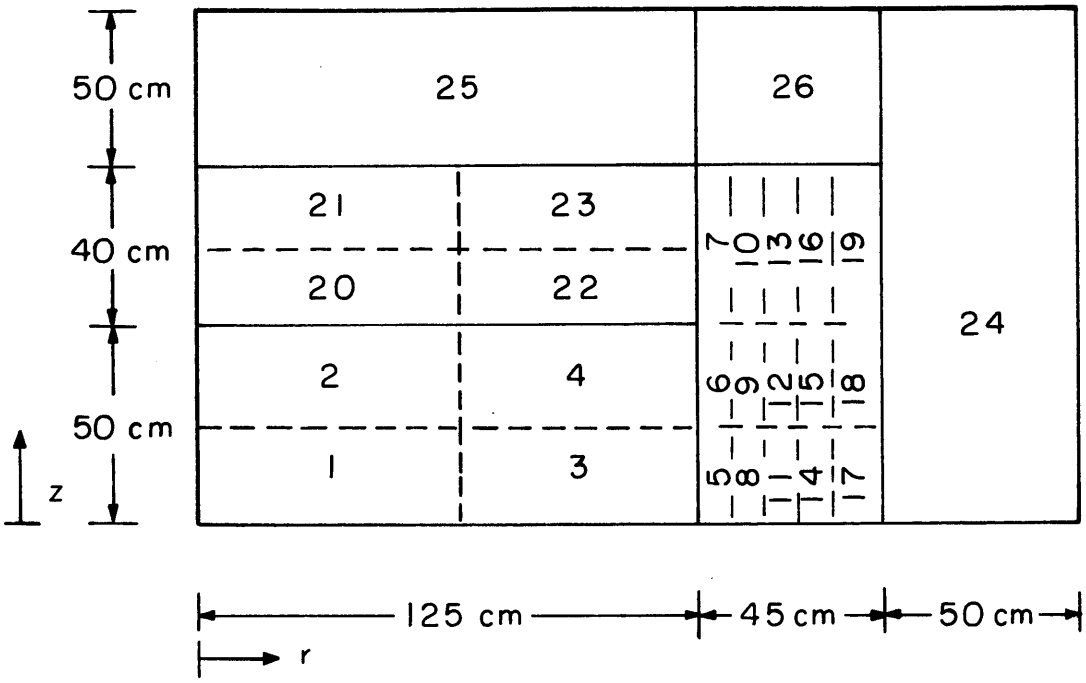

VOLUME FRACTIONS (%)

REGION	CORE	RADIAL BLANKET	AXIAL BLANKET	RADIAL REFL.	AXIAL REFL.	AX. REFL. FOR RAD. BKT.
ZONE	1-4	5-19	20-23	24	25	26
SODIUM	50	30	50	100	50	30
OXIDE	30*	50	30	0	0	0
SS CR-FE-NI	20	20	20	0	50	70

*INITIAL CORE ENRICHMENT = 14 %

FIG. 12.1 REFERENCE LMFBR CONFIGURATION

TABLE 12.1 Pu^{239} Concentrations (10^{-4} atoms/barn-cm)

No parentheses ≡ Run A (26 groups)
Parentheses ≡ Run B (1 group)

Time (days):		0	150.0	300.0	300.0*	450.0	600.0
	Zone						
Core	1	9.100 (9.100)	7.792 (7.811)	6.787 (6.828)	9.100 (9.100)	7.853 (7.868)	6.893 (6.925)
	2	9.100 (9.100)	8.137 (8.140)	7.328 (7.339)	9.100 (9.100)	8.184 (8.184)	7.415 (7.419)
	3	9.100 (9.100)	8.393 (8.395)	7.780 (7.786)	9.100 (9.100)	8.413 (8.414)	7.811 (7.818)
	4	9.100 (9.100)	8.586 (8.580)	8.114 (8.103)	9.100 (9.100)	8.602 (8.594)	8.139 (8.129)
Rad BKT (zones along mid-plane)	5	0.000 (0.000)	2.242 (2.219)	4.075 (4.067)	4.075 (4.067)	5.540 (5.524)	6.726 (6.695)
	8	0.000 (0.000)	1.822 (1.812)	3.392 (3.413)	3.392 (3.413)	4.722 (4.748)	5.870 (5.889)
	11	0.000 (0.000)	1.253 (1.287)	2.422 (2.509)	2.422 (2.509)	3.492 (3.603)	4.492 (4.616)
	14	0.000 (0.000)	0.6859 (0.7670)	1.390 (1.549)	1.390 (1.549)	2.092 (2.301)	2.807 (3.056)
	17	0.000 (0.000)	0.2920 (0.3872)	0.6226 (0.8020)	0.6226 (0.8020)	0.9782 (1.222)	1.370 (1.671)
Ax BKT	20	0.000 (0.000)	2.595 (2.567)	4.314 (4.349)	0.000 (0.000)	2.487 (2.465)	4.161 (4.203)
	21	0.000 (0.000)	1.413 (1.499)	2.697 (2.882)	0.000 (0.000)	1.349 (1.435)	2.573 (2.760)
	22	0.000 (0.000)	1.464 (1.473)	2.695 (2.744)	0.000 (0.000)	1.434 (1.437)	2.645 (2.681)
	23	0.000 (0.000)	0.7607 (0.8336)	1.533 (1.677)	0.000 (0.000)	0.7454 (0.8135)	1.500 (1.634)

*New core and axial blanket.

The shape and magnitude of the total flux and power density agreed well between Runs A and B. In view of this, and the minor variation of cross sections which enter the nuclide rate equations as coefficients, it is understandable that nuclide concentrations predicted by Runs A and B agree closely. The earlier conclusions regarding core depletion results[3] were confirmed.

In the blanket, the spectrum and therefore the effective one-group cross sections vary with position, but change only moderately with time (less than 10% change in $\bar{\sigma}$'s at the outer edge of the blanket in 600 days). A particularly interesting result which arose from these calculations was that the U^{238} capture cross section was found to increase linearly with depth into the blanket.

For the purpose of calculating time-dependent compositions in survey studies, one-group cross sections – fixed throughout burnup – may thus be used in the blanket provided input cross sections have sufficient spatial detail. Cross-section spatial detail is thereby substituted for energy detail, resulting in large savings in computation time with little loss of accuracy in calculating inventories. The 26-group computation (Run A) required 93 minutes running time on an IBM 360/65, while the 1-group computation (Run B) required only 9 minutes on the same machine.

12.4 Conclusions

The purpose of the present work is to study the effect of various blanket design parameters on plant power cost, and to characterize their interrelationship and relative economic importance. This in turn will aid in planning the experimental program of the LMFBR Blanket Physics project beyond Blanket No. 2.

Calculations with the 2DB code have shown that one-group burnup calculations provide satisfactory precision in predicting fissile and fertile inventories in the blanket, provided sufficient spatial detail in the cross sections is substituted for the energy detail. The one-group effective cross sections have been found to vary slowly with time (less than 10% change at the outer edge of the blanket after 600 days), and the U^{238} capture cross section has been found to

increase linearly through the blanket.

The slow variation of the energy-averaged cross sections with time suggests that it might not be particularly useful to simulate partially burnt-up blankets on the Blanket Test Facility (this would be accomplished by loading fuel into a blanket assembly with a suitable U^{235} enrichment gradient).

Presently, the 2DB burnup calculations are being repeated with the steel and sodium outer reflector replaced by a graphite reflector. This will indicate whether or not it would be useful to replace the steel reflector of Blanket Assembly No. 2 by a graphite reflector for Blanket No. 3.

12.5 References

(1) "Fast Breeder Reactor Report," Edison Electric Institute (April, 1968).

(2) Vondy, D., "Basis and Certain Features of the Discount Technique," Appendix F of "A Comparative Evaluation of Advanced Converters," ORNL-3686 (January, 1965).

(3) Little, W. W., R. W. Hardie, L. D. O'Dell and R. B. Kidman, "Fuel Management Models and Analysis for the Fast Test Reactor (FTR)," BNWL-SA-2758 (December, 1969).

(4) Hirons, T. J., and R. D. O'Dell, "Calculational Modelling Effects on Fast Breeder Fuel Cycle Analysis," LA-4187 (September, 1969); Nuclear Applications, Vol. 9, No. 1 (July, 1970).

(5) Hirons, T. J., and R. E. Alcouffe, "Heterogeneity Effects on Large Fast Breeder Fuel-Cycle Calculations," ANS Transactions, Vol. 15, No. 1 (1970).

(6) Little, W. W., and R. W. Hardie, "2DB User's Manual – Revision 1," BNWL-831, Rev. 1 (August, 1969).

(7) Little, W. W., and R. W. Hardie, "1DX, A One-Dimensional Diffusion Code for Generating Effective Nuclear Cross Sections," BNWL-954 (March, 1969).

(8) Little, W. W., and R. W. Hardie, Personal communication (April, May, 1970).

13. SUMMARY, CONCLUSIONS AND FUTURE WORK

M. J. Driscoll

13.1 Introduction

As noted in Chapter 1, this is the first annual report of the LMFBR Blanket Physics Project at M.I.T. As such, one of its major concerns is with the work carried out to complete construction of the basic facility and initial blanket mock-up experiment (Chapters 2 and 3). Likewise, the initial experiments carried out on the facility (Chapter 4) were designed to confirm that performance characteristics matched design specifications. This phase of the research has been essentially completed during the report period.

A second area of research involves work designed to establish the capability for extracting the desired data, primarily material activation and neutron spectra, from the experimental assemblies. Chapters 5 and 6 describe the work which is farthest along, since it involves the use of foil and instrumental techniques upon which considerable prior effort has been expended by other activities in the AEC's LMFBR development program. Chapters 7 and 8, on the other hand, deal with other promising techniques designed to supplement those in Chapters 5 and 6. For the most part, this represents extensions of previous work carried out at M.I.T. in the area of capture gamma spectrometry. Since these latter methods are newer and are being pursued at a lower priority than the former, this work is at a still earlier stage of completion. For the most part, the work described in Chapters 5 through 8 will be completed, or in advanced stage of completion, by the end of the next annual report period.

The final general category under which work has been carried out is concerned mainly with program direction and evaluation, including determination of economic and neutronic features pertinent to the selection of future blanket mock-ups (Chapters 10 and 12), the effects of heterogeneity on mock-up measurements (Chapter 9) and the

characterization of core driving spectra (Chapter 11). This work thus has as its major function the identification of problems requiring increased attention primarily during the third year of the present contract.

13.2 Discussion

The most important conclusions which may be drawn from the performance tests and operating experience on the Blanket Test Facility and Blanket Mock-Up No. 2, to date, are:

1) The facility operates well within all design limits on both operational and shutdown dose rates. Although it was not an essential requirement of the original design, it has been established that midweek access to the blanket mock-up is feasible. This greatly facilitates operational flexibility and improves the productivity of the entire operation.

2) Fundamental-mode cosine flux shapes are achieved in the vertical and horizontal directions in the test blanket. Furthermore, the same shapes are observed using detector foils sensitive to different regions of the neutron spectrum. Thus transverse leakage may be characterized by a simple buckling term and the problem reduced to an effective one-dimensional problem involving traverses through the blanket.

3) Streaming and backscatter effects have been adequately controlled, being confined to a region approximately six inches thick around the periphery of the blanket.

The remainder of the work discussed in this report is not yet at a stage where such definitive conclusions can be drawn. However, a number of potentially important trends are already evident:

1) The poorest agreement between calculations and experiment occur in the steel reflector, quite probably due to the well-known difficulties involved in describing neutron diffusion in iron due to the window in its cross sections near 25 keV.

2) Appreciable heterogeneous effects are observed in the U^{238} capture reaction, which will clearly require both theoretical and experimental clarification.

Finally, some work was completed showing that characterization of core neutron spectra could be achieved using only two simple indices.

13.3 Future Work

During the coming contract year, July 1, 1970 through June 30, 1971, the following work is scheduled:

1) Completion of material activation traverses, including those using Pu^{239} foils, through Blanket Mock-Up No. 2. These traverses will be compared with results from ANISN S_8, 16-group calculations.

2) Completion of neutron spectrum measurements in Blanket No. 2, using both foil and instrumental methods.

3) Evaluation of the feasibility of inferring ambient neutron spectra from capture gamma-ray spectra. This work and that in 2) above should permit us to standardize on two independent methods for application in future studies.

4) Construction of Blanket No. 3 subsequent to a more detailed evaluation of economic and neutronic trends in blanket design. At present, it is tentatively considered that Blanket No. 3 will be a two-row version of Blanket No. 2 having a moderating reflector (probably graphite).

5) Evaluation of heterogeneous effects, especially on U^{238} capture, but also on the activation of foil materials having prominent capture resonances. This will include measurements in a realistic blanket subassembly constructed of UO_2 fuel, stainless steel cladding and Na coolant.

6) Definition and distribution of a benchmark problem corresponding to Blanket No. 2 to interested LMFBR activities to enable them to test their calculational methods against measured data.

The third year of the contract, July 1, 1972 through June 30, 1973, will be devoted to completion of work on Blanket No. 3 and on Blanket No. 4 (for which a final composition has not yet been specified).

Appendix A

THESIS RESEARCH TOPICS

Thesis research topics currently under way are as follows:

(a) T. C. Leung, "Foil Activation Measurements in Blanket No. 2," Sc. D. Thesis; measurements completed by 12/31/70, analysis by 6/1/71, topical report by 9/1/71.

(b) N. R. Ortiz, "Instrumental Spectrum Measurements in Blanket No. 2," Sc. D. Thesis; same schedule as (a) above.

(c) S. T. Brewer, "Blanket Burnup Effects Calculations," Ph. D. Thesis; computations completed by 9/1/70, topical report by 12/31/70.

(d) C. Tzanos, "Blanket Optimization Analyses," Sc. D. Thesis; started 6/1/70, estimated completed by 12/31/71.

(e) M. K. Sheaffer, "Simple LMFBR Calculation Methods," Ph. D. Thesis; topical report by 10/1/70.

(f) C. S. Kang, "Prompt Gamma Spectroscopy on Blanket No. 2," Sc. D. Thesis; same schedule as (a) above.

(g) N. A. Passman, "Neutron Spectrometry on Blanket No. 2 Using Foil Methods," S. M. Thesis; completed by 8/31/70.